POLITECNICO
MILANO 1863

SCUOLA DI INGEGNERIA INDUSTRIALE
E DELL'INFORMAZIONE

CFD analysis of Ducted Injection in a Constant Volume Vessel

Tesi di Laurea Magistrale in
Mechanical Engineering - Internal Combustion Engine and Turbomachinery

Author: **Simone Pavesi, Gabriele Sacchetti**

Student ID: 10571685, 10789382
Advisor: Prof. Gianluca D'Errico
Co-advisors: Andrea Schirru
Academic Year: 2022-2023

Abstract

In the attempt of reducing soot production, to make the combustion process more efficient and also not harmful to the environment, some investigations have been done for improving the quality of diesel combustion: the Ducted Fuel Injection (DFI) technique, experimentally analyzed by Sandia National Laboratories, turned out to be very effective in soot reduction, due to its capability of generating a leaner air-fuel mixture compared to the conventional process. In the present work a numerical approach has been adopted for investigating the experimental state-of-the-art associated with the following duct geometry: D2L16G3.9-δ. The numerical analysis had the target of determining the quality of the chosen spray model through a comparison between experimental data and the ones achieved by considering two different combustion models: PSR and ADF. The most accurate model was then used to base a comparison between FJ and DFI technologies for what concerns the soot production. All CFD simulations were defined for a Low-Temperature Combustion (LTC) case (from 850K to 950K) and for the ambient O_2 concentrations of 0%, 15%, 21%.

Keywords: Alternative Injection, Combustion Models, DFI, Soot

Abstract in lingua italiana

Nel tentativo di ridurre la produzione di particolato, così da rendere il processo di combustione più efficiente ma anche meno dannoso per l'ambiente, diverse indagini sono state fatte nell'ottica di migliorare la qualità della combustione diesel: la tecnica dell'iniezione di carburante canalizzata (DFI), analizzata in via sperimentale da Sandia National Laboratories, è risultata essere davvero efficace nella riduzione di particolato, data la sua abilità nel generare una miscela aria-combustibile più magra rispetto al processo convenzionale. Nel seguente lavoro è stato adottato un approccio numerico con l'obiettivo di investigare lo stato dell'arte sperimentale associato alla seguente geometria del condotto: D2L16G3.9-δ. L'analisi numerica ha l'obiettivo di determinare la qualità del modello di spray scelto attraverso un confronto tra i dati sperimentali e quelli dedotti considerando due diversi modelli di combustione: PSR e ADF. Il modello più accurato è stato quindi scelto per basare un'ulteriore analisi di confronto tra i casi FJ e DFI per quanto riguarda la produzione di particolato. Tutte le simulazioni numeriche sono state definite nel campo della combustione a basse temperature (da 850K a 950K) e per le seguenti concentrazioni di O_2 in ambiente: 0%, 15%, 21%.

Parole chiave: Iniezione Alternativa, Modelli di Combustione, DFI, Particolato

Contents

Introduction

Soot deriving from combustion processes is a significant pollutant in the earth's atmosphere and the second most critical climate-forcing species after carbon dioxide CO_2. The necessity of lowering the emissions to avoid harmful consequences on the environment is also underlined by the emission regulations which are becoming increasingly stringent, posing great challenges to diesel engine combustion and emission. By virtue of that, new solutions acting directly on the combustion process, rather than on the exhaust gases like diesel particulate filters and selective catalytic reduction which add cost and come with fuel-economy penalties, are proposed and investigated to find a new and efficient way to burn diesel fuel and produce power. Among the already proposed solution, some advanced combustion strategies can be appreciated such as globally premixed, low-temperature combustion (LTC), and Leaner Lifted-Flame Combustion (LLFC): but they are characterized by different drawbacks concerning the process control, bringing it difficult at high load and without specific injector geometries. This reduced range of application prompted researchers to think of a novel method for achieving an enhanced charge-gas mixing upstream of the lift-off length by using a small tube placed at a short distance downstream of the injector orifice, termed Ducted Fuel Injection (DFI). Sandia National Laboratories have already tested this new technology experimentally, through a particular optical gear able to replicate the most common operating conditions that can be observed in conventional diesel engines, discovering that DFI approach determines an order-of-magnitude reduction in the soot luminosity signal compared to the one of a free-spray at the same charge-gas conditions. The work here proposed has the main purpose of replicating the experimental data achieved by Sandia National Laboratories during its campaign, by developing a numerical spray model able to show a high level of accuracy in the description of the combustion process that can be appreciated for both FJ and DFI technologies: in this way, numerical data have been collected by considering two different combustion models and different condition, so to create a wide range of considerations relative to the evaluated process. Thus, the campaign has been conducted so to bring the Politecnico of Milan in the wake of the results obtained and present in the state of the art.

1 | Diesel Engine

1.1. Combustion Process

The Diesel engine belongs to the family of Internal Combustion Engine, generating power by burning a mixture composed of fuel and air. Of course, the process is complex and regulated by different and complex variables. The following paragraphs aim to describe as clearly as possible the process, underlying some important aspects of combustion development and emission production, that have to be limited. Never like today an effort in limiting the production of harmful substances assumes importance, and this can be done by acting at the base: by understanding and improving the combustion process.

1.1.1. Process Characteristics

The compression ignition engine *CI* (or Diesel cycle) [1] [2] is characterized by a high volumetric compression ratio, $16 \div 20$, able to produce a temperature increase up to $500°C \div 600°C$ of the fresh charge inside the combustion chamber, after the intake phase. Fuel is injected in form of spray inside this air at high temperature and pressure, then it vaporizes and mixes with air creating an air-fuel mixture that, due to the condition at which is subjected self-ignites, after an ignition delay of the order of a millisecond. The process develops and the pressure increases, accelerating the pre-oxidation reactions of that part of the air-fuel mixture already formed, which ignites and burns, bringing the gas temperature to over 2000°C and level of pressure of $15 \div 20$ MPa, the vaporization and vapor diffusion of the remaining fuel accelerates further. Injection continues until all the fuel quantity corresponding to the applied load is injected, passing through the processes of vaporization, diffusion and combustion. During the expansion phase, the mixing of the remaining air with the burnt or partially oxidized gases leads to the completion of the combustion process inside the combustion chamber.
The following diagram, within abscissa the times and in ordinate the pressures, represents the pressure $p(t)$ trend during a regular combustion process, the dashed line is instead the pressure $p(t)$ trend without fuel injection.

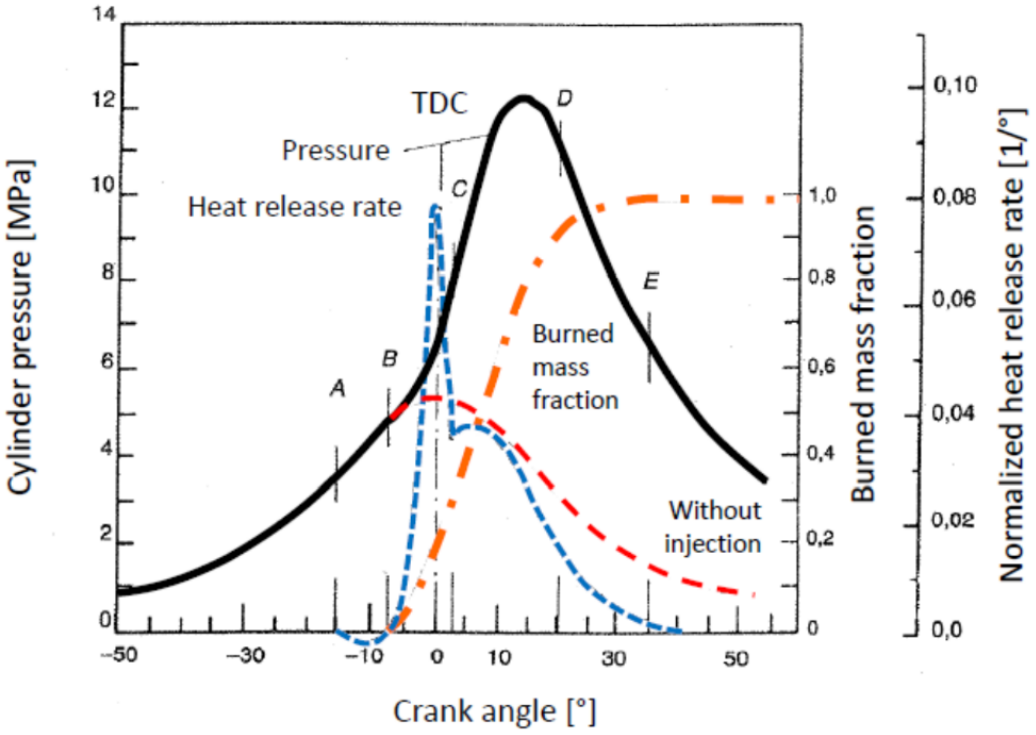

Figure 1.1: Pressure Vs. Time in Diesel engine combustion process

It is possible to distinguish four different phases, subsequently listed:

1. *Delay*: starts when Diesel is injected into the combustion chamber and ends when combustion starts;
2. *Rapid combustion*: phase characterized by rapid propagation of the combustion of the premixed charge air-fuel formed during the ignition delay period, generating a rapid increase of pressure and energy release;
3. *Controlled combustion*: phase of combustion regulated by diffusive process, of the jet central nucleus and of the fuel successively injected, as that enters into the combustion chamber so that the energy release can be regulated by the quantity of injected fuel and its subdivision in more phases;
4. *Completion of combustion*: injection is over but the combustion process proceeds till all the Diesel previously injected burns.

Premixed and Diffusive Combustion

In the Diesel combustion process, the major problem is the correct mixing between the injected fuel with air. This fact forces to improve the characteristics of injected fuel spray

and to increase the level of turbulence inside the combustion chamber. As shown in figure (1.2), when the spray is injected into the combustion chamber, different zones can be appreciated: the central core, which appears compact, and small dimension droplets that are dragged from turbulence and air motion towards peripheral areas, where they are surrounded by abundant air, which quickly heats and vaporizes them. In this zone, fuel vapors and air can be considered mixed, so the combustion generated is premixed, which is fast with a high peak in the associated heat release rate curve. From the point of view of pollutants production, this zone is lean so un-burned hydrocarbons are not present, however, can be formed NO_x due to high temperature and high level of oxygen present.

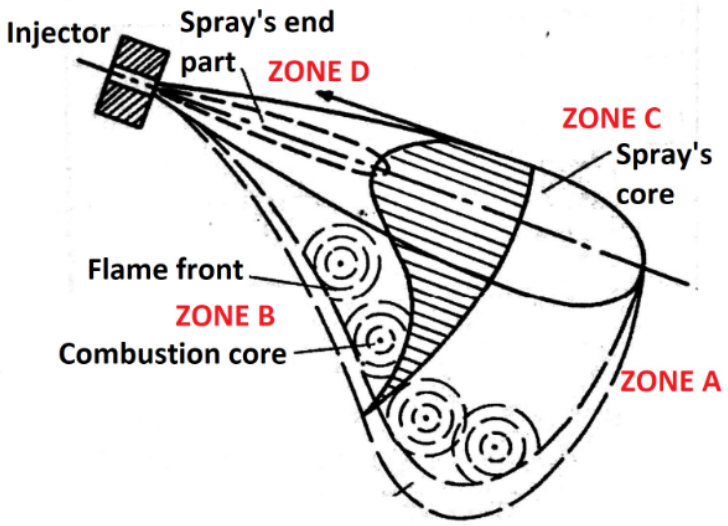

Figure 1.2: Diesel jet schematization

After ignition, combustion starts and the flame propagates to the central core of the spray, where larger fuel droplets are found. These, heated by irradiation, evaporate quickly and the vapors diffuse into the surrounding charge. Many of these droplets in the central part of the spray evaporate, but only partially, so are surrounded by diffusive flames which regulate the evaporation and diffusion of fuel vapors through the flame.
If the combustion chamber has a high level of turbulence, able to guarantee a sufficient level of oxygen replacement, the combustion of these vapors can happen satisfactorily. Otherwise, due to lack of oxygen and bad mixing, can be generated products of incomplete combustion (HC), of partial oxidation like aldehydes and peroxides and carbonaceous particles.

1.1.2. Diffusive Combustion

As briefly described in the previous paragraph, fuel droplets, suspended in air, burn differently from a premixed fuel-air charge because a large influence on this is exercised by the diffusion process of fuel vapors inside the air: commonly, this process develops as a diffusive combustion. This kind of combustion influences a conspicuous part of diesel inside the cylinder. Many droplets may be surrounded by a flame front when they are still in the liquid phase; then, hot gases give heat that brings them to evaporation. The heat flux $\dot{Q}$, transferred by convection and conduction, increase enthalpy h and promotes evaporation:

$$\dot{Q} = m\frac{dh}{dt} - H_v\frac{dm}{dt} \tag{1.1}$$

where:

- m, mass of droplets a time t;
- H_v, latent evaporation heat of fuel.

Fuel vapors form a mixture, with air, that burns when an opportune ratio (typically stoichiometric) is reached. The mixing phase, after the evaporation of fuel droplets, is mainly influenced by the turbulent motion and the diffusion velocity is inversely proportional to the turbulent mixing time τ_t. This is defined as the ratio between the turbulent kinetic energy k with the dissipation velocity ϵ

$$\tau_t = l/u \approx k/\epsilon \tag{1.2}$$

Inside the cylinder, during the mixing time, the big eddies on scale l lose a part of their kinetic energy in a time equal to that of the turbulent turnover (l/u) transferring it to micro-eddies. At equilibrium, the times of kinetic energy dissipation (k/ϵ) from micro-eddies is equal to the times of receipt of the same from the macro-eddies. At high temperatures, during the combustion process, chemical times τ_a are lower than the turbulent mixing time τ_t ($\tau_a \ll \tau_t$). At the beginning of the combustion process, instead, the situation is the opposite ($\tau_a \gg \tau_t$) and the control of the time process is exerted by chemical kinetics.

1.1.3. Ignition Delay

In the studies of Diesel engines, great importance is attributed to the ignition delay: the time interval from the start of injection to the start of combustion. The start of combustion can be determined in different ways, among which:

- individuation, in the pressure vs. time diagram of the cylinder, the point where the pressure increase due to combustion generates the detachment of the curve from the one of pressure without fuel injection;
- time instant where the flame appears inside the cylinder, done with a photodiode;
- measurement of chemical composition change of a fraction of mixture with the formation of combustion products.

The importance of ignition delay calculation lies in the fact that it is the cause of the subsequent combustion phase: the rapid one, which can be approximated to constant volume combustion. The quantity of premixed charge, generated during the ignition delay time, depends on pressure and temperature increase, which consequently influence the level of noise of the engine, the thermal stresses and vibrations.
Returning to the simulation environment, a definition of an accurate and unique method for the ignition delay calculation assumes further importance since consent to compare the value found from the simulation with the experimental one; this part of the work allows to find similarities or differences between the two times and defines whether the simulations results are sufficiently accurate or a further simulation set-up tuning is required. This tuning, increasingly refined, allows copying reality as best as possible in order to have better final results.

1.1.4. Physical and Chemical Process

Talking about ignition delay, it is possible to differentiate and appreciate these two different processes:

- *Physical delay*, that modify the aggregation state of fuel molecules and mix them with air;
- *Chemical delay*, that oxidize the mixture and modify the chemical composition.

Going deeply into details, the physical delay brings to:

1. disintegration of the fuel jet turning it into droplets;
2. heating of the droplet with the subsequent evaporation;

3. diffusion of these vapors into the air till the formation of an air-fuel mixture able to auto-ignite.

with a large influence on these processes of atomization fineness of the fuel jet, which depends on the injection pressure and the geometry of the injector; motion condition of the air, which depends on combustion chamber geometry and rotation speed; pressure and temperature, which depends on compression ratio, cooling and level of supercharging.

The chemical delay instead is associated to:

1. high molecular mass hydrocarbon decomposition in lighter compounds due to thermal effect;
2. their attack by oxygen with the formation of intermediate oxygen compounds, such as peroxides and aldehydes, which are not very stable;
3. initiation of the chain reactions which lead to self-ignition of the fuel.

these processes are influenced by the nature of the fuel, till the formation of a critical concentration of intermediate components able to initiate fast chain reactions that bring to the auto ignition and to final combustion products. So, the chemical component of the delay can be mainly associated with the structure and dimension of the fuel molecule which makes it more or less susceptible to oxygen.
Certainly, it is difficult to clearly distinguish the two different delays, however, the main chemical reactions take place only after the fuel vapors have come into contact with the air, i.e. after the fuel has come into contact with the comburent, therefore it can be assumed that the first part of the delay is dominated by that physical, while the second one from the chemical which leads to self-ignition.

1.1.5. Ignition Delay Calculation

Over the years have been proposed different correlation to calculate the ignition delay as a function of engine parameters, fuel and charge characteristics, with many of these derivatives from experimental and semi-empirical foundations from engines, closed volumes and reactors. However, it is worth mentioning and commenting on the two most significant ones:

- from *Wolfer*
- from *Hardenberg e Hase*

The first proposed a simple formula to give an indication of the possible ignition delay, emphasizing chemical aspects, and related to temperature T [K] and pressure p [MPa],

using the exponential term proposed by *Arrhenius*:

$$\tau_a[ms] = Ap^{-n} \exp^{\frac{E_a}{RT}} \tag{1.3}$$

w/o the constants:

$$A = 0,029 \quad n = 1,19 \quad \frac{E_a}{R} = 4650 \tag{1.4}$$

Although the equation *(2.1)* has been widely applied to Diesel engines, results from the calculations and from experimental measurements show discrepancies, underlying as simple correlation as the *(2.1)* approximate the measured data just in the interval of the parameter values that define the conditions of the engine and the charge in the cylinder. To extend the validity of correlation is required to make the constant A assumes different values as a function of turbulence in the combustion chamber and E_a from fuel characteristics. To achieve the goal of extending the validity interval of the correlation and obtaining results closer to the measured reality, the correlation from Hardenberg and Hase tries to be more precise, taking into account the motion conditions of the air, making them dependent on the average speed of the piston $\overline{u}_p$ *[m/s]* and on the chemical properties of the fuel, through its cetane number *(NC)*. In this case, the ignition delay is expressed in crank angle $\Delta\theta_a[^\circ]$ using:

$$\Delta\theta_a[^\circ] = (0,36 + 0,22\overline{u}_p)e^Z \tag{1.5}$$

w/o:

$$Z = \frac{61,884}{NC + 25}(\frac{1200}{T_2} - 0,582) + \frac{6,85}{(10p_2 - 12,4)^{0,63}} \tag{1.6}$$

in which temperature T_2 and pressure p_2 of the charge are evaluated in correspondence of the top death center *(TDC)* at the end of the compression using a polytropic model for the compression stroke, with the relation:

$$T_2 = T_1 r^{n-1} \quad p_2 = p_1 r^n \tag{1.7}$$

where T_1 and p_1 express the condition in the intake manifold and the exponent n of the polytropic is in the range of 1,1 ÷ 1,4 as a function of engine rotation speed and thermal

regime. Results from *(2.3)* are demonstrated in accordance with the experimental results in a wider interval of working conditions and engine characteristics.

Inside a numerical simulation environment, like the one that has based the following studies, other techniques can be used:

- search for the $max(\frac{dT}{dt})$ inside the file of temperature *T(t)* [K] over time t [s] of the simulation: in this way, it is possible to find the time instant in which temperature undergoes the higher increase, ignition symbol inside the cylinder;
- once defined a T_{amb} [K] and a T_{peak} [K], respectively the ambient and the maximum peak temperatures, the time in which ignition occurs, traduced also in ignition delay, can be found starting from the calculation of the ignition temperature T_{ign} [K]: $T_{ign} = \frac{1}{2}\ (T_{amb} + T_{peak})$, from which, in the file temperature over time, the associated time can be pointed out.

1.1.6. Energy Release Calculation

The calculation of the energy release due to the combustion process inside the combustion chamber in a Diesel engine can be calculated from an experimental relief of the pressure *p(θ)* inside the cylinder. To obtain this is sufficient to apply the energy conservation principle to the gaseous system contained in the combustion chamber, and what can be obtained is:

$$\frac{dQ_r}{d\theta} + \Sigma_i h_i \frac{dm_i}{d\theta} = \frac{dU}{d\theta} + \frac{dW}{d\theta} + \frac{dQ_d}{d\theta} \tag{1.8}$$

Where all the terms are explicit for a generic position θ of the crankshaft and:

- $\frac{dQ_r}{d\theta}$: energy flux released during the chemical reaction of the combustion process;
- $\Sigma_i h_i \frac{dm_i}{d\theta}$: energy contribution due to the passage of mass through the boundary surface;
- $\frac{dU}{d\theta}$: internal energy variation of the system;
- $\frac{dW}{d\theta}$: mechanical power exchanged by the piston;
- $\frac{dQ_d}{d\theta}$ heat dispersion through the walls of the combustion chamber.

Being the modern injection technology, in Diesel engines, defined as direct, it is possible to neglect the sensible enthalpy contribution due to the injected fuel and the mass variations of the system due to leakage through the piston rings.
So, considering $\frac{dm_i}{d\theta} \approx 0$ and the fluid as a perfect gas, the temperature variation over the camber angle change is derived:

$$\frac{dT}{d\theta} = \frac{p}{mR}\frac{dV}{d\theta} + \frac{V}{mR}\frac{dp}{d\theta} \tag{1.9}$$

and the energy release during the combustion process $\frac{dQ_r}{d\theta}$:

$$\frac{dQ_r}{d\theta} = \frac{\gamma}{\gamma - 1}p\frac{dV}{d\theta} + \frac{\gamma}{\gamma - 1}V\frac{dp}{d\theta} + \frac{dQ_d}{d\theta} \tag{1.10}$$

After an accurate measure of the pressure inside the cylinder $p = p(\theta)$ and knowing the volume variation $V = V(\theta)$, the equation *(2.5)* consents to obtain the temporal evolution of the mean temperature inside the combustion chamber, and from which it is also possible to derive the heat loss through the wall $\frac{dQ_d}{d\theta}$ with a suited thermal model. Following these steps, the energy release $\frac{dQ_r}{d\theta}$ or the fraction of burned fuel $\frac{dx_b}{d\theta}$ can be derived, being:

$$Q_r = \int_{\theta_i}^{\theta_f} (\frac{dQ_r}{d\theta})\, d\theta \approx m_c H_i \tag{1.11}$$

and,

$$\frac{1}{Q_r}\frac{dQ_r}{d\theta} = \frac{1}{m_c}\frac{dm_c}{d\theta} = \frac{dx_b}{d\theta} \tag{1.12}$$

In the end, the fraction of burned fuel:

$$\frac{dx_b}{d\theta} = \frac{1}{m_c H_i}\frac{dQ_r}{d\theta} \tag{1.13}$$

The typical trends of the heat release curves present two consecutive maximums: the first relative to the energy released due to fuel mass premixed with air and the second due to the diffusive combustion process. Despite being a simplified analysis, this can underline the relative importance of these two different combustion processes, showing how the second peak becomes more and more preponderant as the temperature in the chamber increases or, in general, as the maximum power of the engine decreases, with which the weight of the delay is reduced when turned on.

1.2. Emissions Production

Pollutants formation during the combustion process in Diesel engines is strongly affected by the inhomogeneity of the charge inside the combustion chamber, due to the continuous variable distribution of fuel and air during the time. ***HC***, ***NO_x***, ***CO*** and ***soot*** are the main pollutants produced in diesel engines due to the combustion of a diesel spray injected in air endowed of turbulent motion, at partial and full load.

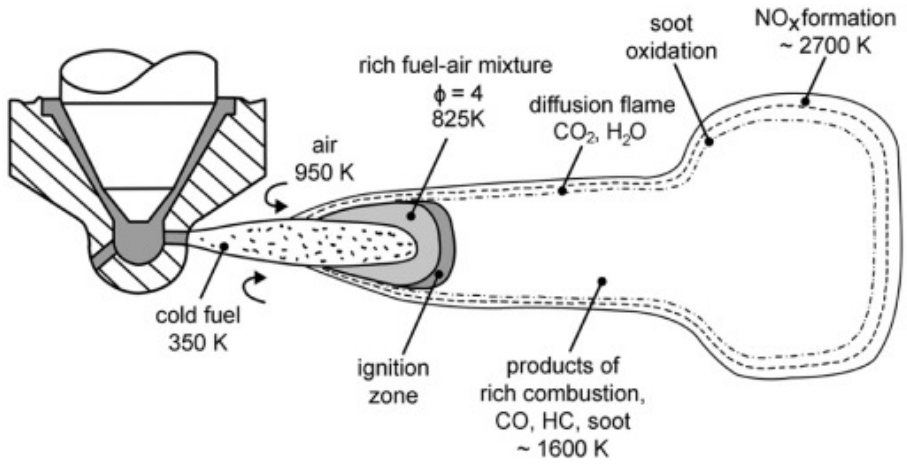

Figure 1.3: Pollutants formation mechanism

1.2.1. HC

In a diesel engine, unburned hydrocarbons can have different origins:

- Peripheral zone of the spray, where the fuel concentration is too lean to bring to the auto-ignition and to the propagation of the flame front and thus can be a zone of partial oxidation and thermal cracking (dissociation of big molecules in smaller ones);
- Central zone of the spray, where the fuel concentration is too rich, HC can also be generated at the end of the injection process and at full load due to a lack of air to completely oxidize the remaining fuel;
- In small engines bore diesel can reach the cylinder walls and piston and evaporates. if the last evaporated vapors do not have sufficient oxygen with which oxidize can have burning difficulties;
- Additional contribution to the HC formation is due to the aspiration of the fuel entrained in the zone between the needle seat and holes of the injectors.

1.2.2. NO_x

Nitrogen oxide production is due to the presence of both oxygen and nitrogen in the atomic state, mainly due to dissociation produced at high temperatures of gases after the flame passages. In general, the chemical kinetics of the production process is equal to the one of the spark ignition engine, with the difference that the inhomogeneity of the fuel inside the combustion chamber.
Conditions where NO_x could be created are:

- Slightly lean region around the jet, which burns first, due to high oxygen availability and high temperature.
- Central nucleus of the spray, where there are the maximum temperatures and high oxygen availability when the load is not at the maximum level.

With the proceeding of the process, so with the expansion, temperatures reduce and NO_x concentration freezes bringing to values higher than the ones predicted from chemical balances.

1.2.3. CO

the CO species, called carbon oxides, is an intermediate product of hydrocarbon oxidation. If there is sufficient oxygen availability, the CO generally is oxidized into CO_2, with the inconvenience of incomplete reaction due to low temperature and residence time, due to the high velocity of the process. Except for occasions, like the central part of the spray core or diesel deposited onto walls, in a diesel engine the availability of oxygen guarantees sufficient oxidation of the CO, and so the presence of carbon oxides at the exhaust is one order of magnitude lower than in an Otto cycle engine.

1.2.4. Particulate Matter

Particulate Matter (PM) is the suspension in the exhaust fumes of carbon particles, also called *soot* generated by the incomplete combustion of the fuel. Due to its danger to human health, PM is a pollutant that requires major attention.
Going more in detail, the PM formation starts during the combustion process and develops till the discharge of the exhaust gases into the atmosphere, continuously changing chemical composition and size. In particular, its formation starts from *precursors* which forms after the start of the combustion, in the central part of the spray characterized by a lack of oxygen and the combustion develops with a diffusive flame. In these zones hydrocarbon molecules, initially with a ratio $H/C = 2$, subjected to high thermal flux without oxygen

decompose due to thermal effect and loss hydrogen, a process called *pyrolysis*, generating molecules poor of hydrogen, with a ratio $H/C = 0.1$. The precursors can react with molecules of unsaturated hydrocarbon and hydrogen-poor radicals, going to create the so-called *primary elements* constitutive of *PM*. These primary elements can increase their dimensions with a process of superficial growth, due to attaching on to the surface of other species rich in carbon, generating the *nuclei*, also called *spherules* due to shape. Much of these nuclei are transported in suspension to the exhaust gases, while others become constitutive elements of particles of bigger dimensions resulting from the agglomeration of many nuclei due to collision, coagulation and aggregation.

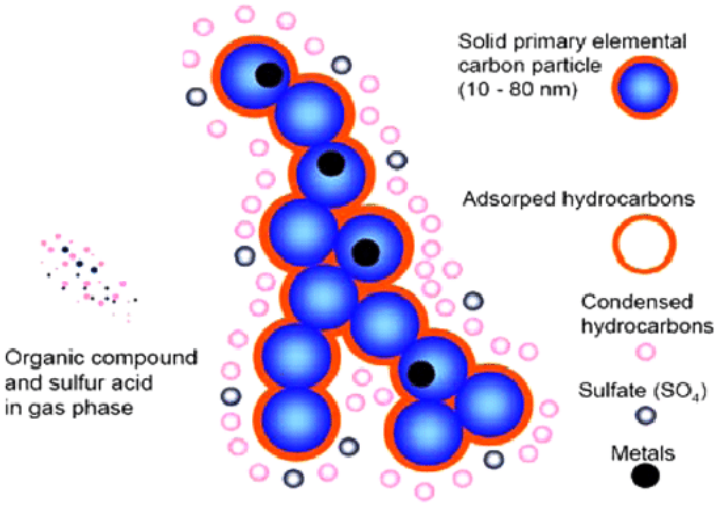

Figure 1.4: Particulate matter representation

At the exhaust of a Diesel engine, particulate matter is a set of carbonaceous nuclei singles or agglomerated in complex clusters. Generally, these carbonaceous nuclei are coated with high molecular weight organic compounds, such as ketones, esters, ethers, organic acids and polycyclic aromatic hydrocarbons (*IPA*) which have been adsorbed on their porous surface or have condensed on it.

The chemical composition of the particulate is a part of solid material, mostly carbon, called dry or solid fraction (*SOL*) and a soluble organic fraction (*SOF*).

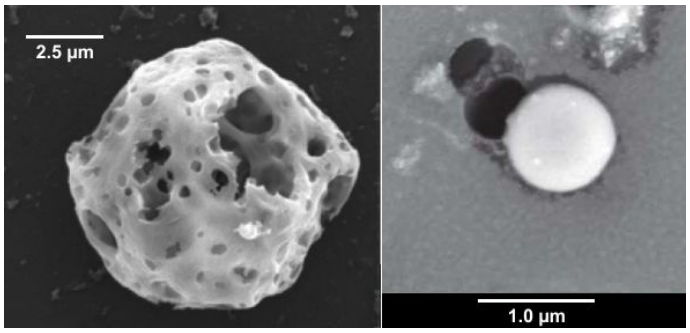

Figure 1.5: Particulate Matter at microscope

It is possible to see the shape: irregular and generally not spherical; it is so defined as an (*equivalent diameter Dp*) of a spherical particle which has the same volume or external surface or dynamic behavior of the irregular particulate matter agglomerate.
In a Diesel engine, the emitted particles' dimensions are in the order of 10 and 10^4 *nm*, values influenced by the kind and the working condition of the engine.

1. *Nuclei* ($Dp < 50\ nm$);
2. *Particles* ($50\ nm < Dp < 1000\ nm$);
3. *Agglomerates* ($Dp > 1000\ nm$).

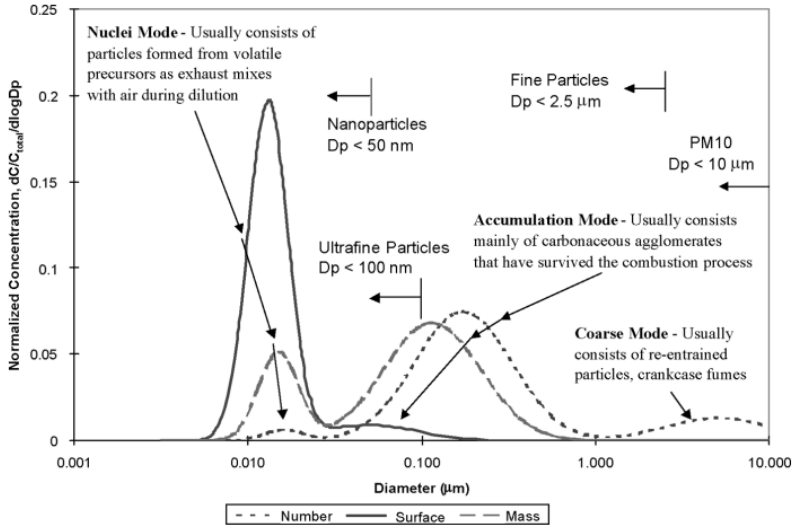

Figure 1.6: Typical diesel particle size distribution weighted by number, surface area and mass

1.3. Emissions Controlling

It is clear that there are active actions with which it is possible to reduce and contain the emission in diesel engines, and these are:

- Exhaust gas recirculation (EGR) in order to reduce the maximum temperature of the combustion;
- Optimized injection time, which depends on pressure and temperature development inside the cylinder;
- Division of the injection phase in more than one;
- high injection pressure in order to produce a better pulverization and so penetration of the combustible spray;
- Optimization of the aspiration process, as the aspiration ducts, to increase the turbulence and the mixing efficiency;
- Use of a turbo-supercharger with intermediate inter-refrigeration of the compressed charge to reduce temperatures and compression ratio;
- Maintenance of the engine and the aspiration system to maintain the parameters to an optimal value, as project;
- Use of clean diesel fuel with better characteristics, like the low presence of sulfur.

1.3.1. EGR

The *EGR* technology is used only during partial load in order to not reduce the power developed at higher load. Essentially this technique provides to the combustion chamber part of the exhaust gases, which replaces part of the air (which is in excess with respect to the quantity required for the combustion). This solution generates the following two effects:

1. Dilutes the charge inside the combustion chamber, reducing the oxygen quantity;
2. Increase the thermal capacity of the mixture, reducing the maximum temperature reached during the process at the same energy released during combustion.

This second effect is in reality not so strong in Diesel engines since the recirculated exhaust charge is not so different in terms of concentration of N2 from the air which substitutes. Different techniques can be applied to make an effective *EGR* and in particular, they can be divided into:

- Internal
- External

The first one can be regulated by the opening and the closure of intake and exhaust valves which are completely variable, in terms of lifts and timing. The kinds of internal *EGR* are:

1. Through the intake valve, bringing back part of the exhaust charge flowed into the intake manifold during the contemporaneous opening of the valves.;
2. Through the exhaust valve, re-intake part of the exhaust charge gone into the exhaust manifold;
3. Avoiding the exhaust charge leaves the combustion chamber.

Specifically, there are opening laws that make possible this valves management:

- Open the intake valves in advance with respect to the top death center (TDC) in order to transfer part of the exhaust charge into the intake manifold so to be re-intake during the following intake phase;
- Close the exhaust valves behind to the (TDC), in order to intake part of the exhaust charge already into the exhaust manifold;
- Open the exhaust valve during the intake phase;
- Hold part of the exhaust charge into the combustion change anticipating the exhaust valve closure and delaying the opening of the intake valves.

For what concerns the external *EGR* there are essentially two main configurations:

1. High pressure and short route: the exhaust gases just after the exhaust manifold or just after having traveled the first part of the exhaust duct are brought back to the intake manifold, downstream the compressor;
2. Low pressure and long route: the exhaust gases are picked up from the end of the exhaust system, after the post-treatment group, and directed to the intake manifold, upstream of the compressor.

1.3.2. Diesel Particulate Filter

The most effective action to reduce *PM* from exhaust gases is to filter it. A filter, called *Diesel particulate filter* or only *FAP* is a component that forces the exhaust gases to pass through it: a porous barrier. The working mechanism is simple: particles bigger

than the pores are trapped inside the barriers, instead exhaust gases pass through them. The carbon compounds accumulate on the filtering surface, which periodically has to be cleaned, oxidizing the stacked deposits. The material which are constituted these filters is ceramic in order to make them resistant to high thermal stress, with a monolithic honeycomb structure. A common way to create them is by extrusion of a ceramic porous material, based on silicon carbides, in order to obtain cylindrical elements with internal squared channels arranged parallel to each other. Each channel is open in one extremity and closed to the other, and is arranged in order that channels near this are closed on the opposite extreme, this feature consent to increase the wet surface. Exhaust gases that enter a channel, open at the entrance, are forced by its final plug to cross the porous walls, to reach the adjacent channels open at the exit, depositing on them the carbonaceous particles transported in suspension.
The image helps the understanding of the structure:

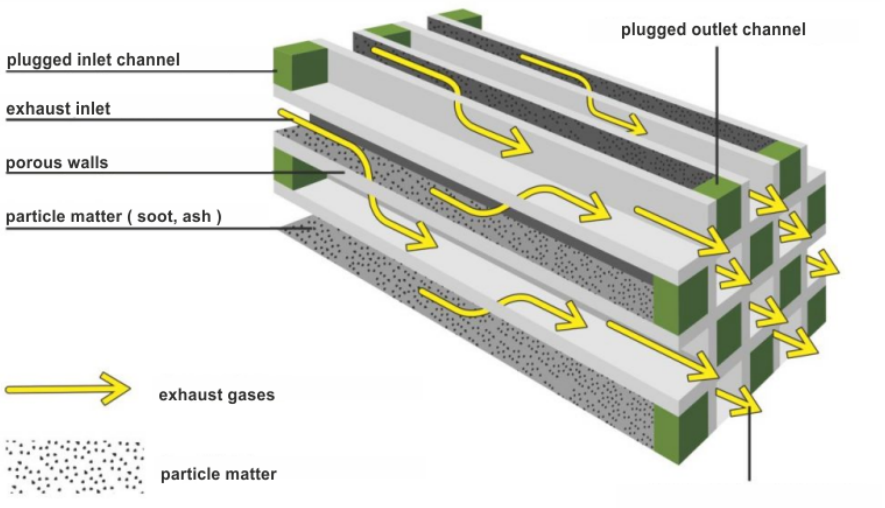

Figure 1.7: Diesel Particulate Filter structure

Vantages of adopting the anti-particulate filter are:

- Filtering efficiency, over 90%;
- Low-pressure drops;
- High thermal and mechanical resistance;
- Good accumulation power of carbonaceous particles.

Due to high thermal resistance and low costs, filters are mostly generated with ceramic material. In recent periods filters are also generated with the sintering of metal powders.

The operating principle remains the same: the gases entering from one end will find the opposite end closed, forcing the passage through the porous channel on which the particulate will be deposited. The advantages that bring this technology are:

1. Possibility of accurately controlling the porosity of the sintered filter;
2. Better thermal conductivity.

FAP Regeneration

Independently on the material used for the generation, on the filtering surface a progressive accumulation of particulate matter takes place that if on the one hand increases the filtering action (because reduces the mesh size of the filter) on the other hand increases the resistance to the passage of the gases, increase the back pressure, reducing the performance and increasing the fuel consumption of the engine. A *regeneration* process is so required. This kind of process can be conducted in different ways, depending on:

1. *Oxidant* agent:
   - Oxygen O_2, which is largely present in the exhaust gases of a Diesel engine; the required temperature is greater than 600°C;
   - Nitrogen dioxide NO_2, which has to be produced by the NO oxidation; the advantage is that reaction can happen at lower temperatures, starting from 250°C;
2. *Periodicity* of the operation:
   - w/o *Continuity*: particulate matter is burned after the deposit onto the filter whenever temperature and minimum quantity of oxidant reagent are reached;
   - *Intermittently*: the regeneration starts thanks to a controlling system which at pre-set intervals like every $4 \div 8$ hours or every $400\ km \div 600\ km$
3. *Cause* that produces regeneration:
   - *Active* regeneration, when the oxidation reactions of the particulate matter are activated from a controlled contribution of energy coming from outside the exhaust gas system, and this can be:
     (a) from the engine, with a calibrated controlling strategy like delayed fuel injection and post-injection during the exhaust phase;
     (b) from a separate source of energy, in order to produce gases sufficiently hot, like electrical heating and micro-waves;

- *Passive* regeneration, when the use of opportune catalysts makes possible the oxidation reactions of particulate matter at the temperature of exhaust gases developed during the combustion process, in normal working conditions:
  (a) being added to the fuel;
  (b) coating the channels.

These last two strategies are the most common techniques for the regeneration of the filter. Entering more in detail: the first strategy consists in adding additives into the fuel, like cerium oxides, that during the combustion process modify the composition of the carbonaceous particles deposited on the filter, this new chemical composition lowers the trigger temperature to a value of 400°C (respect the initial 600°C).

$$C + 2NO_2 \rightarrow CO_2 + 2NO \tag{1.14}$$

$$2C + 2NO_2 \rightarrow 2CO + 2NO \tag{1.15}$$

With the proceeding of these reactions, which are exothermic, the temperature of the filter increase. In the meanwhile that the temperature is in the interval between 250°C $\div$ 450°C the oxidation action of the particulate with NO_2 is prevalent, but with the temperature increase the reaction with O_2 become the most important.

$$C + O_2 \rightarrow CO_2 \tag{1.16}$$

$$2C + O_2 \rightarrow 2CO \tag{1.17}$$

At the end, the regeneration process depends on:

1. catalytic channel coating;
2. temperature and mass slow of exhaust gases;
3. oxygen content in the exhaust gases;
4. content of incomplete combustion product (HC, CO);
5. characteristics of carbonaceous particles filtered.

1.3.3. Selective Catalytic Reduction (for NOx)

Selective Catalytic Reduction (SCR) is a technique used for nitrogen oxides (NOx) reduction when the reduction acting through the combustion process is not sufficient. To

remove (NOx) from exhaust gases the focus is on selective catalytic reduction operated by the use of ammonia. Since ammonia is toxic and easily flammable is preferred the use of a solution of urea ($CO(NH_2)_2$) in demineralized water. This urea solution is injected after the catalytic converter for NOx. The correct quantity of urea injected during the process is optimized during the engine tuning, taking into account that an insufficient quantity of urea brings a lower converter efficiency instead an excessive quantity brings a presence of ammonia into the exhaust gases discharged into the atmosphere. Ammonia in high quantities discharged in the ambient brings even more damages than NOx so it is preferred to reduce the efficiency of the converter to a value of 85% and, in addition, to add downstream the converter an oxidizing part in which the excess of ammonia is oxidized into N_2 and H_2O. At the beginning of the process, the urea solution introduced in the exhaust gas flow is decomposed for thermolysis and hydrolysis into NH_3 and H_2O. In addition, one critical point in the project phase is the % of NOx that generally is very small, in the order of 1% so the drawing of the converter should be such as to ensure good mixing between the exhaust gas and the ammonia formed, to consent at the reagents to come into contact. The structure of the converter is a ceramic monolith with a honeycomb structure, the channels of which have a catalytic coating based on noble metal oxides (vanadium, titanium and tungsten) capable, at temperatures of 250°C ÷ 450°C, to make the base reactions of the process. The base reaction of the reduction process of NOx to N_2 and H_2O by the ammonia are:

$$2NH_3 + 2NO + \frac{1}{2}O_2 \rightarrow 2N_2 + 3H_2O \tag{1.18}$$

$$2NH_3 + NO + O_2 \rightarrow 2N_2 + 3H_2O \tag{1.19}$$

The action of the converter is selective (which brings the name) because favorites the oxidation reactions of NH_3 due to NOx and not from O_2. In addition, being the second reaction is predominant at temperatures of 250°C ÷ 300°C, is better to oxidize the exhaust gases at the first of the converter in order to prepare H_2O and oxidize the exhaust product of incomplete combustion (increasing so the temperature of gases). The SCR converters are widely used in Diesel engines due to the efficient conversion of NOx from exhaust gases.

2 | Ducted Fuel Injection

2.1. DFI Introduction

In modern times, internal combustion engines (ICEs) fed with fossil fuels still remain the dominant powertrain solution for personal and commercial transportation in the world [3]. Based on the market, in 2016, 99.8% of the approximately one billion light-duty passenger cars and trucks on Earth were powered by ICEs burning fossil fuels [3]. ICEs due to the high energy content per unit mass of liquid fuels make them well-suited to transportation applications, where lightweight, long-range, and the ability to refuel quickly are critical. Alongside the high development and some of the benefits just mentioned, there are also drawbacks related to the pollutants emission and the fuel origin. In fact, the combustion of fossil fuels releases carbon dioxide (CO_2) into the atmosphere, ICEs can produce carbonaceous particulate matter (i.e. soot), a known toxin that, together with the CO_2 are two of the main climate-forcing species [3]. Hence, new solutions, developments and improvements of ICEs, in the direction of lowering emissions can bring environmental and societal benefits, especially in the sector where battery-powered vehicles face larger practical challenges, like heavy-duty applications [3]. The action aimed at limiting the impact of the transport sector on the environment should be continuous, and one of them is to increase engine efficiency and eliminate soot emissions while transitioning to renewable liquid fuels. Increase engine efficiency leads to lower CO2 emissions per unit of engine work output. Eliminating soot emissions removes a toxic and critical climate-forcing species. And shifting from fossil fuels to truly renewable, sustainable fuels – using liquid fuels made from waste biomass and/or from solar energy – can slow or even reverse the trend of increasing atmospheric CO2 [3]. It is important to underline that, from a CO_2 perspective, ICEs are not the problem but is instead the carbon inside the fossil fuel, so the use of renewable fuels which do not change the Earth CO_2 equilibrium can be one viable solution in the direction of a cleaner world. Certainly is not the only one, in fact, research is focused also on combustion strategies for mixing-controlled compression-ignition (CI) engines, due to: their inherently high efficiencies, arising from higher compression ratios and lower pumping work during the intake and exhaust strokes [3]. By virtue of

the above, numerous studies have been devoted to overcoming the challenges of higher emissions of soot and nitrogen oxides with mixing-controlled CI combustion.
Starting from 2004, *Pickett and Siebers* proposed different paths to make combustion in CI engines that do not form soot, using various fuels [3]. The idea was to reduce the equivalence ratios in the premixed auto-ignition zone of the combusting diesel jet below approximately two. Although the results were representative of thermodynamic conditions found in diesel engines, the experiments were conducted in conditions remote from those actually found in diesel engines: the use of a CVCV (i.e. constant volume combustion vessel), with a single-hole injector tip (i.e. without interactions between sprays), without interaction with the walls and without a moving piston. All these differences from the reality of operation, although they led to satisfactory results in the elimination of pollutants, including soot, did not give any indication of whether it was the same for real diesel engines.
In the same period *Upatnieks et al.* also found that it was possible to have combustion in diesel engines that did not produce soot, using neat oxygenated fuel at high loads. In this case, the problem lay in the availability of neat oxygenated fuel, which was too low to cover the total requirement and make it an effectively applicable solution.
Polonowski et al. and *Andersson et al.* proposed a so-called leaner lifted-flame combustion (LLFC) using diesel fuel and different injector tip configurations. Even here, although the results obtained were satisfactory, the conditions for which they were found were too far compared to the real ones in a diesel engine: two-hole injector tip at light engine loads were too limiting.
Gehmlich et al. proposed a middle solution between the two previous ones, using a 50 vol% oxygenate in diesel fuel through an LLFC combustion, showing how it could be used with a 6-hole injector tip to loads above 5 bar gross indicated mean effective pressure. In this case, it was not possible to sustain LLFC at significantly higher loads without going beyond the realm of feasible engine operating conditions or the already high level of fuel oxygenation.
Analyzing the various proposed solutions, it is possible to summarize them in attempts such as the use of fuel oxygenation, high injection pressures, small injector orifices, cool intake conditions, and retarded combustion phasing. All the proposed solutions go in the direction of increasing the level of local fuel/charge-gas premixing upstream of the flame lift-off length Seeking to further increase the extent of premixing at the lift-off length, *Mueller* proposed the idea of injecting a fuel spray down the axis of a small duct positioned within the combustion chamber some distance downstream of the injector orifice exit.
This concept is termed ducted fuel injection (DFI), and is, in reality, a 160 years old idea,

as evidenced by the invention and employment of the Bunsen burner in early studies of photochemistry [3]. Although it was thought up several years ago, the DFI concept has not been studied previously in the context of fuel injected through a tube for reciprocating ICE applications. Contemporary approaches use a numerical approach to solve the flow field using turbulence models, allowing detailed analysis of both mixing and entrainment characteristics. A summary of the current state of the art is proposed in the next paragraph.

2.2. State of the art of the DFI technology

After having introduced and described the current treatment systems for emissions reduction in Diesel engines, this chapter will give a description of the DFI method, designed to reduce harmful emissions at the exhaust, acting directly on the combustion process. Differently from what is done by the most recent technologies in terms of abatement for the pollutants emission, the DFI solution is aimed to reduce them during the combustion process itself rather than post-process. The DFI method promises a significant reduction in soot emissions in direct injection CI engines, but still being an immature method, investigations are today done and, in particular, a resume of the actual state of the art can help in the understanding of the actual state of the art. In the modern period, there are two main actions to reduce emissions: one eliminating harmful emissions, only after being produced, and the other acting directly onto the combustion process, which is what DFI does. The DFI concept has been patented by Sandia National Laboratories and is based on the fuel injection inside the combustion chamber down the axis of a small cylindrical pipe in the combustion chamber in order to enable and sustain the Leaner Lifted-Flame Combustion (LLFC). An initial proof of the advantages brought by this concept is observed by *Mueller at al.* [4] who experimentally showed the effectiveness in reducing soot emission, by reducing the natural luminosity of two orders of magnitude with respect to the conventional free spray in a constant volume vessel. Subsequent works developed by *Gehmlich et al.* confirm the result already found and the capability of the DFI to reduce soot, after measurements in the vessel. *Nilsen et al.* [5] [6] implement the method in an engine combustion chamber, which has shown how DFI attenuates engine-out soot emission at low load by approximately an order of magnitude with respect to the conventional diesel combustion and breaks soot/NO_x trade-off with dilution at medium load. Till now, benefits decrease when the load increases. The potentials are known, but an accurate understanding of the process is necessary and *Li et al.* [7] [8] [9] investigated the DFI macroscopic characteristics, in non-reacting conditions via Schlieren imaging, finding how the DFI spray penetrates more than the Free Jet one, with also a larger cone angle

downstream of the duct with more fluctuating peripheries. That is how *Svensson et al.* [10], after the analysis of *Gehmlich et al.* of a duct with a rounded inlet and a tapered outlet, analyzed this duct shape for a ducted injection in a high-temperature pressure vessel varying stand-off distance and duct length and finding that the longest duct was the most efficient geometry in reducing soot. Preliminary investigation and optimization, using CFD, was done by *Fitzgerald et al.* [11], who employed a combustion model (based on *Hiroyasu* model for soot prediction) for DFI. They justified the DFI effectiveness by suggesting that the ducted jet is richer and cooler inside the duct, leading to an elevated turbulence level at the duct outlet, which promotes mixing and a lower equivalence ratio at the Lift-Off Length (LOL). *Tanno et al.* [12], after experimental tests, concluded that DFI homogenizes the mixture narrowing the equivalence ratio distribution because of the more air entrainment sent toward the spray core. Also *Nilsen et al.* [13], using a calibrated spray model, confirm the enhancement of the upstream air entrainment, but reduce the overall one. However, the higher mixing compensates, leading to a lower equivalence ratio at the duct outlet and at the LOL, concluding that a shorter duct cause lower air entrainment inhibition and, thus, better equivalence ratio distribution at LOL. *Millo et al.* [14] [15], after experimental measurements in a constant-volume vessel confirm as DFI, in non-reacting condition, raises the turbulent kinetic energy (TKE), lowering and homogenizing the equivalence ratio distribution.

2.3. Why DFI?

The introduction of the DFI technology could provide some benefits with respect to the actual state of conventional Diesel combustion, characterized by a free spray injection. Hereafter, a list of the main advantages is presented:

1. The presence of the duct could dramatically increase the velocity gradients responsible of the turbulent mixing within the spray, reducing the equivalence ratios of the most fuel-rich mixtures within and downstream of the duct. Soot formation could be prevented if the richest mixtures can be maintained at equivalence ratios of approximately two or lower in the autoignition zone [3].

2. The presence of the duct wall could also limit over-mixing at the radial periphery of the spray, enriching the most-fuel-lean mixtures, increasing the combustion efficiency and lowering hydrocarbon and carbon monoxide emissions. In other words, the duct could help to reduce and narrow the distribution of equivalence ratios reacting at the lift-off length, LOL [3].

3. The proximity of the duct inlet to the cooler wall of the combustion chamber could

tend to draw cooler charge gas from the thermal boundary layer into the duct; furthermore, the duct itself might be cooler than the ambient in-cylinder gases. Both of these phenomena could lead to cooler mixtures within the duct, allowing more mixing to occur during an increased ignition-delay period [3].

4. The duct could prevent, or at least delay, entrainment of combustion products into the spray upstream of the established LOL, preventing an undesired, rapid shortening of that feature leading to increased soot formation [3].

5. Leaner mixtures at the duct exit could have longer ignition delays due to chemical-kinetic effects (i.e., leaner mixtures typically have longer ignition delays), providing more time for premixing [3].

6. The higher strain rates and/or lower temperatures at the exit of the duct create a region, at the duct outlet, where the ignition is unlikely to happen, thereby enabling additional entrainment and premixing downstream of the duct but upstream of the LOL [3]. In addition, if soot, hydrocarbon, and carbon monoxide emissions from the engine were no longer a problem, dilution (e.g., via exhaust-gas recirculation) could be employed as an inexpensive means to control emissions of nitrogen oxides [3].

Since the DFI method enhances air-fuel mixing, the equivalence ratio distributes more uniformly than CDC (Conventional Diesel Combustion), around the auto-ignition region. Because of the homogeneous distribution of the equivalence ratio in the cylinder, the equivalence ratio around the lift-off length results lowered and a relatively uniform temperature occurs from the combustion starting point. As a consequence, the soot concentration inside the cylinder decreases with this method. The DFI method also increases the velocity vectors consenting to a higher spray penetration. In the end, we can say that DFI produces significantly longer, leaner, and faster spray. Globally due to the combined action that the ducted injection brings, soot emission reduction reaches 67% with DFI, whereas HC and CO emission reductions are only 8% and 20%, respectively; it is observed that NO_x emission increases. Hereafter, the DFI technology is depicted in terms of flame structure:

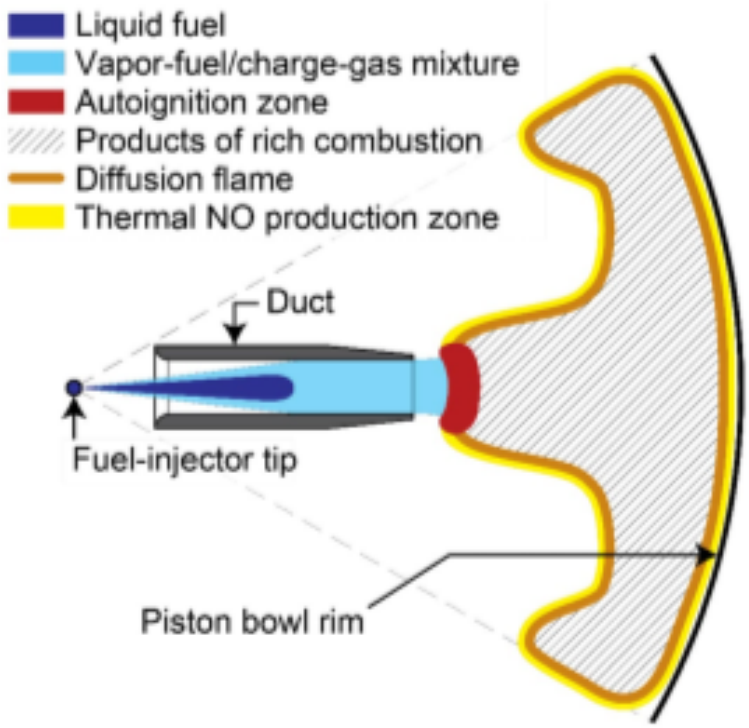

Figure 2.1: DFI technology and flame structure

2.4. Main Parameters Effect

As explained before, the introduction of the DFI technology is focused on the necessity of reducing the soot production with respect to the conventional combustion process, once the thermal and chemical boundary conditions have been fixed for both cases: the soot reduction is obtained by creating a more homogeneous air-fuel mixture, and this is made possible by delaying the auto-ignition phase thanks to the introduction of the duct after the injector nozzle. The overall effect is a strong reduction of soot and partially-oxidized products, like HC and CO, compared to the conventional diesel combustion process. On the other side, it is possible to notice an increase in the NO_x production compared to the reference case.

The experimental activity related to the DFI configuration is aimed to understand the process and the most influent aspects, so the air entrainment, the mixture formation, the combustion development, and the soot precursor formation. With this purpose, observing that the phenomena affecting the turbulent flame structure are quite sensitive to the duct geometry so that, by changing it and also the location of the duct in the vessel, the flame stabilization and mixture auto-ignition may change significantly. The DFI spray is analyzed by varying the following geometrical parameters:

- Duct diameter (D)
- Duct length (L)
- Stand-off distance (G)

Another important aspect able to classify the duct is its internal and external shape. Considering this aspect, the most common geometries are:

1. α-*Duct*: this is, in general, the simplest possible geometry being that a duct obtained by extrusion of length L of a circular crown, without any bevels at the inlet and at the outlet. This geometry is also called "Sharp Duct"
2. β-*Duct*: this is similar to the "sharp" geometry, with the addition of a full radius chamfer at the duct inlet and sharp edges at the outlet section. This geometry is also called "Blunt Duct"
3. γ-*Duct*: this is characterized by sharp edges at the inlet section of the duct, whereas at the outlet section, we can observe a taper, so that the wall thickness diameter is 0.5mm smaller than the inlet one, in order to minimize recirculation zones at this location. This geometry is also called "Tapered Duct"
4. δ-*Duct*: this can be considered a mixing between the shapes β and γ since it presents rounded edges at the inlet section and tapers at the outlet one.

In the picture reported hereafter, a brief sum up of the different geometries that can be experienced in the DFI technology is considered:

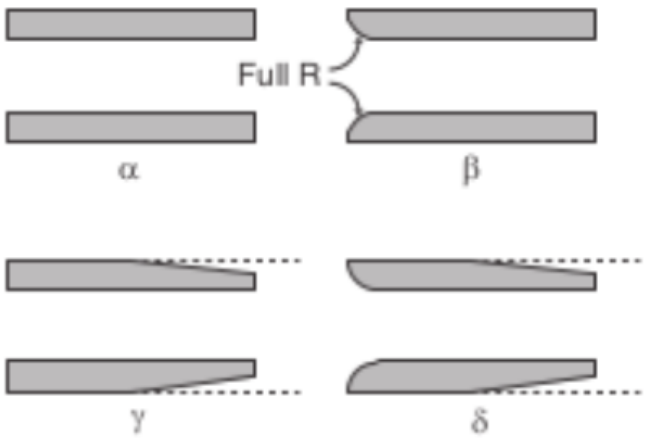

Figure 2.2: Common shapes for the DFI technology

In general, the kind of duct considered for the analysis is univocally defined by a combi-

nation of $D[mm]-L[mm]-G[mm]-ductshape$: for the thesis activity, the D2L16G3.9-δ geometry has been considered.

The geometry of the duct and its change can determine strong effects on the phenomena related to the diffusion flame, like its stabilization, measured in terms of *Lift-Off Length*, the auto-ignition delay with respect to the injection time, but also the soot production: all these aspects influence the combustion development so that the duct shape and geometry needs to be defined so to optimize each aspect of the whole process. Generally speaking, the following figure gives a brief scheme of the duct geometry, by pointing out all the previous quantities:

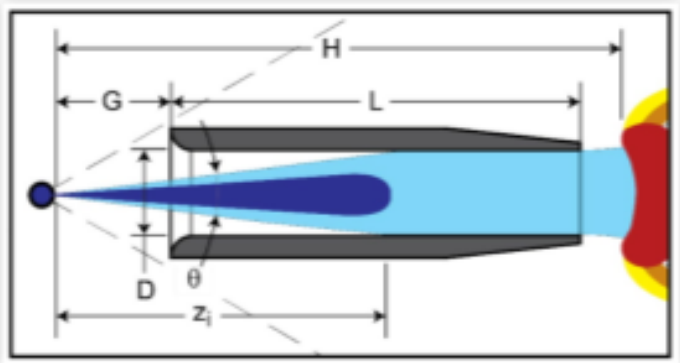

Figure 2.3: Duct Geometry

From the experimental campaign, Sandia showed how the combustion efficiency associated with the DFI technology is quite sensitive both to the duct geometry and also to the ambient thermal boundary conditions wherein the process is studied. Under particular configurations, it has been possible to observe a critical operating condition, called *failure mode* [3], that leads to a reduction of all benefits introduced with the DFI purpose. In this case, the reactive mixture auto-ignites inside the duct, always leading to an increase of the produced soot volume, going against the purpose of leaner combustion: the reasons for this problem are several, since the premature ignition may be associated to :

- a low thermal conductivity of the duct walls, typical of quartz with respect to steel
- high ambient thermal properties, that accelerate the reaction rate of the system, and thus its instability
- large diameters and stand-off distances. In this case, the air volume that can be introduced in the duct is larger, and the formation of a more homogeneous mixture is anticipated.

In the following sections, a qualitative analysis has been made according to the impact

each geometrical parameter has on varying the DFI combustion performances, assuming that the variation of a parameter implies the constancy of the others: starting from the experimental results achieved by Sandia related to ignition delay, flame lift-off and soot production, an explanation of the results has been given, by considering the case of an LTC (Low-Temperature Combustion). Moreover, the following pictures [16] offer a comparison between combustion techniques for different ambient oxygen concentrations:

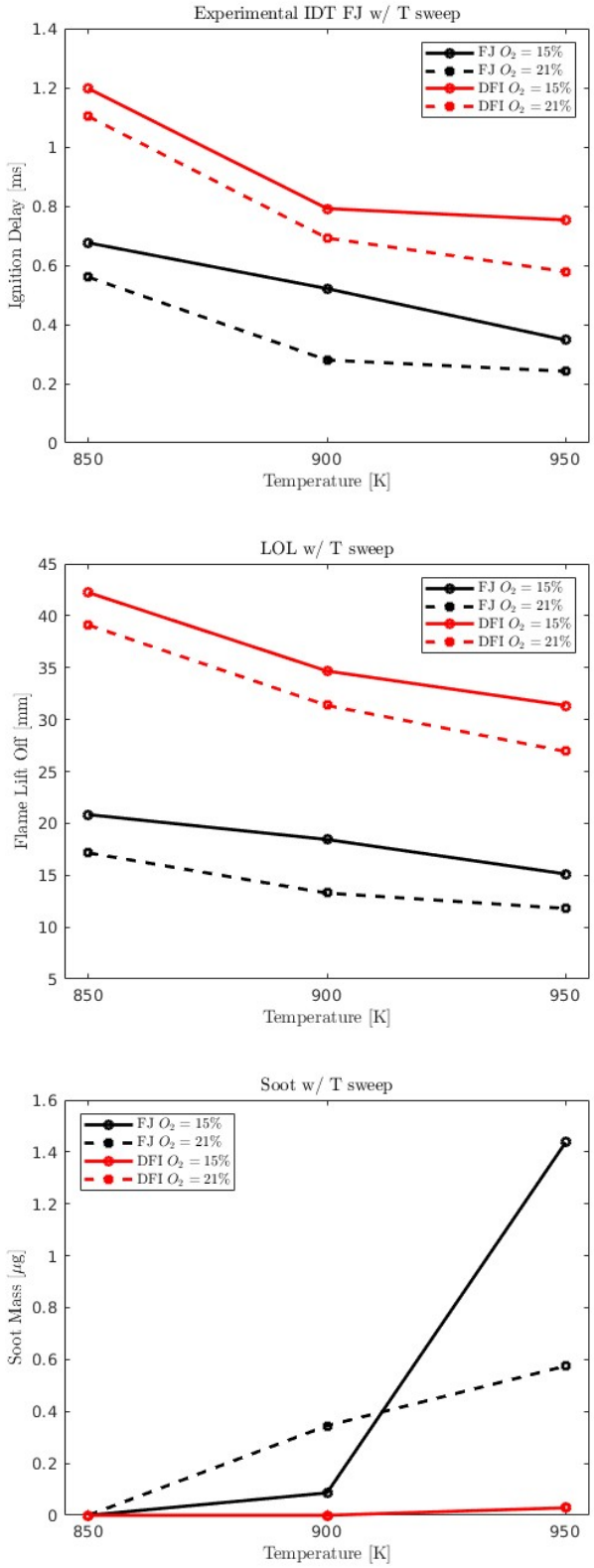

Figure 2.4: Representation of the most significant results achieved by Sandia during its experimental campaign: in these graphs, it is possible to observe, for both FJ and DFI, trends of ignition delay, flame lift-off, and soot production

2.4.1. Duct Diameter D

For what concerns the duct diameter it is possible to observe that, among the values Sandia experimentally analyzed by keeping the same length and stand-off distance, the optimal one that enables to achieve the maximum soot reduction is 2mm: in this condition, the amount of air present in the duct is the optimal one for determining the onset of the jet disruption due to turbulence, avoiding that the amount of released heat can trigger the mixture ignition inside the duct. This allows to observe an extended ignition delay, the subsequent formation of a mixture with a high level of homogeneity, and a subsequent tendency of producing the lowest amount of soot.
Generally speaking, by increasing the duct diameter with respect to the optimal value, it can be observed that the local counter-pressure acting against the fuel jet raises up since the amount of ambient air that can be dragged within the duct increases: in fact, for the same injected fuel mass, enlarging the duct diameter means to increase the air volume that can be entrapped in the duct. The higher counter-pressure acting against the jet penetration speeds up the dissipation of the turbulent kinetic energy due to viscous effects, accelerating the heat production within the duct. By summing up, increasing too much the duct diameter with respect to the 2mm value would mean considering a situation similar to the free spray injection, and all the benefits introduced with the *DFI* technology, in terms of the leaner mixture formation, would be neglected.
On the other side, considering smaller diameters compared to the optimal value means reducing the counter-pressure acting against the fuel jet propagation, since a smaller air volume can be dragged into the duct: this means that the viscous effects associated with the presence of boundary layers become smaller and smaller so that the fuel jet can maintain a higher turbulent kinetic energy level along the duct. Thus, it will be possible to notice higher equivalence ratio regions at the duct exit so that the richer mixture will lead to the formation of a larger amount of partially-oxidized compounds.
By summing, the duct diameter gives a measure of the air volume that can be entrapped inside the duct due to the fuel jet motion, so some consequences on the combustion performances can be appreciated by looking at the parameter variation. Starting from an optimal value of the diameter, deduced from experimental analysis, both lower and higher values can bring, respectively, to the introduction of a small air volume, with a consequent rich mixture formation, or the possibility of observing mixture auto-ignition inside the duct, and both these situations reduce the benefits introduced with the *DFI* technology.

2.4.2. Duct Length L

For what concerns the duct length it is possible to observe that, among the values Sandia experimentally analyzed by considering a 2mm duct diameter and a fixed value for the stand-off distance, the one that enables to achieve the optimal compromise among all the combustion performances is 16mm. In the situation of low-temperature combustion (from 850K to 950K), although the experimental campaign has allowed noticing that the soot production is independent from both the duct length and also the ambient oxygen concentration in the combustion vessel, the adoption of a 16mm duct length has brought some improvements on what regards the overall combustion efficiency, due to the ability to delay the auto-ignition phase and subsequently allowing the creation of a leaner mixture, compared to the free-spray case and to the other studied duct lengths.
By increasing the duct length with respect to the optimal value, the region where the fuel jet is affected by the presence of boundary layers gets extended, and so the higher counter-pressure acting against the fuel penetration determines a stronger turbulent kinetic energy dissipation: in this way, the jet is continuously disrupted into smaller and smaller droplets that mix with the surrounding air due to turbulence. Moreover, the dissipated kinetic energy is converted into heat that rapidly diffuses to raise up the local temperature, leading the mixture to be more unstable due to the fact that now a lower amount of energy is required to reach the auto-ignition phase. Under this scenario, there could be the possibility that the reactive mixture auto-ignites before reaching the duct exit, in particular for ambient temperatures generally higher than 1000K. Generally speaking, the maximum duct length has to be chosen according to the application field: for example, if the duct was mounted inside the combustion chamber of an engine, an excessive length would interfere with other components, like the piston bowl. On the other side, considering smaller lengths than the optimal one means reducing the positive effects due to the presence of the boundary layers and viscosity: in this case, the duct extension is limited and its influence on the fuel stream is poor and thus, it can maintain a higher momentum along the pipe; thus, at the exit section, it will be possible to observe a region where the equivalence ratio is high, leading to the production of a larger amount of soot.

2.4.3. Stand-Off Distance G

The stand-off distance represents the axial space in-between the inlet section of the duct and the injector nozzle: likely to what has been already observed for the duct length, this is a geometry-constrained parameter since it has to respect the limitations offered

by the actual size of the combustion environment. According to the Sandia experimental activity, by considering a duct diameter and length equal to 2mm and 16mm respectively, the value of stand-off distance that optimizes all the combustion performances is 3.9mm: it is possible to notice that, in the case of low-temperature combustion (from 850K to 950K), both soot production and ignition delay seem to be independent on the stand-off distance, when its value is in the range from 1mm to 4mm; in general, it is possible to sum up the analysis of Sandia by noticing that the soot production decreases with the axial gap between injector and duct. The choice of a 3.9mm stand-off distance is due to the necessity of optimizing the combustion efficiency, so that the auto-ignition phase has been delayed, allowing the formation of a leaner air-fuel mixture compared to the free-spray case. Of course, the optimization process has to include the duct-alignment procedure. By increasing the axial gap beyond 4mm, it is possible to observe an extension of the region wherein the fuel is affected by viscous and aerodynamic action of the surrounding air, before entering the duct. In this sense, the situation has some similarities to the free-spray case, so there is a large soot production compared to the DFI solution: thus, the presence of the duct could be irrelevant to the evolution of the combustion process. On the other hand, considering axial distances lower than the optimal one means reducing the initial air-fuel viscous and aerodynamic interactions, so that the jet kinetic energy is lower affected by the surrounding environment: this means that, at the exit section of the duct, a high equivalence ratio region can be observed, that leads to an enhanced soot formation.

2.4.4. Duct Shape

Generally, the duct shapes that are commonly tested and validated are 4: α, β, γ, δ. As said before, these configurations are different in terms of the geometry that describes both the inlet and outlet sections, and this limitation has some consequences on the combustion performances and DFI efficiency. According to Sandia's experimental campaign [30], two different analyses are conducted: the first enables to observe of the impact the inlet geometry has on combustion, in terms of soot production and flame stabilization, so that there is a comparison between geometries α-β and between γ-δ; the other method shows the way combustion is affected by the geometry of the duct outlet sections, by considering the eventual presence of taper. In this sense, it is possible to observe α-γ and β-δ comparisons.

Looking at the impact of the inlet section, it is possible to notice that the effects on both mixture auto-ignition and flame stabilization are negligible. By considering a rounded-edge inlet section, the amount of air that can be introduced within the duct due to the

fuel jet inertia is higher so that it is possible to achieve a leaner mixture. Thus, the risk of observing large amounts of partially-oxidized compounds is limited, reducing soot production.
Looking at the impact of the outlet section, it is possible to appreciate that the introduction of the taper enables to reduce the risk of re-circulation that might encourage anchoring of combustion to the exit of the duct, by limiting its beneficial effects. In fact, by reducing the exit cross-section, the counter-pressure acting against the fuel jet is reduced, so that it can maintain acceptable inertia for flowing away from the duct. Generally speaking, variation of the exit section does not bring any evident variation in combustion performances.
By resuming, the adoption of a rounded-edge inlet section is preferable for the abatement of the soot production, because of the larger amount of air that can be introduced within the duct, and the subsequent creation of a leaner mixture; whereas the adoption of a tapered outlet section does not bring so evident benefits with respect to the conventional case, but it enables to avoid auto-ignition of the mixture within the duct or in the closeness of the outlet section. The $\delta - duct$ shape is the best one for reducing soot production.

3 | Modelling Fundamentals

To analyze the way the duct can affect the injection and the subsequent combustion process for the case of a constant-pressure combustion vessel, the usage of *OpenFOAM* has been adopted, a C++ software aimed to model and solve CFD problems: in particular, it is able to use numerical methods, like the finite volume approach, to discretize and solve the equations that govern a generic fluid system, including the Navier-Stokes ones: in this way, it is possible to approximately find a solution from a numerical point of view, limiting the computational effort that would be required by adopting an analytical process.
Usually, when Computation Fluid Dynamics (CFD) problems are evaluated, the attention is focused on complex fluid flows that are affected by turbulence and viscosity, heat transfer, and chemical reactions, and all those aspects strongly influence the way the fluid system moves and evolves in space and time. As introduced before, the behavior of the fluid flow is accurately described by the Navier-Stokes equations, a framework of PDEs used to express, for each point of the feasible domain, the conservation equations applied to the system and, generally speaking, they can be classified into:

- Continuity Equation
- Momentum Equation

For a better understanding of the conservation laws for a fluid system, it is possible to analyze the way a generic flow extensive property X varies in time and space inside the control volume. To do that, a quite useful tool is the Reynolds Transport Theorem that, from an analytical point of view, can be expressed as:

$$\frac{d}{dt}\int_{\Omega} X(x,t)\,d\Omega = \int_{\Omega} \frac{\partial\, X(x,t)}{\partial t}\,d\Omega + \int_{S} X(x,t)(\vec{V}\cdot\vec{n})\,dS \tag{3.1}$$

where:

- $\boldsymbol{X(x,t)}$ is the flow extensive property of interest (e.g., velocity, pressure, temperature, etc.) evaluated in space and time: a property is extensive when it is defined according to the size of the chosen control volume

- $\boldsymbol{\Omega}$ is the control volume, which can be any arbitrary region of the feasible analysis domain
- $\boldsymbol{S}$ is the boundary surface of the control volume
- $\boldsymbol{\vec{V}}$ is the velocity of the fluid at the boundary
- $\boldsymbol{\vec{n}}$ is the outward unit normal vector to the surface S

The Reynolds theorem can also be expressed in differential form by introducing the Gauss theorem, which enables to express the flux of the property X through the control volume boundaries by using the concept of spatial gradient:

$$\int_S X(x,t)(\vec{V}\cdot\vec{n})\,dS = \int_\Omega \nabla\cdot\ (X(x,t)\vec{V})\,d\Omega \tag{3.2}$$

In particular, once the reference system has been defined, the gradient of a generic property X shows the rate of change of that parameter along each principal direction of the domain.
By doing some mathematical steps, the differential definition for the Transport theorem is hereafter reported:

$$\frac{d}{dt}\int_\Omega X(x,t)\,d\Omega = \int_\Omega (\frac{\partial\ X(x,t)}{\partial t} + \nabla\cdot\ (X(x,t)\vec{V}))\,d\Omega \tag{3.3}$$

The Reynolds theorem states that the absolute rate of change of a fluid property X inside the control volume is mainly due to 2 different contributions:

1. by considering the flow is not moving, there is the possibility that a given flow property X is changing in time
2. by considering the flow is moving at a given speed, the flow property X can change inside the control volume due to the fact that mass flow is crossing the boundaries

Once the Reynolds Theorem and its benefits on the conservation principle have been introduced, the analysis can move deeper into detail in distinguishing between the 2 Navier-Stokes laws.

3.1. Conservation Equations

As said before, the conservation principle for a generic fluid system can be accurately expressed by the Navier-Stokes equations, which are used to express how a generic property X of the flow changes in time and space within the control volume, by taking into

account different complex fluid-dynamic patterns, like turbulence and viscosity, and thermodynamic conditions, just like the heat exchange and the presence of chemical reactions (i.e. combustion). The fact a turbulent environment has been introduced for the CFD analysis leads to describe the conservation laws by using the Reynolds Averaged Navier-Stokes (RANS) conditions: these are time-averaged conservation equations that are able to properly evaluate the global behavior of a turbulent fluid system, by giving an approximate solution to the actual Navier-Stokes laws. The innovation is related to the Reynolds decomposition of the fluid extensive property: since the turbulence introduces a sort of instability for what concern the fluid-dynamic behavior, a generic flow extensive property $X(x,t)$ can be separated into 2 main components:

$$X(x,t) = \bar{X}(x) + X^{'}(x,t) \tag{3.4}$$

where the first contribution is referred to the time-averaged property:

$$\bar{X} = \frac{1}{T}\int_0^T X(x,t)\,dt \tag{3.5}$$

the second one takes into account the fluctuation of the same property in space and time due to the effect of the uncertainty associated with turbulence: the effect also depends on the size of eddies describing the pattern of the system. This way of conservation principle resolution is reported in the OpenFOAM environment as RAS (*Reynolds Averaged Simulations*). Hereafter, a brief explanation for each law has been done

3.1.1. Mass Conservation

By considering a specific control volume for the analysis of the flow, this condition expresses the mass conservation principle inside the domain. It states that the mass rate of change in a fluid volume is equal to the net mass flow rate into or out of that space element. In other words, the continuity equation describes how the mass flow is conserved as it flows through a given region of space. By introducing the Reynolds theorem, the Continuity equation can be expressed as:

$$\frac{dm}{dt} = \frac{d}{dt}\int_\Omega \rho\,d\Omega = \int_\Omega \frac{\partial \rho}{\partial t}\,d\Omega + \int_S \rho(\vec{V}\cdot\vec{n})\,dS = 0 \tag{3.6}$$

or, in differential form:

$$\frac{dm}{dt} = \frac{d}{dt}\int_\Omega \rho\,d\Omega = \int_\Omega (\frac{\partial \rho}{\partial t} + \nabla\cdot\ (\rho\vec{V}))\,d\Omega = 0 \tag{3.7}$$

And so, after simplifying all the terms, it is obtained the actual definition of Continuity for a fluid system:

$$\frac{\partial \rho}{\partial t} + \nabla \cdot (\rho \vec{V}) = 0, \tag{3.8}$$

This equation can be in 2 different ways according to the fact the fluid density can change or not in time and space. Referring to this condition, it is possible to distinguish between:

- Hydraulic Applications: in this case, the density is assumed to be constant at each point of the system and no variation of the extensive property in time can be noticed. The pressure/temperature variation does not affect the fluid density:

$$\frac{\partial \rho}{\partial t} = 0 \tag{3.9}$$

- Thermodynamic Applications: in this case, the behavior of the working fluid can be assumed to be similar to a perfect gas, and thus the time variation of pressure/temperature will lead to a time change for the density according to the law:

$$pV = RT \tag{3.10}$$

3.1.2. Momentum Conservation

By considering a specific control volume for the analysis of the flow, this condition expresses the momentum conservation principle inside the domain. The momentum corresponds to the quantity of motion possessed by a fluid system when it moves at a certain speed along a specific spatial direction. From a mathematical point of view, the flow momentum can be expressed as:

$$\vec{q} = m\vec{V} \tag{3.11}$$

It is quite useful to appreciate the relationship existing between the flow momentum and the set of external forces acting on the control volume, which is nothing but the 2nd Newton dynamic:

$$\frac{d\vec{q}}{dt} = m\frac{d\vec{V}}{dt} = m\vec{a} = \vec{F} \tag{3.12}$$

The set of forces acting on the fluid system can be distinguished into volume (i.e. weight) and surface ones: these are the most critical in the system equilibrium condition. Acting on the surface of the control volume, the external forces generate a state of stress that can be summed up into normal and tangential components. Both of them determine a momentum variation in the flow: otherwise if no external forces are applied to the control

volume, the momentum keeps constant in space and time. Thus, by introducing the Reynolds theorem, and by neglecting the volume forces, the Momentum conservation law can be expressed in differential form as:

$$\frac{d(m\vec{V})}{dt} = \int_{\Omega} \rho \frac{d\vec{V}}{dt}\, d\Omega = \int_{\Omega} \rho(\frac{\partial \vec{V}}{\partial t} + \vec{V} \cdot \nabla \vec{V})\, d\Omega = \int_{\Omega} (\nabla \cdot \bar{\tau} - \nabla\ p)\, d\Omega \tag{3.13}$$

And thus, by re-arranging all the terms, it is possible to find the formulation for the 2nd Navier-Stokes equation:

$$\rho(\frac{\partial \vec{V}}{\partial t} + \vec{V} \cdot \nabla \vec{V}) = \nabla \cdot \bar{\tau} - \nabla\ p \tag{3.14}$$

3.1.3. Energy Conservation

Apart from the Navier-Stokes equations, an additional conservation law that is very useful for describing a generic transient system is the Energy conservation principle, which states that all the energy that enters the control volume boundaries is not dissipated, but it is used to vary the total energy of the system. From an analytical perspective, the total energy of a generic dynamic system is expressed by 3 different contributions:

- Internal Energy, $\boldsymbol{U}$: it is a kind of energy that can be evaluated on a microscale, and it is mainly associated with the particle's motion. It depends on the chemical nature of the considered element and it is very dependent on the instantaneous temperature of the system
- Kinetic Energy, $\boldsymbol{K}$: it is a kind of energy a particular system of total mass m has when it moves at a certain speed. Fixing the mass, the faster the system moves, the higher will be the associated kinetic energy
- Potential Energy, $\boldsymbol{G}$: it is a kind of energy associated with the system when it is characterized by steady-state.

By considering the previous quantities, the total energy, $\boldsymbol{E}$ of a generic transient system can be defined as:

$$E = \int_{\Omega} e\rho\, d\Omega = U + K + G \tag{3.15}$$

where $\boldsymbol{e}$ corresponds to the specific total energy level associated with an infinitesimal mass of the system.
The fluid system may undergo some variation due to the influence of external sources that transfer energy through its control volume's boundaries. The main energy fluxes that can be introduced are:

- Mechanical Power: this can be divided into 2 different contributions, the first associated with the internal volume, the latter to the boundaries. By considering only the second term, this corresponds to the power that has to be provided to the system for changing its total energy. This concept can be better explained by re-introducing the flow motion inside a pipe: a fraction of the mechanical power is introduced for changing the flow momentum between the inlet and outlet sections; the remaining part is spent as friction against the physical walls.
- Thermal Power: this is associated with the presence of some heat sources affecting either the control volume or its boundaries, or it can be related to the presence of some chemical reactions that verify inside the system (i.e. combustion)

In conclusion, the energy conservation law can be re-written in a differential way by introducing the Reynolds theorem as:

$$\frac{\partial(\rho h_t)}{\partial t} + \nabla \cdot (\rho h_t \vec{V}) - \frac{\partial p}{\partial t} = -\nabla \cdot \vec{q} + \nabla \cdot (\bar{\tau} \cdot \vec{V}) \tag{3.16}$$

where $\boldsymbol{h_t}$ is the specific total enthalpy, expressed as

$$h_t = e + \frac{p}{\rho} \tag{3.17}$$

3.2. Numerical Setup

Once the main conservation laws that allow studying the behavior of a generic fluid system have been introduced, the attention is focused on the way OpenFOAM can use all these informations to set and solve the CFD case. Some considerations have been made for creating a numerical model able to reproduce in the best way the actual process and to point out the main performances associated with the turbulent combustion, just as the flame generation and stabilization, and the soot production during the process. The software framework is based on a set of libraries that include the basic data structures, linear algebraic tools, and numerical methods used to solve fluid flow equations, so there is the possibility to model and simulate different complex fluid-dynamic cases. OpenFOAM also provides a variety of utilities that can be used to pre-process and post-process simulation results, including tools for mesh generation, visualization, and data analysis.
The creation of the numerical model has been determined by the same dictionaries and utilities, which can be grouped into 3 different folders:

1. *0*

2. *system*
3. *constant*

that contain all the useful and necessary informations relative to the analysis domain, the kind of geometries the fuel interacts with, and the kind of working fluid taken into account for the CFD model. Hereafter, a brief explanation of these folders and their utility in the case setup will be given.

3.2.1. 0

The folder *0* contains all the informations related to the initial thermodynamic conditions for the environment and the initial state of the working fluid. Since the activity is based on the fuel injection study inside a vessel, the notions here listed are referred to the thermodynamic state inside the vessel (i.e. pressure and temperature), but also the initial chemical composition inside it (i.e. oxygen percentage inside the chamber, initial soot concentration, air chemical structure ...).
By resuming, the folder *0* sets all the boundary conditions necessary to set up the CFD simulation. Thus, by considering a constant density of 22.8 $\frac{kg}{m^3}$, there is the possibility of setting the initial temperature and pressure inside the vessel, by considering that, at the start of injection, the temperature of the unburned mixture T_u is the same of the absolute temperature T. The pressure is assumed to be constant in each point of the computational domain, whereas the temperature value on both domain walls and duct is different from the absolute one, and it has been set to 500K and 300K, respectively.

	density $\frac{kg}{m^3}$	**walls T [K]**	**duct T [K]**
value	22.8	500	300

Table 3.1: Initial thermodynamic boundaries

3.2.2. System

The folder *system* contains all the informations related to the simulation setup (application field, time duration, ...) and the different kinds of solvers employed for the CFD resolution with the associated tolerances. In this directory, some interesting dictionaries and files can be appreciated, like:

- *fvSolution*: this file specifies the set of different solvers used to work out the conservation equations for the fluid system, and also the tolerance level and the maximum number of iterations so to reach the maximum precision.
- *decomposeParDict*: is a dictionary used for parallel processing and specifies how the simulation domain should be partitioned into multiple subdomains for parallel processing.
- *controlDict*: is a dictionary wherein we can find some information related to the simulation process, like its overall duration and the time-step we can apply. This last parameter impacts the final results quality in terms of accuracy, but very small time steps will bring to a very high computational effort to run the CFD case, so, similarly to what was previously discussed for the mesh generation, we need to define a trade-off between the different necessities.

In particular, the injection duration has been set to 4ms, and the simulation time step has been considered as fixed and equal to 1e-8s. Another aspect that has to be considered is the tolerance of the generic CFD result, which has been set to 1e-16 for achieving a quite good accuracy level, and also 3 correctors were considered. In particular, the correctors enable to accelerate the stabilization of the CFD solution:

	endTime [s]	**timestep [s]**	**tolerances []**	**Correctors []**
value	0.004	1e-8	1e-16	3

Table 3.2: Computational boundaries

3.2.3. Constant

The folder *constant* contains all the informations referring to both the analysis domain and the kind of process that is going to be observed from the simulation. Since both injection and subsequent combustion processes are considered in this project, inside this directory it is possible to find some files and dictionaries used to model the way fuel spray evolves in space and time, by considering turbulent and aerodynamic interaction with the surrounding air for the mixture generation. All these aspects also depend on the kind of chosen injection system and the associated operating performances.
In this sense, a breakup model, with the respective limitations, has been considered for describing the fuel jet atomization into droplets; also a heat transfer correlation is

evaluated, so that it is possible to observe the boundary conditions associated with the energy exchange between fuel droplets and air for the onset of the constant-pressure auto-ignition process. For describing the turbulent pattern inside the combustion vessel, the $k - \varepsilon$ model has been considered, whereas the soot production has been modeled by introducing the *Leung-Lindstedt-Jones model*. Moreover, the composition space has been limited between 0.01 and 5.4.

	Model
Breakup	KHRT
Heat Transfer	Ranz-Marshall
Turbulence	$k - \varepsilon$
Collision	*none*
Drag	*standard*
Evaporation	*standard*
Soot	Leung-Lindstedt-Jones

Table 3.3: Models for the analysis of the combustion process

For each of these aspects, an accurate description is offered in the following sections.

Injection System

The fuel is introduced inside the combustion vessel through an injector, whose properties are collected in the file *injectorProperties*: it gives a brief and accurate description of the injection system considered for the numerical model, pointing out some information related to its geometry and orientation in the reference system. Some interesting notions that can be appreciated are:

- the position with respect to the vessel and details about the injection trajectory (spray angle, direction)
- the geometry in terms of L/D ratio and discharge coefficient
- the references to the provided injection law.

The injection law plays a very important role in the evaluation of combustion performances since it gives an idea of the overall amount of fuel mass introduced inside the vessel and

how it gets distributed over time. The injection law has been computed thanks to an injection rate generator proposed by the ECN database [17]: it's possible to appreciate that the injection trend depends on many different parameters, both related to the injector geometry, its operating conditions (injection pressure), and the thermodynamic pattern of the chamber (back pressure, that represents the resistance against the fuel propagation inside the vessel); moreover, also the fuel density and the injection duration have to be considered. The result obtained with this virtual generator is reported in the *sprayA4.txt* file, and hereafter the Rate Of Injection (ROI) adopted for the CFD simulations in this thesis activity is reported:

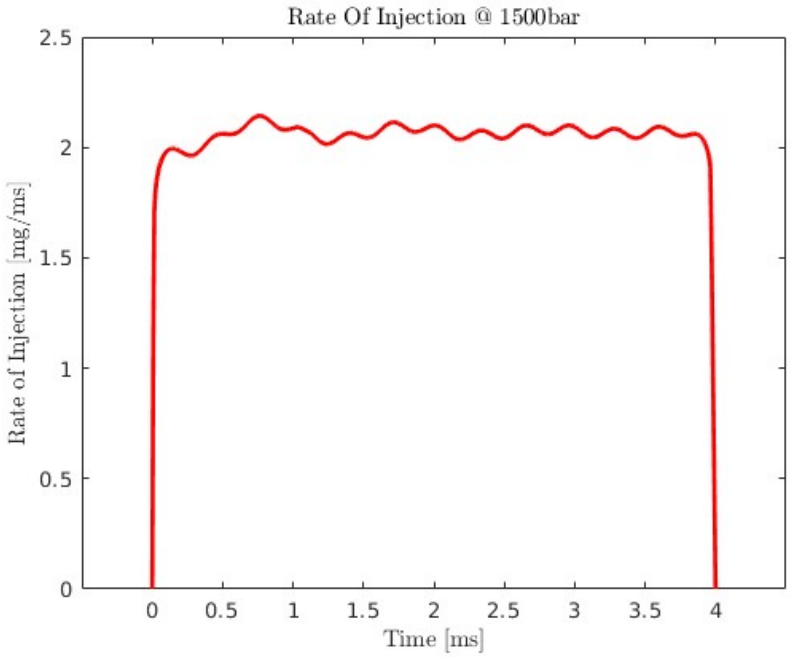

Figure 3.1: ROI profile adopted for the CFD simulations

It's useful to observe that the area below the injection rate curve corresponds to the overall fuel mass injected inside the vessel during the whole duration of the process, that in the present activity has been conventionally set to 4 ms, so to have a complete and exhaustive explanation of all the phenomena occurring during the main case.

Turbulence Model

Turbulence is a common fluid-dynamic phenomenon that, differently from the laminar regime, introduces a sort of continuous instability inside the flow, in the sense that its properties are affected by periodical fluctuations determined by the presence of randomly dispersed vortexes characterized by different sizes so that oscillations are superimposed to

the mean flow properties. In particular, the fluctuations are directly related to the size of the turbulent eddies [18] and, in this way, a possible classification can be defined among 3 different scales, that differ from the point of view of the characteristic length and time:

1. *Integral*
2. *Taylor microscale*
3. *Kolmogorov scale*

The Taylor microscale is usually considered the threshold with respect to which the turbulent vortexes may play a crucial role in the flow regime. Conventionally, the larger scales are not affected at all by the turbulence, whereas the smaller ones are characterized by the presence of high dissipations induced by eddies so the heat production is quite relevant. Generally speaking, the energy is transferred from the largest scale to the Kolmogorov one, which is the most dissipative one, since the viscous effects are predominant (Re is very low). Finally, the turbulent kinetic energy associated with the flow is completely converted into heat. Hereafter, a brief classification of the turbulent scales is represented:

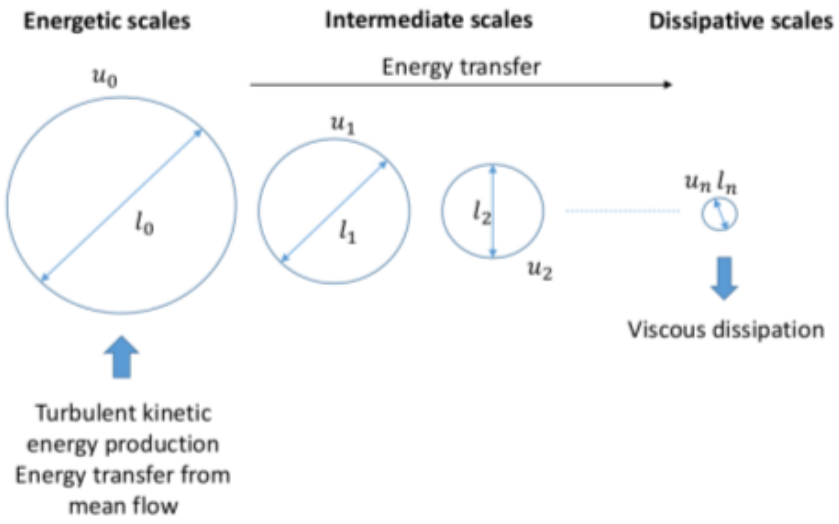

Figure 3.2: Energy transfer through different turbulent scales

As observed by most engine applications, a turbulent environment wherein the combustion process occurs has been considered, due to the fact that turbulence enhances the heat propagation and diffusion through the fuel, so to speed up the chemical process. In particular, to maximize the combustion performances, the turbulence generation has to be optimized and this may lead to a re-configuration of the geometry wherein the phenomenon occurs: by considering Sandia experimental gear, the turbulence is provided by

a fan localized within the chamber. From a numerical point of view, there are different ways to solve the conservation equations in a turbulent environment:

- *Direct Numerical Simulation (DNS)*: the conservation equations are solved by considering the smallest turbulent scale, and thus the Kolmogorov one. So, the grid has to be fine enough to figure out the smallest length scale: on one side, this approach is the most accurate in terms of evaluation of both turbulent kinetic energy dissipations and heat production, but on the other side the required computational effort is very high.
- *Large Eddy Simulation (LES)*: only the largest scale are explicitly solved, whereas the smallest ones are modeled by semi-empirical techniques.
- *Reynolds Averaged Navier-Stokes (RANS)*: in this case, all the turbulent scales are considered to have a complete overview of the flow system behavior. To do that, a statistical approach is considered, so that a generic flow property can be described by means of a mean value and a term considering all the fluctuations around it, according to the Reynolds decomposition. This approach is the most used since it is less demanding in terms of computational efforts. In the RANS model, the turbulent behavior of the environment is represented by the viscous shear stress μ_t and it is described as:

$$\mu_t = C_\mu \rho u l \tag{3.18}$$

  where u is the turbulent characteristic velocity field, l is the turbulent length scale and C_μ is a characteristic turbulence constant.

In this thesis activity, the model considered for simulating the presence of turbulence inside the combustion vessel is the $k-\epsilon$ [19], and it is completely described inside the file *momentumTransport*: this model is based on the resolution of 2 different PDFs, one associated to the turbulent kinetic energy and the other to its dissipation rate. In particular, these 2 quantities are defined as:

$$k = \frac{1}{2}(\bar{V_1'}^2 + \bar{V_2'}^2 + \bar{V_3'}^2) \tag{3.19}$$

$$\epsilon = \frac{k^{\frac{3}{2}}}{l} \tag{3.20}$$

$$\mu_t = C_\mu \rho \frac{k^2}{\epsilon} \tag{3.21}$$

In particular, the 2 equations of the model in the given reference system are:

$$\frac{\partial k}{\partial t} + \bar{V_i'}\frac{\partial k}{\partial x_i} = \frac{\partial}{\partial x_i}(\frac{\mu_t}{\rho C_k}\frac{\partial k}{\partial x_i}) + \frac{\mu_t}{\rho}\frac{\partial \bar{V_j'}}{\partial x_i}(\frac{\partial \bar{V_j'}}{\partial x_i}\frac{\partial \bar{V_i'}}{\partial x_j}) - \epsilon \tag{3.22}$$

$$\frac{\partial \epsilon}{\partial t} + \bar{V_i'}\frac{\partial \epsilon}{\partial x_i} = \frac{\partial}{\partial x_i}(\frac{\mu_t}{\rho C_\epsilon}\frac{\partial \epsilon}{\partial x_i}) + \frac{\mu_t}{\rho}\frac{\partial \bar{V_j'}}{\partial x_i}C_1\frac{\epsilon}{k}(\frac{\partial \bar{V_j'}}{\partial x_i}\frac{\partial \bar{V_i'}}{\partial x_j}) - C_2\frac{\epsilon^2}{k} \tag{3.23}$$

where $C_\mu, C_\epsilon, C_k, C_1, C_2$ are constants whose values depend on the problem, but generally they are found through data fitting processes, and in the current project, C_1 is set to 1.5. The $k-\epsilon$ model enables to obtain accurate results far away from the walls, where the adverse pressure gradient acting on the flow is quite small, but it might not be the best model to analyze problems in the closeness of physical surfaces, where the adverse pressure gradients are relevant, and thus the impact of turbulent viscosity. This is why this is the simplest way to numerically model the turbulence inside a system.

Spray Modelling

One last aspect that has to be considered is the generation of the fuel jet and the way it propagates and diffuses inside the combustion chamber: all these aspects are collected inside the file *sprayCloudProperties*, which gives informations on the way the fuel spray evolves in space and time from the injection point, once the location of this point and the flow direction have been defined. For analyzing the way the fuel jet evolves over time, it needs to be considered that the fuel is introduced inside the system with certain inertia mainly dependent on the injection pressure, so the higher this quantity, the higher the flow stability. In terms of jet shape, this means to have a smaller cone angle, and thus higher values of mixture fraction at a given distance from the injection point. On the other side, the air present inside the combustion chamber plays as an active resistance against the flow penetration, and the level of counter-pressure mainly depends on the initial thermal boundary conditions. The presence of turbulent eddies leads to a continuous division of the fuel jet into smaller and smaller particles: this process is called *jet breakup* and it is necessary for the non-premixed combustion since we need to create a mixture with a certain chemical composition so that it is able to auto-ignite. In this project, the KHRT breakup model [20] has been introduced.

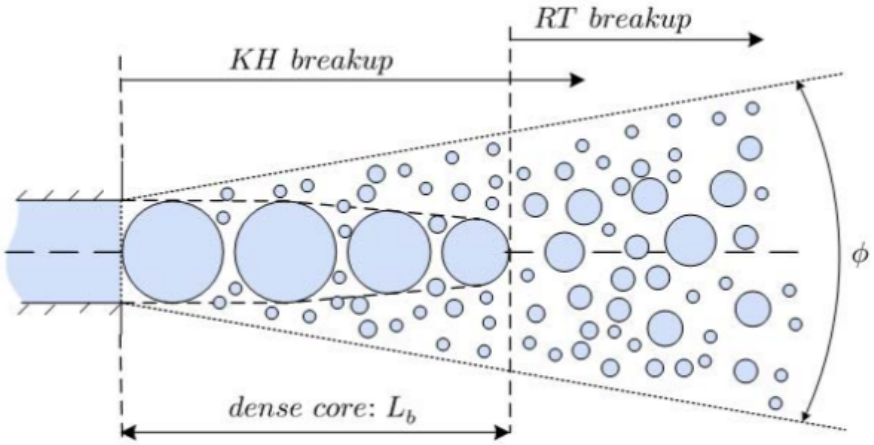

Figure 3.3: Description of the KHRT breakup model

From a physical point of view, the jet breakup is a consequence of the turbulent kinetic energy dissipation induced by the vortexes and thus, since the flow inertia is lowering, this means that the fuel is more affected by the external action of the turbulent air that can be summed up, in particular, with the aerodynamic forces acting on the jet surfaces (i.e. drag and viscous stresses), but also the turbulent pattern that can be observed inside the jet due to different sources of instability (i.e. eddies). Although the influence of the turbulence, it is possible to point out a specific region of the fuel jet, the *breakup length,* L_b, as the distance from the injection nozzle where the fuel jet can be considered as a continuum, and thus not disturbed by the presence of turbulence and aerodynamic forces. Generally speaking, the fuel breakup can be divided into 2 phases:

1. *PRIMARY BREAKUP*: the fuel is injected inside an environment characterized by a smaller pressure than the injection one. The very high-velocity gradient due to pressure difference may induce the presence of cavitation, which promotes and accelerates the atomization process. This first phase is mainly due to the injection pressure and the thermodynamic state of the combustion chamber: moreover, the size and geometry of the injector are responsible for the breakup. This first phase is completely described by the Re number, which gives the ratio between inertial and viscous forces.

2. *SECONDARY BREAKUP*: far away from the injection nozzle, the air mass entrained inside the fuel jet increases and enhances the turbulence, by means of further eddies that contribute to a secondary breakup. This phenomenon is completely described by the Weber number, which gives the ratio between the inertia forces (relative motion between 2 layers of different fluid systems) and the surface tension

of the fluid.

For accurately describing the whole process of disgregation for the fuel jet when it is introduced inside the combustion chamber, the KHRT breakup model joints 2 different instabilities to explain all the different causes of perturbation that affect the process and constitute the preamble to the effective combustion:

- *KEVIN-HELMOLTZ INSTABILITY*: is a phenomenon of dynamic instability that verifies every time there is a relative motion between 2 different fluid systems and the shear stresses induced at the interface by velocity and pressure gradients (viscosity effects) are usually greater than the maximum fluid surface tension. The KH principle observes that, when a cylindrical fluid jet of diameter d_0 penetrates a stationary incompressible gas at a certain speed u_{rel}, it is possible to appreciate the presence of sinusoidal waves acting onto the jet surface, determining the onset of pressure fluctuations and thus leading to a perturbed state. In particular, when the wave oscillating frequency ω induces a state of stress that equalizes the maximum surface tension at the frequency Ω_{KH}, the jet gets divided into new droplets.

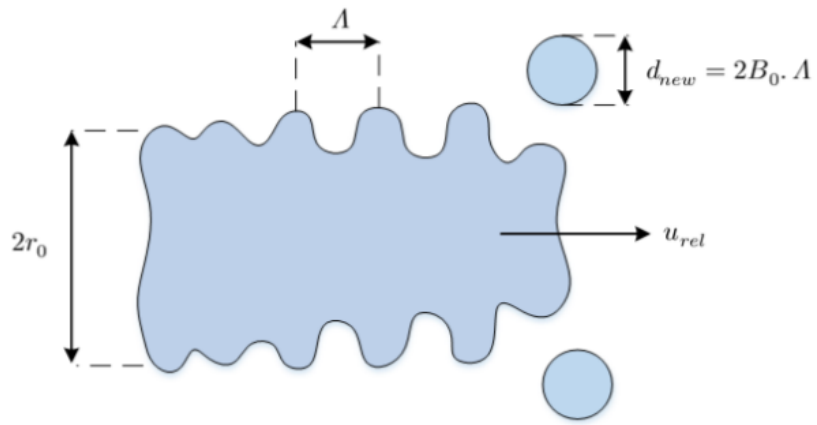

Figure 3.4: Graphical representation of the KH instability

Thus, starting from an initial size r of the jet, the new size r_{new} of the droplets is determined by looking at the following equation:

$$r_{new} = B_0 \Lambda_{KH} \tag{3.24}$$

where B_0 is a model constant, and Λ_{KH} is the critical wavelength we can observe on the jet surface before the jet gets atomized into new parcels, and this quantity is linked to the critical frequency Ω_{KH} through a dispersion equation, obtained by adopting curve fitting methods. Thus, the critical wave frequency and the associated

wavelength are expressed by the following correlations:

$$\Omega_{KH} = \frac{0.34 + 0.38We_g^{1.5}}{(1+Oh)(1+1.4Ta^{0.6})}\sqrt{\frac{\sigma}{\rho_f r^3}} \tag{3.25a}$$

$$\Lambda_{KH} = \frac{9.02r(1+0.45\sqrt{Oh})(1+0.4Ta^{0.7})}{(1+0.865We_g^{1.67})^{0.6}} \tag{3.25b}$$

where:

- We_g is the Weber number and it is an adimensional parameter used in fluid-dynamics problems every time there is an interface between 2 different fluids, especially for multi-phase ones. It gives a measure of the relationship existing between the flow inertia and its surface tension, σ, and it is defined by the following formula:

$$We_g = \frac{\rho_g r u_{rel}^2}{\sigma} \tag{3.26}$$

- Re_l is the Reynolds number and it is an adimensional parameter used to observe the inertia associated with a generic flow stream that moves at a certain speed. It gives a measure of the relationship existing between the flow kinetic energy and the viscous forces that obstacle its propagation in space and time, and it is defined by the following formula:

$$Re_l = \frac{\rho_l r u_{rel}}{\mu} \tag{3.27}$$

- Oh is the Ohnesorge number and it is an adimensional parameter used to relate the viscous forces to the inertial and surface tension ones. It is defined as:

$$Oh = \frac{\sqrt{We_l}}{Re_l} \tag{3.28}$$

- Ta is the Taylor number and it is defined as:

$$Ta = Oh\sqrt{We_g} \tag{3.29}$$

As the droplet penetrates the incompressible gas, the state of stress acting onto its surface follows to increase, so that it continuously loses mass and the rate of

shrinking can be described as:

$$\frac{dr}{dt} = \frac{r - r_{new}}{\tau_{bu}} \tag{3.30}$$

where τ_{bu} is the *breakup time*, defined as:

$$\tau_{bu} = \frac{3.788 B_1 r}{\Omega_{KH} \Lambda_{KH}} \tag{3.31}$$

B_1 is a model constant that takes into account the effects of both nozzle geometry and perturbations like turbulence and cavitation that may occur inside the injector: in general, this parameter assumes values within the range from 1.73 to 60. Thus, the KH model is used to predict the initial break-up of the intact liquid core.

- *RAYLEIGH-TAYLOR INSTABILITY*: it is a phenomenon of static and subsequent dynamic instability that occurs at the interface of 2 fluid systems characterized by different densities in case of acceleration or deceleration normal to this interface. When the fuel droplet moves with respect to the air at a certain speed u_{rel}, the presence of aerodynamic and viscous forces creates a state of stress in the back side of the drop, under the form of sinusoidal waves: in this sense, we experience a pressure gradient that opposes the density gradient. In particular, the set of aerodynamic forces that affect the droplet and the subsequent induced deceleration can be expressed as:

$$F_{aero} = \pi r^2 C_D \frac{\rho_g u_{rel}^2}{2} \tag{3.32a}$$

$$a = \frac{3}{8} C_D \frac{\rho_g u_{rel}^2}{\rho_l r} \tag{3.32b}$$

where C_D is the drag coefficient acting on the droplet due to the presence of turbulent and viscous air surrounding it. In the same way as the KH model, the RT instability is described as a sinusoidal wave characterized by wavelength and oscillating frequency, respectively defined as:

$$\Lambda_{RT} = C_3 2\pi \sqrt{\frac{3\sigma}{a(\rho_l - \rho_g)}} \tag{3.33a}$$

$$\Omega_{RT} = \sqrt{\frac{2}{3\sqrt{3\sigma}} \frac{[a(\rho_l - \rho_g)]^{1.5}}{\rho_l + \rho_g}} \tag{3.33b}$$

The wavelength is compared to the droplet diameter to assess whether the breakup occurs or not: until the perturbation wavelength is smaller than the droplet diameter, the instability due to aerodynamic and viscous forces leads to the breakup into smaller and smaller drops. In this case, an important parameter for controlling the breakup is C_3, which is quite similar to the parameter B_1 for the KH model: by increasing C_3, the wavelength increases too, and thus the breakup trend is limited. Usually, this variable assumes values contained between 1 and 5.33. In particular, when the wave oscillating frequency ω induces a state of stress that equalizes the maximum surface tension at the frequency Ω_{RT}, the drop is assumed to break up into smaller droplets characterized by a diameter equal to Λ_{RT}.

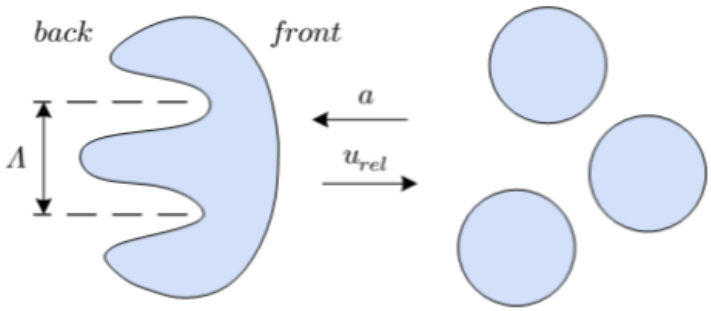

Figure 3.5: Graphical representation of the RT instability

By resuming, the Kelvin-Helmoltz model expresses the main processes of spray disintegration in the closeness of the injector nozzle, whereas the Rayleigh-Taylor model is responsible for the spray breakup in the remaining regions: generally speaking, both the 2 instability simultaneously participate in the fuel disgregation into smaller and smaller particles. By introducing the concept of a liquid breakup length to the KH-RT hybrid model, we can observe that the fuel disgregation occurs at a different rate within and beyond the length of this liquid core, and generally speaking, the RT model was introduced such that the related perturbation influences not only are the drops beyond the breakup length but also those drops that are adjacent to the liquid core. The break-up length is calculated from Levich's theory as:

$$L_b = C_b d_o \sqrt{\frac{\rho_{fuel}}{\rho_{air}}} \tag{3.34}$$

where C_b is an adjustable constant of the previous theory. In the following table, the main parameters for the KHRT model and their values adopted for the CFD simulations are reported:

	B0	B1	C_τ	C3	C_D	We_{cr}
values	0.61	25	0.1	15	0.44	6

Table 3.4: KHRT breakup model coefficients

In particular, We_{cr} represents the critical value of the Weber number that leads to an atomization process due to the RT instability.
Another aspect that needs to be considered is the energy transfer between the fuel droplets and the surrounding turbulent air for determining the onset of the evaporation phase, once the diffusive phenomena have generated a certain mixture with suitable properties for the auto-ignition. The advantages of turbulence in combustion processes have been already discussed, and they are related to the improved thermal diffusivity inside the system. The generic scheme for this kind of process is described in the figure hereafter:

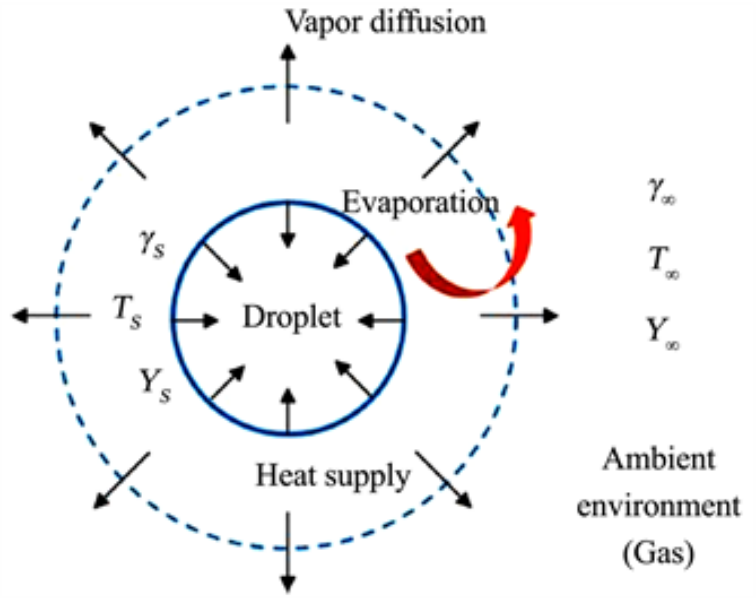

Figure 3.6: Evaporation of a fuel droplet

For the present analysis, the Ranz-Marshall model [21] has been adopted for modeling the heat transfer between the two systems. In this approach, it is possible to observe that, in the closeness of the droplet surface, there is a very small region called *thermal boundary layer*, that is strictly related to the dynamic one, although there are some differences for the definition of the respective thicknesses. In particular, the boundary layer thickness defines the extension of the region, close to the physical and steady

surface, wherein a generic flow property varies until it reaches the free-stream condition. If an infinitesimal portion of the droplet surface is considered so that it can be assumed as planar, the case study can be re-conducted to the one of a generic flow impinging a flat surface, just as depicted in the following figure:

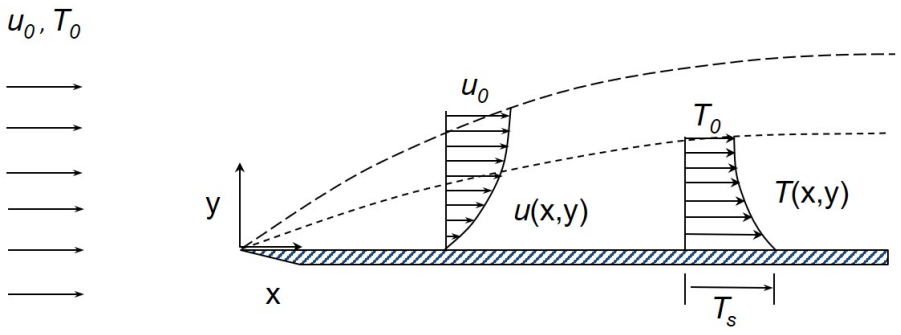

Figure 3.7: Comparison between dynamic and thermal boundary layers

In particular, u_0 and T_0 are the velocity and temperature of the free-stream air surrounding the droplet, whereas u_s and T_s are the velocity and temperature detected onto the droplet surface: since the no-slip condition is introduced also to take care of the viscosity affecting the process, u_s is set as equal to 0.
For a laminar flow, the relationship between thermal and dynamic thicknesses is defined through the Prandtl number, as:

$$\delta_t = \delta_v Pr^{-\frac{1}{3}} \tag{3.35}$$

whereas, for a turbulent flow, their comparison is defined by introducing the Reynolds number:

$$\delta_t \approx \frac{0.37x}{Re_x^{\frac{1}{5}}} \tag{3.36}$$

In the absence of chemical reactions occurring on the droplet surface, the thermal gradient observed in the boundary layer is only due to convective and conductive phenomena associated with heat exchange. The relationship between these 2 mechanisms is pointed out by introducing the *Nusselt number*, also used for characterizing the shape of the thermal boundary layer associated with the droplet surface of diameter d_p. In the case described in this thesis activity, a forced convection process has been considered, and the Nusselt number is defined as a function of the Reynolds and the Prandtl numbers:

$$Nu = h\frac{d_p}{\kappa} = a + cRe^m Pr^n \tag{3.37}$$

where h is the convective heat transfer coefficient, κ is the conductive heat transfer coeffi-

cient, and a, c, m, n are coefficients depending on the kind of fluid system and its geometry. In the thesis activity, for defining the Ranz-Marshall model, the following values have been used for the coefficients:

	c	m	n
values	0.6	0.5	0.33

Table 3.5: Ranz-Marshall heat transfer model coefficients

For a fluid speed equal to 0, the heat is only transferred by conduction, and so the Nusselt number is commonly expressed as:

$$Nu = 2 + 0.6Re^{0.5}Pr^{0.33} \tag{3.38}$$

As said before, by only considering heat transfer in correspondence of the droplet surface, the conservation equation for taking into account both the effects induced by convection and conduction is defined as follows:

$$\rho c_p \frac{dT}{dt} + \rho c_p V \nabla T = \nabla(\kappa \nabla T) + q \tag{3.39}$$

where V is the velocity field derived from the incompressible Navier-Stokes model. In particular, the thermal flux vector q is given by

$$q = -\kappa \nabla T + \nabla c_p T V \tag{3.40}$$

3.2.4. PolyMesh

As said before, OpenFOAM adopts different numerical methods to solve the conservation equations that univocally describe the fluid-dynamic system of interest. One of them consists of the finite volume approach so that the available control volume is divided into several parts to have a more accurate resolution and comprehension of the phenomenon. The creation of a mesh is a strategy that surely needs to be a little bit clarified: by generating a denser subdivision of the domain, an improvement on the numerical solution quality can be achieved, but on the other side, the computational time will be dramatically increased so that it's necessary to find a trade-off between the 2 purposes. This case-solving strategy is completely stored inside the folder *constant/polyMesh*, wherein there

is an accurate description of the kind of generated mesh according to the presence of additional geometries inside the spatial domain. In particular, the mesh generation [22] is determined by the presence of 2 different dictionaries:

1. *blockMeshDict*
2. *snappyHexMeshDict*

The first step for creating the CFD model is to limit the analysis space where the process is verifying, by defining the shape and the extension of the domain. This can be done by using the *blockMeshDict*, a useful dictionary for generating the physical domain wherein the CFD case will verify: in this case, the set of commands are used to define the geometry of the vessel wherein the injection and combustion occur. First, the main dimensions are defined by means of a set of vertexes and then, considering the presence of such additional geometries (i.e. duct), the original domain is subdivided into blocks and each of them could be characterized by a different mesh size according to the precision level that has to be guaranteed (logically, in all those critical points of the domain it is preferable to decrease the cell size so to have a more precise solution). Thus, *blockMeshDict* defines the domain extension and subdivides it into different regions according to the presence of critical surfaces, by giving a preliminary mesh grid.
The actual mesh grid used for running the simulation is generated by the *snappyHexMeshDict*, used to create a mesh subdivision in the closeness of the complex geometry, once it has been introduced inside the domain (it is described inside a ***file.stl*** commonly extracted by a CAD software). A particular trait of this process is the possibility of choosing a sub-region of the initial domain where this kind of refinement can be applied: the sharper the variation of mesh size with respect to the background one, the higher will be the number of refinement layers that should be introduced so to have a more accurate final solution. Once the critical features have been identified, the mesh size starts to be reduced in their closeness according to a level previously set, always considering the trade-off related to the mesh refinement. This process is known as "Mesh Castellating", and it is followed by "Mesh Snapping": in this phase, the mesh cells get deformed so to reproduce as well as possible the actual profile of the complex geometry.
The whole mesh generation process can be summed up in this way by considering this example:

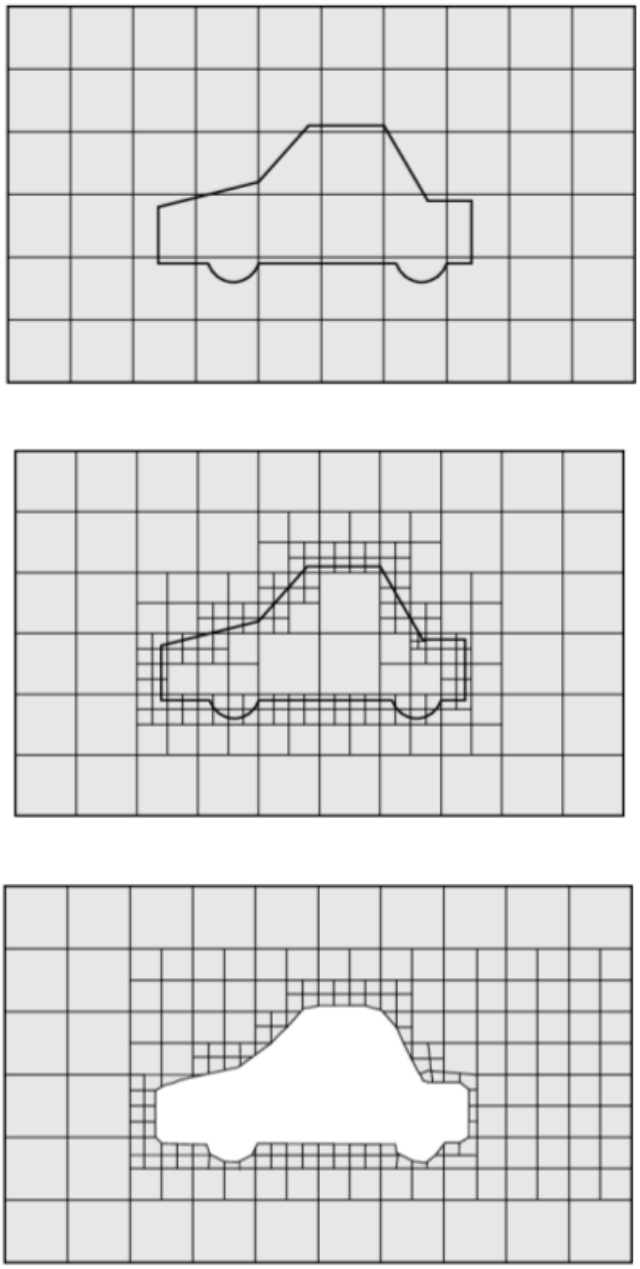

Figure 3.8: Graphical representation of the process aimed to snap a particular geometry introduced within a hexahedral computational grid

Computational Domain

Thanks to the adoption of the CFD software OpenFOAM and the related dictionaries and utilities, a particular computational domain was introduced by adopting both the dictionaries *blockMeshDict* and *snappyHexMeshDict*, so to reply in the most accurate way the experimental one adopted by Sandia and described in the ECN website: the idea is

the generation of a simplified wedge type mesh. In particular, this kind of domain consists of a very small slice of a cylinder that represents the actual combustion vessel: the slice angle is 3 degrees. The choice of a 2D CFD computational domain rather than a 3D one is due to some considerations, mainly related to the reduction of the required computational time for dealing with the CFD case. Moreover, by considering an axisymmetric problem, the transient evolution of the system in the 2D domain will be representative of the one of the 3D domain. Hereafter, a description of the adopted 2D domain is depicted:

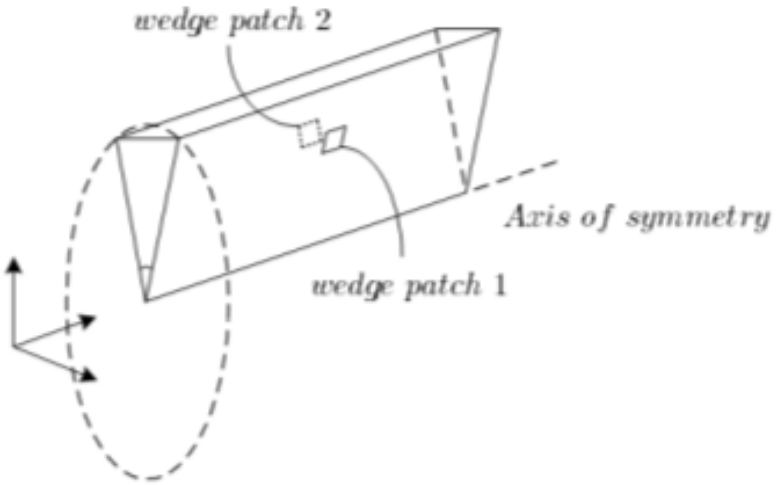

Figure 3.9: Considered 2D CFD domain

Looking at the picture above, the injection point is located at the origin of the reference system and, by considering the main dimensions of the adopted domain:

- **width** = 50mm
- **height** = 108mm

Since both the Free Jet and the Ducted Fuel Injection cases have been analyzed, 2 different computational domains need to be introduced, due to the need of taking care of the complex geometry that characterizes the duct. For what concerns the mesh grid, the common usage of the *blockMeshDict* enabled to subdivide of the domain into 9 different blocks and to consider a variable cell size along both the X and Z directions so that in the closeness of the injection axis the grid density is sufficiently high to have an accurate solution of the CFD computation. In the table hereafter, a brief description of the domain subdivision into blocks and their geometries is depicted, by focusing on the way each block is meshed: as it is possible to observe from the table, the first 6 blocks are the ones closest to the injection axis, since their width is quite small and the mesh density is high, due

to the fact that this region of the domain is the most critical one in terms of accuracy on the final results. The reference system is located in the lower left vertex of the domain so that all the following dimensions are considered with respect to this point.

	Width [mm]	Height [mm]	X cells [mm]	Z cells [mm]
Block 1	0→ 1	0→ 88.1	10	92
Block 2	0→ 1	88.1→ 104.1	10	62
Block 3	0→ 1	104.1→ 108	10	18
Block 4	1→ 2	0→ 88.1	10	92
Block 5	1→ 2	88.1→ 104.1	10	62
Block 6	1→ 2	104.1→ 108	10	18
Block 7	2→ 50	0→ 88.1	95	92
Block 8	2→ 50	88.1→ 104.1	95	62
Block 9	2→ 50	104.1→ 108	95	18

Table 3.6: Size and mesh of the domain blocks

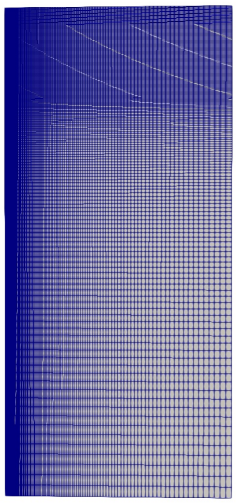

Figure 3.10: Computational Grid for the FJ case

For the definition of the DFI domain, there is also the necessity to consider the *snappyHexMeshDict* due to the presence of a complex geometry inside the environment that influences the evolution of the fluid-dynamic system: in this sense, the realization of

a proper grid in the closeness of the duct shape is due to the necessity of achieving high quality and reliability of the results.

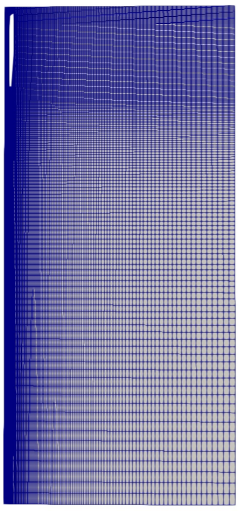

Figure 3.11: Computational Grid for the DFI case

3.2.5. Soot Production

The production of soot is something that must be accurately considered in the analysis of every kind of combustion process since it gives some informations on the pollutant emissions level and moreover on the combustion efficiency: indeed, the higher the amount of soot, the lower will be the portion of injected fuel that has been correctly employed in the flame generation. Furthermore, emissions abatement is a fundamental target many factories are concerned with, in order to reduce the harmful effect on the environment. To efficiently consider and analyze the soot production in the overview of combustion processes associated with both the free-spray and the DFI technologies, in this project the *Leung-Lindstedt-Jones* [23] soot model has been introduced: this is a semi-empirical approach, based on shock-tube studies of hydrocarbon mixtures conducted at different pressures, adopted for the soot analysis in CFD simulations, and it is described in the *thermophysicalProperties*, stored in the folder *Constant*. The main advantages introduced by this model, with respect to the others, are:

- the compatibility with the flamelet concept, so that it can be used to estimate the production of partially-oxidized elements in the case of laminar non-premixed flames
- the assumption, validated from experimental measurements, that the soot production does not depend on the amount of fuel mass injected in the combustion chamber, but actually it depends on the presence of some regions in the flame structure

where *pyrolysis products* are generated from the fuel breakdown path: it has been discovered that such products are crucial in the soot formation process

In particular, this model considers the acetylene C_2H_2 as the most important soot precursor, as experimentally observed by *Harris and Weiner*, but the choice of this element is not so strict: in fact, *Smyth et al.* experienced that other species commonly associated with soot formation, just like C_6H_6, C_4H_2 and C_4H_6, show profiles of similar shape to the acetylene, but with different magnitudes. Thus, the Leung-Lindstedt-Jones approach enables to figure out different steps in the soot formation process, and these phases are:

1. soot nucleation
2. soot surface growth
3. soot oxidation

Numerically speaking, these steps are evaluated by solving a system of 2 different transport equations, one associated with the soot mass fraction and the other with the soot number density, N:

$$V\frac{\partial Y_s}{\partial x} = -\frac{\partial}{\partial x}(\rho V_{T,s} Y_s) + S_m \tag{3.41a}$$

$$\frac{\partial N}{\partial x} = -\frac{\partial}{\partial x}(\rho V_{T,s} N) + S_N \tag{3.41b}$$

where Y_s is the soot mass fraction, N is the soot density number, which is defined as the number of particles contained in a unit of mixture mass, V is the axial mass flow rate and $V_{T,s}$ is the thermophoretic speed of the particle, defined as:

$$V_{T,s} = -\frac{\mu}{\rho T}\frac{\partial T}{\partial x} \tag{3.42}$$

This is the velocity at which a particle moves inside a flow due to the presence of a temperature gradient along the x direction. S_m and S_N are 2 source terms respectively accounting for the whole process and the nucleation/aggregation phases. According to *Smyth et al.*, the nucleation of soot particles verifies in those regions of the flame structure wherein there is a high concentration of pyrolysis products deriving from the fuel breakdown: among them, the acetylene C_2H_2 is the most influent one during the nucleation, defining very rapid mass growth. Experimental measurements showed that typically less than 10% of the total soot mass is formed by incipient particle formation, and the nucleation phase commonly verifies for an activation temperature (E/R) belonging to the range 15000K-25000K. This step is described by the following formula:

$$C_2H_2 \rightarrow 2C(s) + H_2 \tag{3.43}$$

The definition of the reaction rate constant is determined by considering a trade-off between 2 different necessities, on one side there is the necessity of accurately describing the high activation energy process, and on the other, there is the observation for which the nucleation rate of the particle is not uniform, since the reactivity of their surfaces decreases with the aging. To simplify this issue, some measurements from *Harris and Weiner* pointed out the relationship existing between the soot formation rate and the local concentration of acetylene, and also that the reaction step is activated only for a minimum particle size, conventionally set at 100 carbon atoms. Thus, the nucleation rate constant can be expressed in the following way:

$$R_1 = k_1(T)[C_2H_2] \tag{3.44a}$$

$$k_1(T) = A_\alpha e^{-Ta_\alpha/T} \tag{3.44b}$$

The other reaction responsible for the soot formation is the particle surface growth due to the absorption of C_2H_2, and this reaction step can be written as:

$$C_2H_2 + nC(s) \rightarrow (n+2)C(s) + H_2 \tag{3.45}$$

and the associated reaction rate constant can be expressed in the following way:

$$R_2 = k_2(T)f(S)[C_2H_2] \tag{3.46}$$

where $f(S)$ represents the function of soot surface area for unit volume. Experimental results have shown how the assumption of a linear relationship existing between the surface growth and the particle surface S gives poor accuracy and reliability on the actual phenomenon occurring in the flame. However, for the sake of simplicity, a linear relationship has been suggested in this work; so, the reaction rate can be re-written as:

$$R_2 = k_2(T)S[C_2H_2] \tag{3.47a}$$

$$k_2(T) = B_\beta e^{-Ta_\beta/T} \tag{3.47b}$$

In this reaction step, experimental measurements based on shock tube studies showed how the activation energy (E/R) required for triggering the surface growth process is of around 12100K. For the oxidation phase, it has been assumed that it verifies only in a narrow region close to the flame front, and it can be schematized by the following formula:

$$C(s) - \frac{1}{2}O_2 \rightarrow CO \tag{3.48}$$

and the associated reaction rate constant is expressed as:

$$R_3 = k_3(T)S[O_2] \tag{3.49a}$$

$$k_3(T) = C_{OX}T^{0.5}e^{-Ta_{OX}/T} \tag{3.49b}$$

The processes of nucleation and agglomeration above-introduced lead to a variation of the density of the particles in the environment, due to the fact that the particle surface growth brings to a situation where few bigger particles are generated in the combustion chamber. Thus, these reaction steps introduce a source term S_N in the number density transport equation, that can be defined as follow:

$$S_N = \frac{2}{C_{min}}N_A R_1 - 2C_\beta(\frac{6M_{C(s)}}{\pi\rho_{C(s)}})^{1/6}(\frac{6\kappa T}{\rho_{C(s)}})^{0.5}[C(s)]^{1/6}[\rho N]^{11/6} \tag{3.50}$$

where:

- N_A is Avogadro's number
- C_{min} is the minimum amount of carbon atoms required for triggering the soot formation
- $\rho_{C(s)}$ is the soot mass density
- C_β is the agglomeration rate constant
- κ is the Boltzmann constant
- $[C(s)]$ is the soot concentration in the environment, and it can be defined as:

$$[C(s)] = [\frac{\rho_{C(s)}Y_{C(s)}}{M_{C(s)}}] \tag{3.51}$$

  where $Y_{C(s)}$ is the soot mass fraction and $M_{C(s)}$ is the soot molar mass

In the table hereafter, all the values associated to the previously introduced coefficients are reported:

	Value
A_α	10000
Ta_α	21100 [K]
n	0.5
B_β	100000
Ta_β	12100 [K]
C_{OX}	0.08
Ta_{OX}	19800 [K]
C_{min}	100
C_β	3
$\rho_{C(s)}$	1800 $[\frac{kg}{m^3}]$

Table 3.7: Leung-Lindstedt-Jones model coefficients

3.3. Results Accuracy and Reliability

All the reasoning previously done on both the computational domain and the numerical model reflects the necessity of achieving the highest feasible level of accuracy on final results, so to have a reliable method for evaluating the actual process. In any kind of CFD analysis, the parameter that most indicates the accuracy level and the stability of a given process is the Courant Number. In particular, it can be defined as:

$$CoNum = \frac{u\Delta t}{\Delta x} \tag{3.52}$$

where Δt is the time-step set for running the simulation, Δx is the main size of the mesh cell, and u is the characteristic speed of the fluid system.
The Courant number (CoNum) represents the ratio of the distance a fluid particle can travel in one time step to the grid spacing. This ratio determines how accurately the fluid flow is captured by the numerical method used for the simulation: if it is too large, the simulation becomes unstable and the numerical solution oscillates or diverges because the fluid particles can move too far in one time step, and the numerical method is unable to capture the flow accurately. On the other hand, if CoNum is too low, the simulation becomes too expensive from the computational point of view.
Theoretically speaking, the average CoNum that gives the optimal result in terms of

solution accuracy is lower or equal to 1: this means that, for each time step, the fluid particle moves inside an adjacent cell. In this thesis activity, the adopted numerical setup and computational grid size have been chosen so to obtain an average CoNum lower than 1 for each time instant of the process.

3.4. Chemical Kinetic

Up to now, it has been described how the generic setup of a CDF case is organized from the numerical point of view, pointing out the main folders and dictionaries required to define the boundary conditions for the specific problem. These limits are referred to a wide range of different aspects, like the geometry (i.e. to define the shape and the boundaries of the control volume), the thermodynamic state of the actual system (pressure/temperature, turbulence model, chemical composition of both fuel and air), but also the set of solvers used to simulate the CFD case. Since the thesis is based on the study of fuel injection and subsequent combustion inside a constant pressure vessel, another important scheme that needs to be introduced in order to complete the overall setup is related to the mechanism of interaction between fuel and air during the whole process: this can be efficiently analyzed by pointing out the concept of chemical kinetic for a generic reaction.
Generally speaking, combustion is a thermo-chemical reaction where fuel and oxidizer interact with each other in order to generate energy (i.e. heat) and products, like soot that has to be limited to avoid harmful consequences to the environment. Regarding reactants, 2 macro-classes can be distinguished:

- *OXIDIZER*: air is the most common oxidizer in this kind of process. It is a mixture of gases with different chemical properties but, for the sake of simplicity, it can be assumed that its chemical structure can be approximated in a good way by only considering oxygen and nitrogen
- *FUEL*: a very wide class of elements can be considered, that differ from both thermochemical and physical aspects (we can observe solid, liquid and gaseous fuels and, for this, different thermochemical properties, like ignition point and activation energy level). For simplicity, fuel is chemically described as a macromolecule composed of Carbon, Nitrogen, Hydrogen, Oxygen, and Sulphur, and the concentration for each of these elements is expressed by a molar coefficient.

The chemical reaction that involves both fuel and oxidizer can be accurately expressed by the following formula:

$$C_xH_yO_uS_tN_s + \alpha_s(O_2 + 3.76N_2) \rightarrow xCO_2 + \frac{y}{2}H_2O + tSO_2 + 3.76\alpha_sN_2 + \frac{s}{2}N_2 \quad (3.53)$$

In the formula above, the stoichiometric air-to-fuel ratio α_s, a fundamental parameter for defining the combustion process, gives a measure of the exact amount of oxidizer required to not have residual oxygen as a combustion product. Moreover, the actual air-to-fuel ratio α_a corresponds to the amount of oxidizer used to consume the available amount of fuel. The ratio between the stoichiometric and actual quantities gives the equivalence ratio, Φ.
The spatial region at constant pressure where the interactions described above take place is called *flame* and, in the present project, the *non-premixed* case was considered: this means that the fuel and oxidizer are well separated in 2 different systems before the chemical reaction starts. One of the several advantages of this solution is that no premixing structure is required so the system is lighter. The mixing phase between the 2 systems verifies at the flame boundary so that, through the mass and energy diffusion, the flame can self-sustain and the chemical reaction is able to move on. Moreover, chemical and kinetic phenomena can be decoupled, observing that the convective and diffusive transport mechanism enhanced by the presence of a turbulent environment is usually slower than the chemical reactions so that flame chemistry can be considered infinitely fast.
The set of chemical reactions that occur in the flame mixing region can be described according to different points of view:

- *Thermo-Chemistry*: it describes the combustion from the point of view of thermal energy release according to the chemical composition of the mixture
- *Chemical Kinetic*: it emphasizes the way the chemical species interact to each other to generate combustion products.

The chemical kinetic is very useful to understand the rate at which reactions occur and the set of several factors that affect them: indeed, according to the concentration of reactants, temperature, pressure, and eventual catalysts, it is possible to appreciate some variations for the speed at which the reactants are converted into products. The fundamental idea of this approach is that the chemical reaction is determined by a series of impacts among reactants molecules involved in the process: in particular, not all the collisions are beneficial for the chemical reaction progress, but only those characterized by an energetic level higher than the minimum activation energy $\boldsymbol{E_a}$. In the following picture, the energy level associated with an exothermic reaction is depicted:

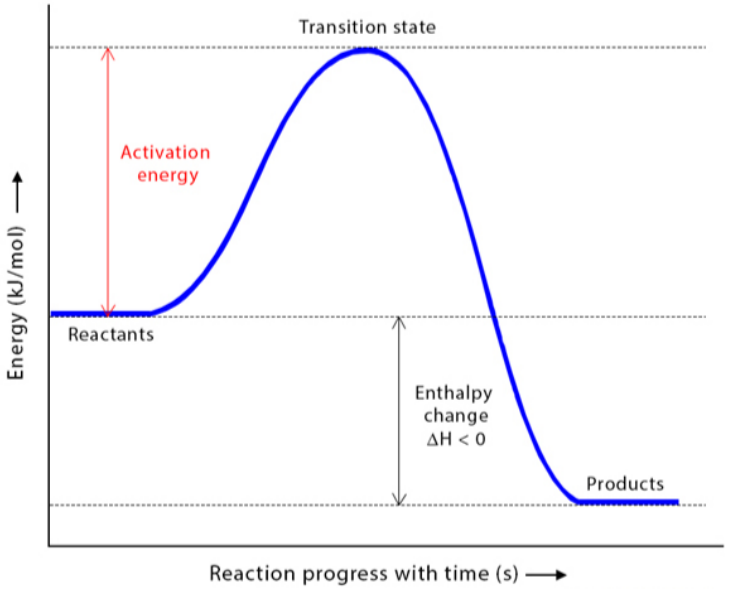

Figure 3.12: Energy level during exothermic reaction

When a set of chemical elements is taken into account, it is useful to introduce an important parameter that enables to understand the way its energy can change in time and because of some applied boundary conditions: Gibbs Free Energy. This feature expresses the maximum amount of energy available for a specific element at a given concentration and thermodynamic state, and it can be used for analyzing whether the reaction can be considered spontaneous or not:

- $\Delta G < 0$: the energy inside the system is decreasing during the process, this means that the chemical reaction is releasing heat as expected for an exothermic process (spontaneous)
- $\Delta G > 0$: the energy inside the system increases during the process, and this is the case of an endothermic reaction: a certain amount of energy has to be provided to the system for triggering and sustaining the chemical reactions, so this process can't be considered as spontaneous
- $\Delta G = 0$: the equilibrium condition for the system has been reached, so that both species concentrations and Gibbs energy do not vary further and this last feature reaches the minimum level during the whole process

By considering the differential field, the variation of Gibbs energy can be seen as:

$$dG = \sum_{i=1}^{N} \mu_i(p, T, n_i)\, dn_i \tag{3.54}$$

where μ_i is the chemical potential associated with the i-th species, and it corresponds to the available energy increase associated with the chemical species whenever it is molar concentration n_i inside the system raises up. In the case of an ideal gas, the chemical potential can be expressed as:

$$\mu_i(p, T, N_i) = \mu_i^0(p^0, T) + RT \log \frac{p_i}{p^0} \tag{3.55}$$

During the exothermic process depicted in the figure above, the reactants interact by means of collisions to generate new chemical species, called products, until the equilibrium condition is reached and the Gibbs Energy for the whole system is the minimum. For a so-defined chemical reaction:

$$\sum_{j=1}^{N} \nu_j^{'} M_j \rightarrow \sum_{j=1}^{N} \nu_j^{''} M_j \tag{3.56}$$

the correspondent process rate related to the i-th chemical species can be defined, that depends on the reactants' concentrations:

$$RR = \frac{d[M_i]}{dt} = (\nu_i^{''} - \nu_i^{'}) k_f \prod_{j=1}^{N} [M_j]^{\nu_j^{'}} \tag{3.57}$$

where k_f is a reaction rate constant that depends on both system temperature and activation energy, according to Arrhenius Law. For the reactants, it gets considered the disappearance rate since their concentrations continuously reduce throughout the process; on the other side, it is defined as the appearance rate for products.
After a certain period of time, the system reaches the equilibrium: in this case, the Gibbs Free Energy reaches the minimum value and also the chemical composition of the system is not going to change further, so the rate of a chemical reaction is null, as shown in the figure below:

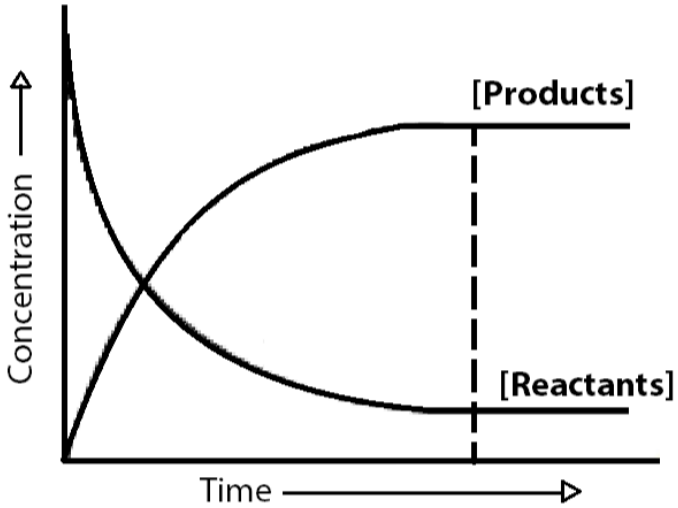

Figure 3.13: Trend of both Reactants and Products towards system equilibrium

In particular, the dashed line represents the onset of the equilibrium condition for the chemical system, where the concentration of each species can be considered constant since the reaction rate is null: from this point on, no more chemical interactions occur inside the system, so that Gibbs Energy will not be characterized by further variations. By resuming all concepts, the equilibrium condition enables to distinguish 2 main regions that can easily be observed by looking at the graph above: before the equilibrium it is possible to observe the *kinetic region*, characterized by the presence of repeated collisions among the reactants molecules; after the equilibrium has reached, it is possible to appreciate the *equilibrium region*, where the system state can be considered as fixed and no more variations from both energetic and chemical points of view will occur.

3.5. Diffusive Flame Model

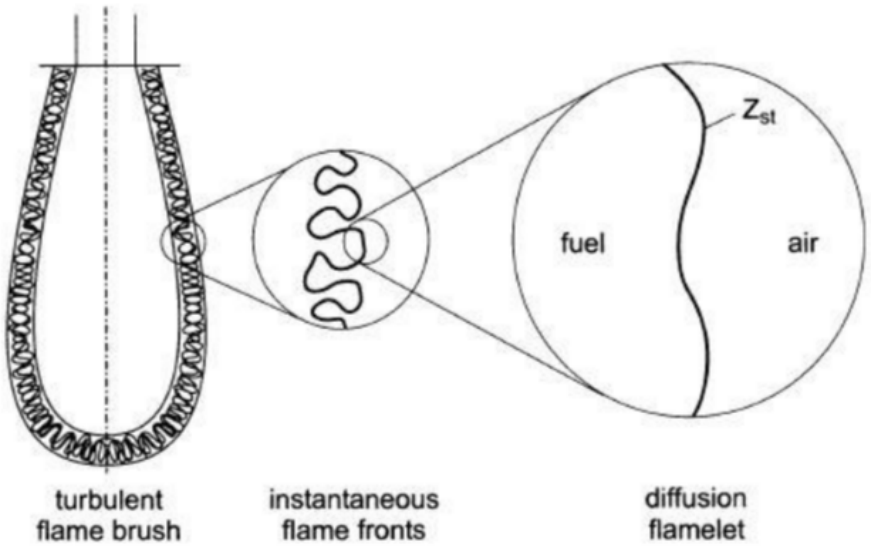

Figure 3.14: Application of flamelet to flame front

The non-premixed combustion process can be accurately described by taking into account the chemical reactions occurring between fuel and oxidizer, and also considering the mass and energy diffusion and convection induced by the turbulent environment, so to promote the continuous mixing and the subsequent flame maintenance over time. At first approximation, it is possible to consider that mass and energy transports are localized in a very thin region of the flame compared to its whole extension and to the adopted turbulence scale, called *flame front*, where the fuel is continuously atomized by the action of the turbulent vortexes: in the case of non-premixed combustion, turbulence plays an important role because fuel and oxidizer are introduced in the combustion chamber in different times and with some discrepancies related to both physical state and temperature. The existing dependence between mass and energy diffusion during the whole phenomenon can be pointed out by introducing the *Lewis number*, a quantity defined as:

$$Le = \frac{thermal\ diffusion\ rate}{mass\ diffusion\ rate} = \frac{Sc}{Pr} = \frac{\alpha}{D_m} \tag{3.58}$$

In particular, both Schmidt and Prandtl adimensional numbers are very useful for defining the flotation phenomena occurring every time a diffusive flame generates, since the first

refers to the mass motion, the latter to the energy transfer inside the system:

$$Sc = \frac{kinetic\ diffusion\ rate}{mass\ diffusion\ rate} = \frac{\mu}{D_m} \tag{3.59}$$

$$Pr = \frac{kinetic\ diffusion\ rate}{thermal\ diffusion\ rate} = \frac{\mu}{\alpha} \tag{3.60}$$

For the purposes here reported, Lewis number has been assumed as equal to 1: it means that energy and mass are characterized by the same diffusion rate during the process, and they can be analytically modeled by an Arrhenius law. So, the flame structure of the system can be completely described in space and time inside the mixture fraction space. The *mixture fraction, Z* defines the concentration of fuel in the environment at a given distance from the injection point, and it's expressed as:

$$Z = \frac{fuel\ mass\ concentration}{air\ mass\ concentration} \tag{3.61}$$

and it is conventionally described as a linear combination of the different species mass fractions considered in the process. If a generic thermo-chemical system is considered, its state is completely defined by the mass fractions Y_k (k = 1, 2, ... n_s), the enthalpy h and the pressure p as follows:

$$\Phi(t) = \Phi(Y_1, Y_2, ..., Y_{n_s}, h, p) \tag{3.62}$$

and its transient evolution can be monitored by considering 2 progress variables:

$$\frac{d\Phi(t)}{dt} = S(\Phi(t)) + M(t) \tag{3.63}$$

Respectively, the first contribution is called *chemistry progress variable, S*, and it is used to track the conversion of reactants into products and the energy balance of the system, by looking at the chemical reaction rate associated with each species under different thermal boundary conditions; the second term is called *mixing progress variable, M*, and it is used to describe the diffusion rate of both mass and energy during the whole process.
An important consideration has to be pointed out: since chemical and physical phenomena are characterized by different time scales (usually the first are very fast compared to the latter), it is possible to decouple the effects induced on the transient evolution of the chemical system state, so that:

$$\frac{d\Phi(t)}{dt} = S[\Phi(t)] \tag{3.64}$$

$$\frac{d\Phi(t)}{dt} = M(t) \tag{3.65}$$

Starting from the initial thermochemical state Φ_o, the transient evolution of the system can be completely described in the mixture fraction space through the
chemistry progress variable: in particular, the way the system changes is described, from the chemical point of view, by a trajectory in the composition space, that shows the conversion of the reactants towards the global equilibrium. There is a powerful tool we can use to efficiently model and solve this combustion case within the Z-space: the *flamelet model*. It enables to consider the flame structure as a series of 1D, thin, and laminar flamelets affected by a turbulent stretch as observed by Karlovitz and Markstein. In particular, the flamelets are assumed to be iso-surfaces of a certain value of mixture fraction Z or species mass fraction Y_j and they can be represented by introducing a curvilinear reference system, where the generic coordinate "s" is locally perpendicular to the profile.

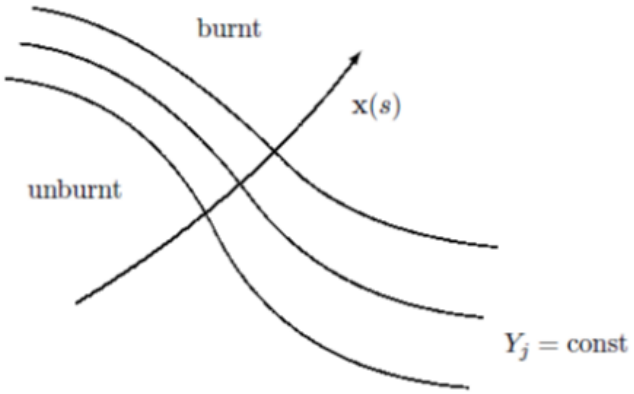

Figure 3.15: Discretization of the flame structure into flamelets

Since flamelets are assumed as thin, the scalar transport equation is only allowed along the direction perpendicular to the local profile, since:

$$\frac{\partial}{\partial x} >> \frac{\partial}{\partial y_{2,3}} \tag{3.66}$$

so that, onto the flamelet surface, a generic scalar quantity like the mixture fraction Z can be considered constant. This means that the variation of the mixture fraction, and thus the chemical composition of the system, is observed only along a generic curve $x(s)$ through the flame structure, locally perpendicular to each iso-surface parametrized by the coordinate s. This brings some simplifications to the flame structure analysis, due to the fact that the evolution of the system is completely described by a single conservation equation defined along a single direction in the space.

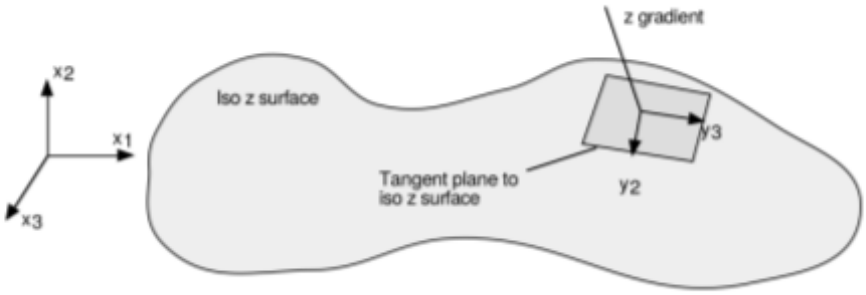

Figure 3.16: Flamelet structure in the Z-space

As said before, the transient evolution of the system can be accurately described in the Z-space, so that the conservation equations for both the system chemistry and energy can be written along the generic curve $x(s)$ as:

$$\rho\frac{\partial Y_k}{\partial t} = \rho\frac{\chi}{2}\frac{\partial^2 Y_k}{\partial Z^2} + \dot{\omega}_k \tag{3.67}$$

$$\rho\frac{\partial h_t}{\partial t} = \rho\frac{\chi}{2}\frac{\partial^2 h_t}{\partial Z^2} + \frac{\partial p}{\partial t} - \sum_{k=1}^{N_s} h_k\dot{\omega}_k \tag{3.68}$$

where:

$$\chi = 2D_m(\frac{\partial Z}{\partial x})^2 \tag{3.69}$$

corresponds to the *scalar dissipation rate*, a quantity that takes into account the diffusion phenomena occurring in the definition of a non-premixed flame.
These equations are also called *flamelet equations* and, since it has been also considered the transient term for the evaluation of the system change, they enable to introduce the *Unsteady Flamelet Model (UFM)*: in fact, if the transient term was not considered, it would not be possible to reproduce the chemical impact of some species that are not in equilibrium, like CO and NO_x, so that the final result would not be accurate to describe the global process. In both the above equations, it is possible to appreciate how the transient evolution is dependent on both chemistry and mixing progress variables: in the energy conservation equation, the term $\sum_{k=1}^{N_s} h_k\omega_k$ represents the overall amount of energy that needs to be spent in order to guarantee the progress of the chemical reactions occurring inside the system.
As said before, to have an accurate understanding of the actual turbulent combustion process, it needs to be taken into account also the mixing phase occurring in the flame front: this process produces a mixture fraction gradient inside the flame, and thus also

the transient evolution of this quantity is represented by a transport equation. Since turbulence introduces a fluctuation of the generic extensive flow property X proportional to the adopted vortexes scale, Z can be defined by exploiting the Reynolds decomposition, so that:

$$Z = \bar{Z} + \tilde{Z''^2} \tag{3.70}$$

This means that turbulence introduces an uncertainty level referred to the sub-grid chemical structure: inside a single cell of the computational domain, the chemical composition is not constant, but it is affected by a well-given gradient imposed by the external turbulence and the greater the vortexes scale, the higher the uncertainty, and thus $\tilde{Z''^2}$. Starting from these considerations, the evolution of the Z-space in time and due to turbulence is depicted by a set of 2 equations, one referring to the mean value and the other to the variance:

$$\frac{\partial \bar{\rho}\bar{Z}}{\partial t} + \nabla \cdot \ (\bar{\rho}\bar{Z}\tilde{u}) = \nabla \cdot \ [(\mu + \frac{\mu_t}{Sc_{\bar{Z}}})\nabla \bar{Z}] + \bar{\rho}\bar{\dot{S}} \tag{3.71}$$

$$\frac{\partial \bar{\rho}\tilde{Z''^2}}{\partial t} + \nabla \cdot \ (\bar{\rho}\tilde{Z''^2}\tilde{u}) = \nabla \cdot \ [(\mu + \frac{\mu_t}{Sc_{\tilde{Z''^2}}})\nabla \tilde{Z''^2}] + \frac{2\mu}{Sc_{\tilde{Z''^2}}}(\nabla \bar{Z})^2 - \bar{\rho}\tilde{\chi} \tag{3.72}$$

Thus, the chemical composition variation of the system at a sub-grid scale can be expressed by means of a $\beta - PDF$, used to model the behavior of random variables. Thus, the mass fractions of species Y_k inside the actual domain are evaluated by integrating the mass fractions in the flame front and furthermore applying a probability function, so that:

$$Y_k(Z, \tilde{Z''^2}) = \int_0^1 Y_i(Z) P(Z, \tilde{Z''^2})\, dZ \tag{3.73}$$

By introducing the flamelet concept, 2 main flame structures can be considered according to the influence turbulence has on the sub-grid chemical frame for the system:

1. *Well-Mixed (WM)*: each cell of the computational domain is characterized by the same chemical composition, and the transient evolution of the system is only due to chemical reaction rates for each species and the associated heat release. At the sub-grid level, it is not possible to appreciate any affection of turbulence on the chemical composition.

2. *Representative Interactive Flamelet (RIF)*: the flame structure is described by multiple flamelets affected by turbulent stretch, and the evolution of the system depends on both chemical reactions and diffusive phenomena so that a sub-grid variation of the chemical composition due to turbulence can be observed. It means that, inside a

cell of the domain, the chemical composition is not constant, but it is characterized by a given distribution expressed by a $\beta - PDF$, and the level of uncertainty is related to the turbulent length scale. By consider a discretization of the flame into many flamelets, it is beneficial for achieving a better understanding of all those stable and unstable phenomena occurring during diffusive combustion, but on the other side, the main drawback is related to the computational cost, since the resolution of flamelet is made during the CFD computation and the increase of complexity in terms of chemistry frame raises the number of transport equations that have to be handled by ODE stiff solvers. This means that only a few flamelets are considered and the modelling of the phenomenon is poor.

3.6. Chemistry Table Generation

To accurately describe all the different aspects related to the case of turbulent combustion, just like the eventual presence of turbulence-chemistry interaction, the flame structure, and the pollutants emission, it is required to generate a precise model of the chemical composition for the system, highlighting the main chemical species involved in the process but also the way they interact to each other for determining the transient evolution towards the equilibrium condition. Since the OpenFOAM environment employs ODE stiff solvers for computing the chemical reaction rates for each species, it means that by increasing the chemical complexity of the system, also the number of transport equations that have to be handled will raise too, leading to a higher computational effort. This is why Direct Integration Solving is not the best way for dealing with very complex chemical systems. To obviate this problem, a solution is represented by the introduction of the *tabulated kinetic* [24]: the chemical kinetic for the system is entirely pre-calculated in a look-up table where the reaction rates are computed, once a given combustion mechanism and flame structure is defined, for a wide range of different thermodynamic boundaries (i.e. temperature, pressure, mixture fraction ...).
By considering the subdivision of the turbulent flame into a set of multiple laminar flamelets, some techniques can be pointed out for generating the chemistry table [25]:

- *Intrinsic Low-Dimensional Manifold (ILDM)*: it enables to realize a simplified kinetic mechanism so that, initially, the evolution of the system only depends on the initial thermochemical boundary conditions and, after a certain time, the advancement towards the chemical equilibrium is only matter of a small number of variables. If N_s species inside the system are considered, it is possible to observe that each of them evolves at a specific rate and, in particular, the fastest ones are negligible

for pointing out the equilibrium condition towards which the system tends. The fastest processes are found by solving an eigenvalue analysis of the local Jacobian of the chemical reaction rates. The eigenvectors associated with all those processes characterized by small time scales are considered to be in *steady-state*: this means that in the equation (3.67), the chemical reaction rate $\dot{\omega_k}$ is equal to 0. On the other side, the eigenvectors associates to slow processes are used to construct a *Low-Dimensional Manifold* in the composition space. By considering the first M species to be the steady-state ones, the manifold will be characterized by a dimension $(N_s - M)$. In this case, *manifold* corresponds to the set of few independent variables used to show the way the system is changing in time. Once the manifold has been introduced, it gets tabulated as a function of the different controlling variables, whose number determines the size of the look-up table: in general, to achieve an accurate evaluation of the combustion phenomenon, at least 3 controlling variables (p, h_u, Z) need to be considered. The main drawback of this technique is that the accuracy is very poor in the "colder" zones of the flame, where the impact of chemical reactions is very low, and phenomena like diffusion play a very important role. So, the ILDM approach is quite used for the modeling of stationary flames rather than diffusive ones.

- *Flamelet-Generated Manifold (FGM)*: this approach is more accurate to simulate the evolution of diffusive flames and all the related non-stationary phenomena, like auto-ignition. The turbulent flame is decomposed into a set of multiple laminar *flamelets* and moreover, the concept of the low-dimensional manifold is introduced to limit the composition space: due to the fact that the major parts of convection and diffusion processes are also present in 1D flamelets, the chemical composition of the general flame can be described by looking at the one of the single flamelet. It is possible to observe that, by considering a single iso-surface wherein the certain species mass fraction Y_j is considered as constant, the resolution of the equations (3.67) and (3.68) gives a solution $(Y_i(s), h(s))$ called *flamelet*, that represents a curve in the composition space parametrized by a single progress variable Y_c, usually expressed as a linear combination of the species mass fractions involved in the process. The set of flamelets defines a manifold in the composition space able to link the points corresponding to the unburned mixture and the equilibrium state, as represented in the following figure:

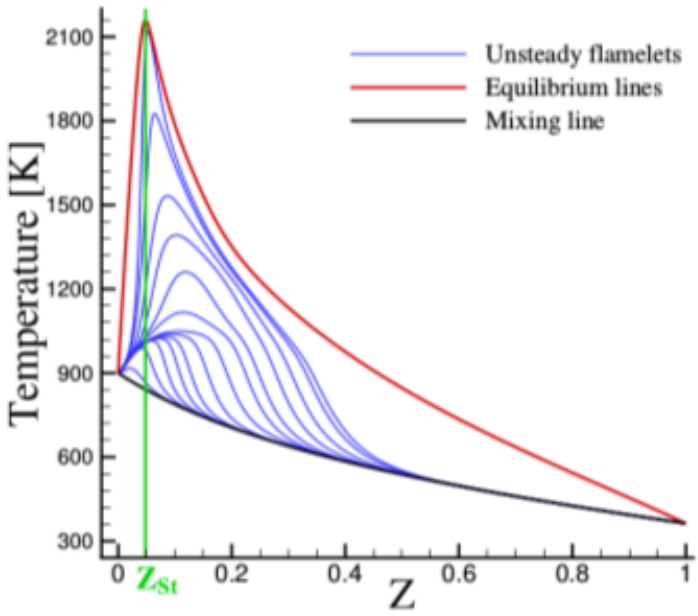

Figure 3.17: Flamelet distribution in the composition space T-Z

As can be observed, the formation of a FGM can be generated from a set of flamelets starting at different points of the 1D curve in the composition space (*mixingline*), where the enthalpy and the element mass fractions are kept constant: in this way, all flamelets rapidly converge to the same chemical equilibrium. This means that one progress variable is enough to describe the chemical state of the system, obtaining a smaller chemistry table than the one with the ILDM approach.

For the thesis activity here described, the table generation is based on simulations related to constant-pressure and auto-ignition processes, by discretizing the flame structure with the flamelet model and considering each of them as a homogeneous reactor: in this sense, it is talking about *PSR Table* [26] [27], where PSR stands for *Perfectly-Stirred Reactors*. By considering this main assumption, it can be observed that the sub-grid chemistry is constant all over the domain since the turbulence is not considered for the evolution of the system: thus the PSR tabulation collects all the informations associated with laminar combustion. Hereafter, it is depicted the basic algorithm for the generation of the chemistry table based on the assumption of homogeneous reactors:

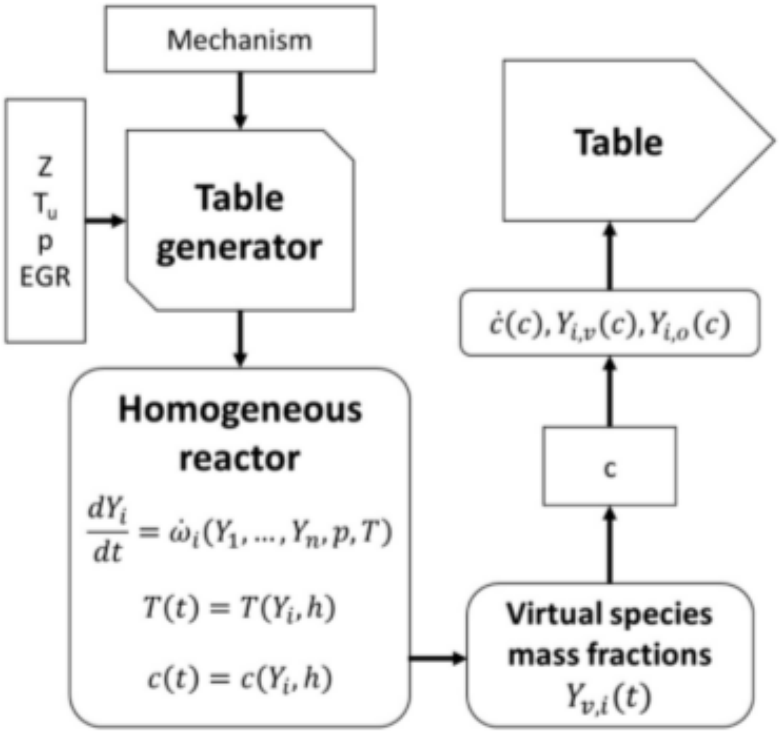

Figure 3.18: Generation of the chemistry table based on the assumption of homogeneous reactors

It is possible to observe that some inputs need to be provided for the table generation:

- *chemical mechanism*: it regards all the aspects related to the chemical kinetic for the considered system, and thus it is necessary to point out the initial chemical structure for the global system, highlighting the composition of both fuel and oxidizer and moreover the way they interact for generating products and for reaching the equilibrium condition. A very important aspect that has to be considered is the set of reaction rates that govern the process, but also the production of intermediate compounds, since they may introduce instability in the process and also pollutant generation.
- *thermodynamic boundary conditions*: some assumptions need to be defined according to the environment wherein the process happens, from the point of view of thermal traits (temperature, pressure), but also from the perspective of the compounds space by limiting the acceptable range for the mixture fraction, Z. All those aspects have a great impact on the chemical reaction rates, since they depend both on temperature according to an Arrhenius law, and on the initial chemical composition of the system that may be affected by the presence of EGR in the combustion

chamber.

- *mixing line*: it corresponds to the thin region where ideally fuel mixes with the already-present air and subsequently evaporates at adiabatic conditions [28]. This assumption is due to the fact that, for non-premixed combustion, fuel and air are introduced inside the combustion chamber at different times and with some discrepancies on what concern both temperature and physical state. In this region it is possible to observe mixing and diffusion between the reactants so that the sub-grid chemical composition is not uniform: since mixture fraction varies, also the temperature changes, because by changing the amount of fuel that mixes with the air, the final temperature of the mixture will be different. The enthalpy balance in the mixing line is defined as follows:

$$h_{mix}(Z) = (1 - Z)h_{air}(T_{air}) + Zh_{fuel}(T_{fuel}) \tag{3.74}$$

$$T_u = T(h(Z)) \tag{3.75}$$

Since the mixing phase verifies without heat dissipation, all the energy is used to increase the fuel temperature until it evaporates, so that air cools down. Actually, the mixing line can be affected by a certain level of dispersion, due to the fact that spray evaporation depends on:

  - *droplet size*
  - *mixing rate*

However, other effects such as heat transfer close to the nozzle tip could affect the mixture fraction and cause a scatter dispersion in the spray mixing line. The general trend for the mixing line is here depicted:

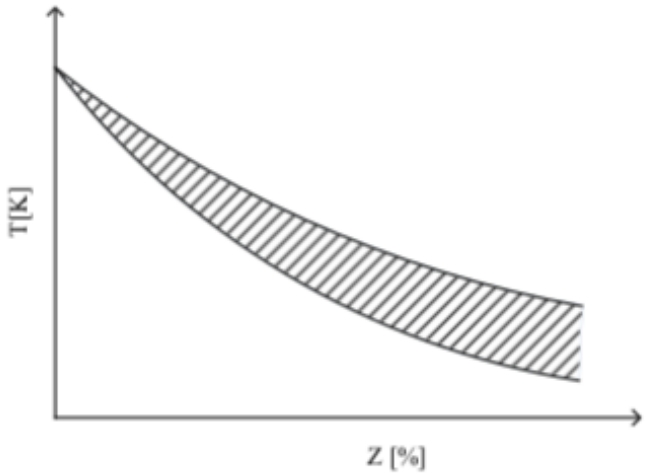

Figure 3.19: Schematic for the dispersion observing the mixing line

Otherwise, if the presence of a mixing line was neglected, it would mean that no mixing between fuel and oxidizer occurs: thus, the temperature of the system does not depend on the mixture fraction. Moreover, it has been introduced the possibility to consider fuel evaporation, which will modify the balance equation of the mixing line.

Once the input parameters are set, the variation of the chemical composition inside the computational domain only depends on the chemical reactions, since the influence of turbulence at a sub-grid scale has not been introduced. Thus, the transient evolution of the system can be monitored by solving the system of transport equations related to both chemical species and energy release:

$$\begin{cases} \rho \dfrac{dY_i}{dt} = \dot{\omega}_i(T, p, Y_1, ..., Y_n) & \text{(3.76a)} \\ \dfrac{dh_t}{dt} = \dot{S}_{Q_r} & \text{(3.76b)} \end{cases}$$

The resolution of the previous system of equations, for each time step, defines the way the chemical composition changes in time. Since the mixture fraction can be expressed as a linear combination of the species mass fractions involved in the process, it turns out that the mixture fraction continuously changes in time towards the achievement of the equilibrium condition and the way it evolves is expressed by the following transport equation:

$$\frac{\partial Z}{\partial t} + \nabla(\rho \bar{V} Z) - \nabla(\mu_t \nabla Z) = \dot{S}_z \tag{3.77}$$

The adoption of a chemistry table for studying the combustion process enables to introduce a very important parameter that describes how the system is changing from the chemical point of view, by looking at the state of conversion from reactants to products: the *progress variable, C*. The progress variable is computed at each time step so to monitor the chemical evolution of the system towards the equilibrium and each value assumed by the parameter univocally defines a thermodynamic state for the system.
There are several definitions for the progress variable, in particular:

1. linear combination of the mass fractions Y_i of the system

$$C(T_u, p, Z, t) = \sum_{i=1}^{N_s} \alpha_i Y_i(T_u, p, Z, t) \tag{3.78}$$

2. sensitive enthalpy for the system

$$C(T_u, p, Z, t) = h_s(T, t) \tag{3.79}$$

3. enthalpy of formation at reference conditions (T = 298K and p = 1bar)

$$C(T_u, p, Z, t) = \sum_{i=1}^{N_s} h_{298,i} Y_i(t) - \sum_{i=1}^{N_s} h_{298,i} Y_i(0) \tag{3.80}$$

   In this case, the progress variable expressed the amount of heat released by the combustion process at reference conditions: for the purposes described in this activity, this definition has been chosen.

Generally speaking, the progress variable must be characterized by a monotonic trend and, for showing the state of advancement for the global process, the
normalized progress variable, c was introduced, which varies from 0 (initial conditions) to 1 (equilibrium condition). It is analytically defined as:

$$c = \frac{C - C_{min}}{C_{max} - C_{min}} \tag{3.81}$$

where C_{min} and C_{max} are respectively the minimum and maximum values for the progress variable, which are found at initial and after auto-ignition conditions. Those values are stored in the table as functions of Z, T_u, and p. As said before, the progress variable C describes the trajectory followed by the system, in the space of the composition, for reaching the equilibrium state starting from the initial conditions of temperature and

chemical composition, and the trajectory trend mainly depends on the chemical reaction rate and heat release during the process. If it would analyze the rate at which the global system is changing, it should introduce the concept of *progress variable reaction rate,* $\dot{c}$:

$$\dot{c}_i = \frac{c_{i+1} - c_i}{t_{i+1} - t_i} \tag{3.82}$$

As each scalar quantity is used for the implementation of the numerical model, the variation of the progress variable C inside the computational domain is expressed through a transport equation, where the parameters used for its definition must evolve according to similar time scales. The analytical definition is hereafter reported:

$$\frac{\partial \bar{\rho}\tilde{C}}{\partial t} + \nabla(\bar{\rho}\bar{V}\tilde{C}) - \nabla(\frac{\tilde{\mu_t}}{Sc_t}\nabla\tilde{C}) = \rho\dot{C} \tag{3.83}$$

where $\dot{C}$ is the *progress variable source term* and it mainly depends on the considered combustion model. In particular, it is defined as a function of the progress variable reaction rate as follows:

$$\dot{C} = \dot{c}(C_{max} - C_{min}) \tag{3.84}$$

Another equation needs to be considered and it evaluates the enthalpy of the unburned mixture, used to estimate the unburned mixture temperature T_u which is one of the independent variables of the table. By introducing the *turbulent thermal diffusivity,* α_t and the density of the unburnt mixture ρ_u, the conservation equation associated with the system enthalpy is the following:

$$\frac{\partial \bar{\rho}\tilde{h_u}}{\partial t} + \nabla(\bar{\rho}\bar{V}\tilde{h_u}) - \nabla(\tilde{\alpha_t}\nabla\tilde{h_u}) = \dot{Q}_s + \frac{\bar{\rho}}{\bar{\rho_u}}\frac{D\bar{p}}{Dt} \tag{3.85}$$

$\dot{Q}_s$ is the term related to the spray evaporation, and it assumes different values according to the fact the mixing line is included or not inside the chemistry table generation process. At each time step, in each cell of the CFD domain the transport equations related to mixture fraction, enthalpy, unburned gas temperature, and progress variable are solved, so that at a given time t^*, the thermochemical state of the system is described by a set of values (Z^*, h^*, T_u^*, C^*). Those values are then used to access the PSR table, in order to compute the progress variable reaction rate and thus the chemical composition, so that the look-up table is updated with the new values.

Since an excessive size for the chemistry table must be avoided, it is useful to simplify the actual chemistry structure of the system, by introducing the concept of *virtual species.*

In this work, 7 virtual species $(O_2, N_2, CO_2, H_2O, CO, H_2, fuel)$ have been considered

and they represent a reduced palette of compounds able to reproduce the thermochemical properties of the actual detailed chemistry and they're defined so to preserve:

1. total number of C, H, O and N atoms
2. mixture enthalpy and specific heat
3. mixture molecular mass

Hereafter, the calculation of the virtual species and their mass fractions is reported so that all the previous points can be satisfied.

$$\begin{cases} \sum_{i=1}^{N_{vs}} x_{v,i} N_{C,i} = \sum_{k=1}^{N_s} x_k N_{C,k} & \text{(3.86a)} \\ \sum_{i=1}^{N_{vs}} x_{v,i} N_{H,i} = \sum_{k=1}^{N_s} x_k N_{H,k} & \text{(3.86b)} \\ \sum_{i=1}^{N_{vs}} x_{v,i} N_{O,i} = \sum_{k=1}^{N_s} x_k N_{O,k} & \text{(3.86c)} \\ \sum_{i=1}^{N_{vs}} x_{v,i} N_{N,i} = \sum_{k=1}^{N_s} x_k N_{N,k} & \text{(3.86d)} \\ \sum_{i=1}^{N_{vs}} Y_{v,i} h_i(T) = \sum_{k=1}^{N_s} Y_k h_k(T) & \text{(3.86e)} \end{cases}$$

The PSR table can be employed in different ways:

- directly with the TWM model
- integrated into the RIF model, so to define the TRIF model
- for generating the ADF table, with the introduction of mixture fraction variance and scalar dissipation rate.

3.6.1. Perfectly-Stirred Reactors (PSR) model

This model is based on the assumption that each cell of the computational domain is similar to a homogeneous reactor since there is constancy in terms of chemical composition. Moreover, the turbulence is not affecting the transient evolution of the system, so the sub-grid chemical composition variation is only due to the chemical reactions. Thus, at each time step, the reaction rates for the compounds are evaluated by solving conservation equations related to both species and energy release, so that a new value of the progress variable is computed and stored in the table.

For the PSR model, the conservation equation for the mixture fraction Z, also by taking into account the fuel evaporation $\dot{S}_z$, is defined by the (3.77); whereas, for evaluating the transient evolution of the chemical system, the same conservation equations (3.83) and (3.85) reported inside the PSR table, related to both chemical species and energy, are considered. Hereafter, the classical algorithm for the PSR model is depicted:

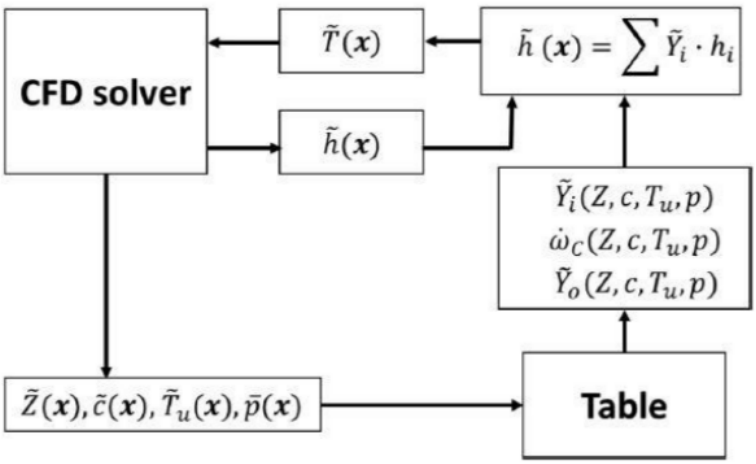

Figure 3.20: Scheme for the PSR model

The general advantage that can be achieved with this model is the simplification in terms of independent variables used to describe the chemical system: Z, c, T_u, p. On the other side, some disadvantages characterize this approach:

1. PSR does not take into account the influence turbulence has on chemistry: thus, it can be considered as an approximation of the effective combustion phenomenon related to a turbulent flame
2. In rich regions ($\Phi > 3$) it is possible to encounter instantaneous ignition of the mixture due to the diffusion of the progress variable C. Thus, the reaction rates are set to 0 where the equivalence ratio is equal to 3, and thus in all those regions where dual-stage ignition does not verify.

3.6.2. Tabulated Representative Interactive Flamelet (TRIF) model

This model is based on the flame structure discretization into multiple laminar flamelets, so that an increase in the number of considered flamelets leads to improve accuracy level in the description of all those phenomena related to non-premixed turbulent combustion,

like flame stabilization and auto-ignition. In this model, according to the decoupling of chemical and physical phenomena due to different time scales, it has been assumed the presence of an undisturbed region where the chemical reactions occur: moreover, the choice of a unitary Lewis number means that both mass and energy diffusions are characterized by the same kind of law, so the evolution of the system can be completely described in Z space. By considering the turbulence impact on chemistry, this leads to a sub-grid variation of the chemical composition, that can be accurately described through a $\beta - PFD$. The local flame structure is evaluated by solving conservation equations related to both the progress variable and the enthalpy:

$$\rho\frac{\partial C}{\partial t} = \rho\frac{\chi}{2}\frac{\partial^2 C}{\partial Z^2} + \dot{C} \tag{3.87}$$

$$\rho\frac{\partial h_t}{\partial t} = \rho\frac{\chi}{2}\frac{\partial^2 h_t}{\partial Z^2} + \frac{dp}{dt} \tag{3.88}$$

where χ is the scalar dissipation rate used to express the mixing effects induced by turbulence: it is used to control the diffusion rate of the species in the mixture fraction space and is a function of the scalar dissipation rate at stoichiometric mixture conditions $\chi_{st,j}$ that is computed for each flamelet:

$$\chi = \chi_{st}\frac{f(Z)}{f(Z_{st})} \tag{3.89}$$

Instead, the progress variable source term $\dot{C}$ is computed by assuming a $\delta - PDF$ distribution for the progress variable and a $\beta - PDF$ function for the mixture fraction:

$$\dot{C} = \int_0^1 \int_0^1 \dot{C}(p, T_u, Z, c)\beta(Z, \tilde{Z''^2})\delta(c)\, dc\, dZ \tag{3.90}$$

At each time step, the conservation equations (3.87) are solved for every flamelet, then the chemistry table is used to compute the progress variable reaction rate term by using the progress variable and thermodynamic properties as input. Hereafter, the classical algorithm for the TRIF model is depicted:

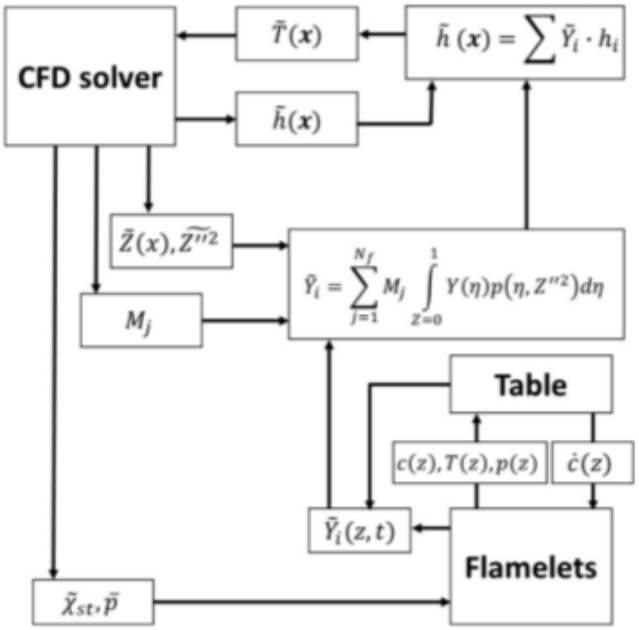

Figure 3.21: Scheme for the TRIF model

The main advantage introduced by this model is basically the decoupling between CFD computation and the resolution of the flamelets set: this enables to reduce the computational effort so that the global phenomenon can be efficiently described by considering a wider set of flamelets with respect to the basic mRIF approach. Thus, the set of laminar flamelets required to reproduce the turbulent flame structure is pre-calculated and all the results are stored in a look-up table in terms of thermochemical parameters. Although several simplifications are introduced with this model, the generation of the flamelet database remains expensive in terms of computational time when fuels with high molecular complexity are considered and also when the boundary conditions span over wide ranges of values. Moreover, it requires a higher computational cost compared to the TWM model.

3.6.3. Approximated Diffusion Flamelet (ADF) model

This model allows to efficient solve all the issues related to the TRIF model, enabling to reduce the computational time for generating a flamelet database and also considering the complex chemistry structure of fuels. The ADF model [29] is based on the same concepts that describe the TRIF model: the turbulent flame structure can be modeled by introducing a set of multiple laminar flamelets, so that it is possible to decouple the effects induced on the combustion process by chemistry and physics, observing that the chemical

reactions take place in an undisturbed region of the flame. In this sense, it is possible to observe that the transient evolution of the system is described in terms of 2 progress variables, one associated with the chemistry reaction rates and the other one referring to both mass and energy diffusion phenomena due to turbulence. The introduction of this last quantity enables to observe that the sub-grid chemical structure of the system is not constant in each cell of the domain, but it is characterized by a given gradient that can be represented through a $\beta - PDF$ model.

In the ADF model, the resolution of the flamelets set for a wide range of thermodynamic properties values, just like temperature, pressure, and scalar dissipation rate, is contained in a look-up table, so that its evaluation is decoupled from the CFD computation and, moreover, the variable source term $\dot{C}$ used to define the progress variable transport equation is pre-calculated by solving the auto-ignition of a set of homogeneous reactors (adiabatic and isobaric) for each value of the mixture fraction stored in the table: thus, at each time-step, for each tabulated value of the mixture fraction Z and the related variance, it is possible to estimate both the chemical composition of the system in terms of virtual species and also the progress variable:

$$Y_i(Z, \tilde{Z''^2}) = \int_0^1 Y_{TRIF}(Z)\beta(Z, \tilde{Z''^2})\, dZ \tag{3.91}$$

$$C(Z, \tilde{Z''^2}) = \int_0^1 C_{TRIF}(Z)\beta(Z, \tilde{Z''^2})\, dZ \tag{3.92}$$

In particular, this model considers the progress variable Y_c as a linear combination of the mass fractions for the species involved in the model, and thus the virtual ones. The transport equation that has to be solved is the following one:

$$\rho\frac{\partial C}{\partial t} = \rho\frac{\chi}{2}\frac{\partial^2 C}{\partial Z^2} + \dot{C} \tag{3.93}$$

where $\dot{C}$ has the formulation expressed in the (3.84). Alternatively, the previous equation can be also expressed in this way:

$$\frac{\partial Y_c}{\partial t} = \frac{\chi(a, Z)}{2}\frac{\partial^2 Y_c}{\partial Z^2} + \dot{\omega}_Y^{HR}(Z, c) \tag{3.94}$$

where $\dot{\omega}_Y^{HR}(Z, c)$ corresponds to the chemical reaction rate evaluated through the PSR table for each value of mixture fraction and normalized progress variable stored inside it. Thus, the ADF model represents an interesting compromise between TWM and TRIF, since the resolution of the 1D transport equation associated with the progress variable

depends on a parameter calculated by considering a PSR table. Hereafter, the schematic of the ADF table generation is reported:

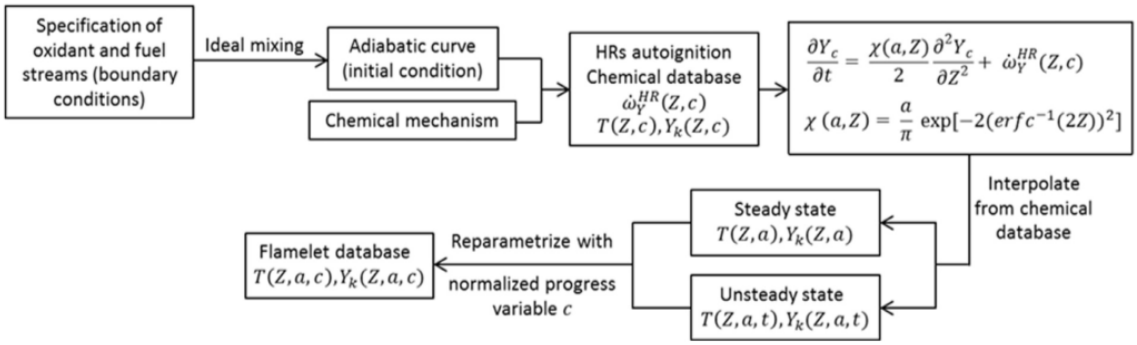

Figure 3.22: Scheme for the ADF table generation

For achieving an accurate description related to the combined effects of mixing and reaction, a small time-step has been chosen for the CFD computation, and also the need of considering different values for the scalar dissipation rate increases the computational time of a 5-10 factor compared to the one needed to generate the PSR table and, in this case, the independent variables that must be considered are: $T_u, Z, c, p, \chi_{st}, \tilde{Z''^2}$. Although the high computational effort, this hybrid chemistry table enables to achieve a very accurate representation of all the phenomena occurring during the analysis of a turbulent flame, just like:

- extinction in the closeness of the nozzle region, where the effects of mixing and diffusion are predominant, and thus the scalar dissipation rate is very high
- re-ignition due to the diffusion of the progress variable
- flame stabilization processes, expressed by the *Lift-Off Length*, and auto-ignition

4 | Experimental Reference: Sandia National Laboratories

In a research activity in which a conspicuous part is numerical, the experimental data present assume great value, especially in the first stage of development. In this case, the experimental activity, adopted as a reference for comparing the numerical results, was the one conducted by Sandia National Laboratories. In particular, Sandia led an experimental analysis for both the free spray and the ducted fuel injection using a Constant Volume Combustion Vessel (CVCV), cube-shaped with optical access. By adopting this kind of setup, it is possible to reproduce and observe the different sets of phenomena occurring during a turbulent combustion case; moreover, thanks to the introduction of fully optical diagnostic techniques for the data analysis, there is the possibility of easily observing the system transient evolution, obtaining accurate and reliable measurements. Another advantage due to this kind of equipment is the facility to align and substitute the duct. In the following sections, the Sandia experimental setup will be explained and described in detail, focusing attention on three main aspects:

- Combustion Vessel and the relative geometry
- Injection system and reference conditions
- Optical diagnostic techniques for data processing

4.1. Combustion Vessel

As it is possible to observe from the ECN website, the experimental equipment is the following:

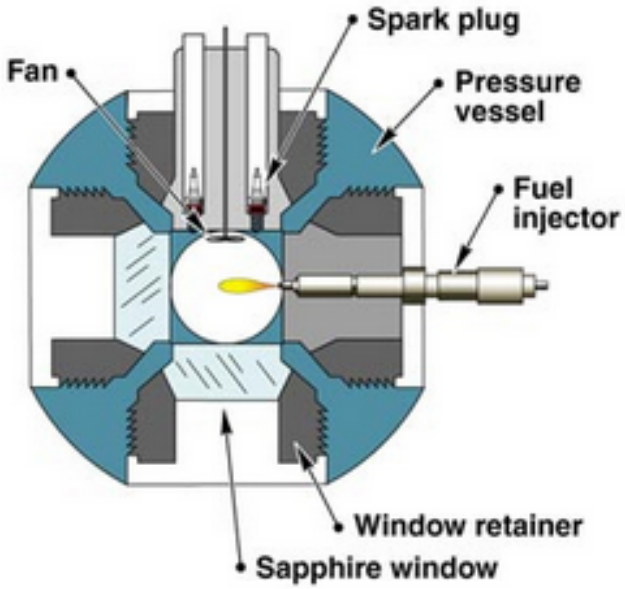

Figure 4.1: Experimental Sandia CVCV

The CVCV is a particular combustion chamber wherein the combustible mixture is injected and subsequently ignited under specific thermodynamic conditions set in advance, similar to the ones that characterize the actual operating field of a conventional diesel engine. The main difference between the CVCV and a conventional CI engine is the possibility, in the first case, of observing in real time the evolution of the system thanks to optical techniques and also the presence of a window placed on the external surface of the volume. Generally speaking, the operating conditions that can be replicated by using the Sandia equipment are limited by its thermal and mechanical properties, but in general, it is possible to analyze different cases, just like:

- Ambient gas temperature from 450K to 1300K
- Ambient gas oxygen concentrations from 0 (non-reacting case) to 21 (reacting case)
- Ambient gas densities from 3 to 60 $\frac{kg}{m^3}$

4.2. Spray A case

One of the most important experimental measurements achieved by using the Sandia combustion vessel is named **Spray A** [30]. This condition is a low-temperature combustion case where there is the possibility of observing a moderate amount of EGR in the combustion chamber. Typically, this case is evaluated at a temperature of 900K, a constant ambient density of 22.8 $\frac{kg}{m^3}$ and thus, by applying the perfect gases equation, an ambient

pressure of 6 MPa: moreover, it is applied to both non-reactive and reactive conditions, but these last ones are limited to an oxygen concentration of 15 % in the environment. The ambient gas is considered near-quiescent, in the sense that the velocity field of the ambient air is negligible to the one associated with the fuel jet, and the adopted fuel is the n-dodecane, $NC_{12}H_{26}$, of 99% purity. In the following table, all the conditions describing the spray A case are reported with the specific reference values:

	Value
Ambient Temperature [K]	900
Ambient Pressure [MPa]	6
Ambient Density [$\frac{kg}{m^3}$]	22.8
Ambient O_2 concentration [%]	0, 15
Injection Pressure [MPa]	150
Injector Nozzle Temperature [K]	363
d_n **[mm]**	0.09
K_n **[-]**	1.5
C_d **[-]**	0.99
L/D **[-]**	5

Table 4.1: Spray A boundary conditions

The actual level of turbulence in the combustion environment is reproduced by adopting a high-RPM rotating fan, that is also used to create uniform ambient conditions after a certain time period. Before the auto-ignition phase occurs, the thermodynamic environment can be assumed as steady; then, the onset of combustion is determined by the presence of spark plugs, used to simulate the auto-ignition process once a predefined value of pressure has been reached in the vessel, that is arranged on the opposite side with respect to the injector, allowing so enough space for optical access. The following figure describes the kind of injector used for dealing with the spray A measurements:

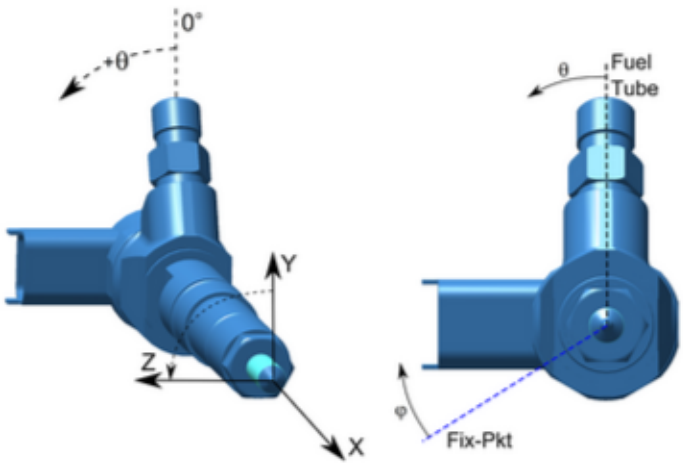

Figure 4.2: Spray A nozzle geometry from ECN

For what concerns the kind of adopted injection system, as it is possible to observe from the ECN website, it is the same one used for analyzing the Spray A condition, the *A*210370, and it is characterized by a single hydro-eroded nozzle, whose orientation is axial (it means that the relative angle between the Z-axis and the injection one is 0°). Moreover, the injector is linked to a common-rail system characterized by a Bosch-solenoid activation, generation 2.4, and operating at a fixed injection pressure of 1500 bar. The injection duration was chosen long, typically around 4ms, as this is representative of a high-load operating field: this is the most challenging condition in modern compression ignition engines due to the fact that many attempts and experimental studies have been conducted with the main target of avoiding high particulate emissions.

4.3. Optical diagnostics

The main advantage of using the CVCV is the possibility of reproducing the combustion phenomenon under different boundary conditions; moreover, the presence of optical windows enables one to analyze and observe the actual evolution of the system inside the chamber, so to have an accurate comprehension of all those phenomena occurring during the turbulent combustion, just like flame stabilization, auto-ignition, and the soot production. To do that, Sandia adopted different data processing techniques based on the usage of optical equipment. These techniques can be grouped into:

1. natural luminosity detection and imaging, indicating regions of hot soot;
2. imaging of chemiluminescence from electronically excited hydroxyl (OH) radicals, indicating where high-temperature reactions occur.

Natural Luminosity (NL)

The natural luminosity (NL) emitted by hot soot and electronically excited species produced during chemical reactions was measured using high-speed cameras. The lens is equipped with a short-wave pass filter to emphasize the contribution to natural luminosity from broadband chemiluminescence.

Chemiluminescence

A high-speed camera equipped with an intensifier was used for chemiluminescence imaging. The lift-off length, LOL is determined by an average of pixel intensity at each point along the spray axis; LOL is determined as the first axial position downstream of the injector where the average axial intensity is above a certain threshold. The threshold level is set as a compromise between being low enough to detect the onset of OH/CL from auto-ignition reactions, but not so low that the LOL value would be susceptible to variations caused by camera noise.

Of course, the cameras used depend on the research institute where investigations were carried out.

5 | Thesis Target and Results

The main target of this thesis activity is the evaluation of the main differences between FJ and DFI combustion technologies both under no-reacting and reacting conditions, in order to find out similarities with respect to the experimental results achieved by Sandia National Laboratories. To achieve the best similarity with the reference results, the adoption of the CFD software OpenFOAM was considered in order to simulate the combustion process for a wide range of different thermo-chemical ambient conditions, and the computational domain has been defined so that its dimensions are the same to the Sandia experimental combustion vessel. Thus, the cases analyzed in this work can be collected into 2 different classes:

- *Non-Reacting*: combustion process is not evaluated, assuming that no oxygen is present in the environment. The target of this analysis is the evaluation of the macroscopic behavior of the fuel jet according to the boundaries associated with the vessel and, for the comparison with experimental results, the ECN database has been chosen as reference.
- *Reacting*: the combustion process is evaluated for 2 different oxygen concentrations (15% and 21%) and for an LTC case, where the ambient temperature varies from 850K to 950K. The attention is focused on the interaction between fuel and air for generating a mixture able to auto-ignite at constant pressure for different thermodynamic conditions. Moreover, the analysis wants to point out the combustion performances, in terms of flame stabilization and soot production

In the following sections, all the results achieved during the CFD simulations are reported for both the non-reactive and reactive cases, and a brief description of both conditions is offered, so to emphasize the target of each analysis. The post-processing has been determined through ParaView for obtaining the graphical evolution of the flame, highlighting its main features. Matlab has been used for processing the trend of the most important quantities associated with the transient evolution of the system, defining a comparison with the Sandia experimental results.

5.1. Non-Reacting Analysis

The non-reacting analysis has been conducted to define the spray evolution in space and time due to the viscous and aerodynamic interaction with the ambient gas, once the thermo-chemical state in the vessel has been set: since no O_2 is present inside the combustion environment, combustion does not occur. In the following table, the considered boundary conditions have been reported:

	T_u **[K]**	**Density** $[\frac{kg}{m^3}]$	**Inj. Pressure [MPa]**	O_2 **concentration [%]**
Values	900	22.8	150	0

Table 5.1: Boundary conditions for the spray model validation

The non-reacting campaign has been divided into 2 different steps:

1. validation of the free-spray technique through comparison with the experimental data achieved by Sandia for the spray A case, so to evaluate whether the numerical model adopted in this project can be considered accurate or not
2. comparison between the FJ and DFI technologies, for determining the main differences in terms of flow evolution in space and time due to the introduction of the duct inside the vessel.

For both cases, the most essential features that have been analyzed under no-reacting conditions, during the jet penetration, are:

- the evolution of the *mixture fraction, Z* along both axial and radial directions
- the evolution of the *mixture fraction variance,* Z_2 along both axial and radial directions, induced by the presence of a turbulent pattern of the ambient air: thus, the trend of such quantity mainly depends on the turbulent length and time scales
- the evolution of the radial and axial *velocity fields*: this aspect mainly depends on the turbulent kinetic energy dissipation due to the surrounding air, which generates a state of stress on the jet due to the presence of both viscosity and aerodynamic forces
- the trend of the *liquid and vapor penetration* during the injection phase: in particular, the trends of these 2 quantities are described by the output files *sp99.Bomb*

and *vapPen1.Bomb*. The liquid length is defined as the distance from the injector nozzle at which the 99% of the total mass is injected inside the chamber; the vapor length is defined as the distance from the injector nozzle at which the 0.1% of the injected fuel mass is converted into vapor.

5.1.1. Spray Model Validation

The main target is to assess whether the numerical model used for the CFD simulations is accurate enough to reproduce and approximate the experimental data, reported in the ECN database, for the free-spray condition. The goodness of the adopted numerical model has been assessed by comparing it with the results associated with the ECN spray A case: in this sense, the same injector system and thermo-chemical conditions inside the vessel have been modeled.
Once the thermo-chemical environment has been defined, the simulation results are reported hereafter: the attention has been focused on the comparison between the numerical mixture fraction and the associated variance with respect to the experimental ones, for evaluating some similarities between the 2 different approaches. In particular, all these quantities are evaluated at 25mm and 45mm away from the injection point, so to have a better understanding of the influence the ambient air has on the fuel jet penetration and a radial distance of 10mm with respect to the injection axis has been considered so to be sure of capturing all the quantity trend.

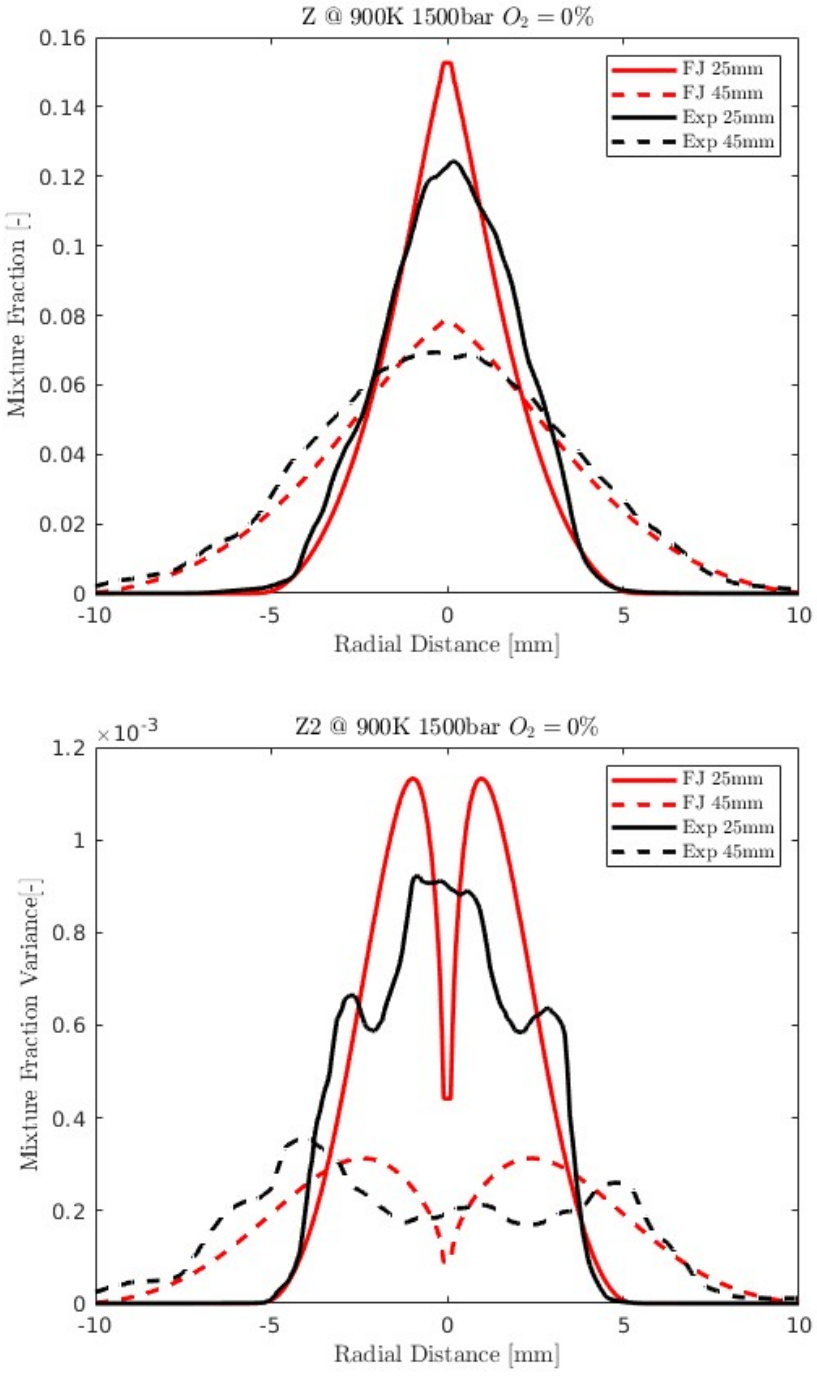

Figure 5.1: Comparison between numerical data achieved from CFD simulations (red) and experimental trends extracted from the ECN database (black)

An interesting aspect can be pointed out: moving from 25 mm to 45mm, the mixture fraction field flattens out. This is due to the viscous and aerodynamic impact the surrounding air has on the fuel stream: as a result of their interaction, the fuel jet loses part of its momentum and it tends subsequently to spread away from the injection axis, by

mixing with the surrounding air. Thus, the fuel concentration along the motion axis is reduced and, by compensation, it increases elsewhere. The same trend is observed for the mixture fraction variance.
Although the numerical and experimental trends are very similar to each other, some differences can be noticed according to the profiles and the maximum fuel concentration. For what concern the profiles, the discrepancy is due to the fact that an axisymmetrical domain has been considered in the numerical simulations, and thus the mixture fraction field has been mirrored with respect to the main vertical axis; instead, experimental results have been achieved by adopting other domain conditions, and thus they appear slightly asymmetrical. By looking at the maximum fuel concentration, it is possible to observe that the difference with the experimental results tends to decrease with the depth: in fact, moving from 25mm to 45mm, the difference passes from 0.03 to 0.01. For what concerns the mixture fraction variance, the same differences with respect to Sandia results are noticeable: in this case, the experimental profile is very irregular, and this tendency seems to increase with jet penetration. This is due to the impact that the turbulent air has on the evolution of the system chemistry.
Another aspect that has to be considered for completing the numerical model validation is the comparison of the vapor and liquid penetration of the fuel jet with respect to Sandia's results:

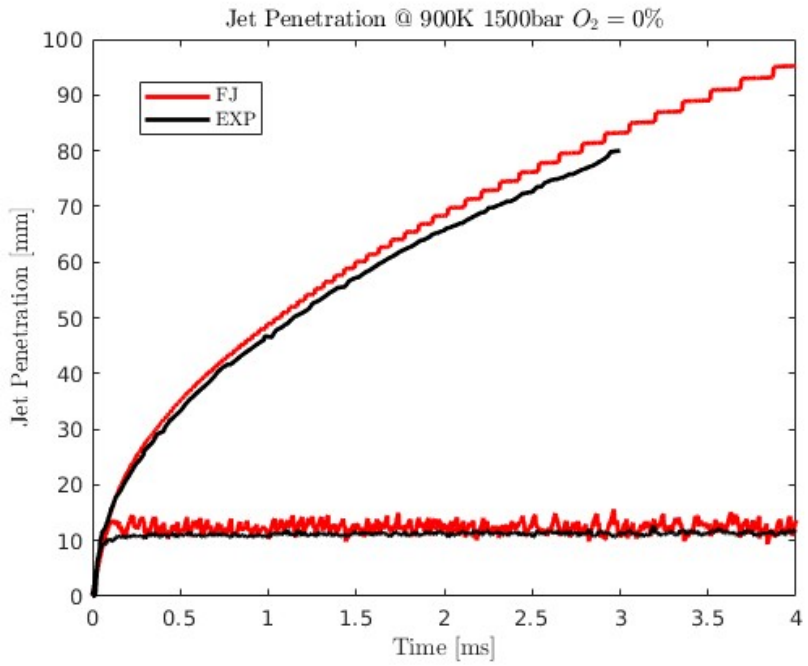

Figure 5.2: Comparison between numerical and experimental results on what concerns the spray penetration inside the vessel

By looking at the graph, it is possible to appreciate how the numerical and experimental trends are very similar to each other. The liquid length stabilizes at almost 10mm from the injection point: it means that, at that distance, 99% of the fuel mass has been injected inside the vessel. Beyond that threshold, the viscous and aerodynamic influence of the surrounding air provokes the jet disruption into smaller and smaller molecules, that diffuse in the environment. Moreover, the difference in terms of temperature between air and fuel determines a heat exchange between them, leading to fuel evaporation. As said before, the absence of O_2 inside the vessel avoids the onset of the combustion process.

5.1.2. Free Jet Vs. Ducted Fuel Injection

Once the numerical model has been assessed to be accurate enough to reproduce the experimental spray A case, a further analysis has been conducted for detecting the main differences between the conventional injection mode and the DFI technology at the same conditions expressed for the validation case. This analysis is necessary for understanding the improvements associated with the duct methodology, focusing on the way the mixture fraction field changes with respect to the conventional case.

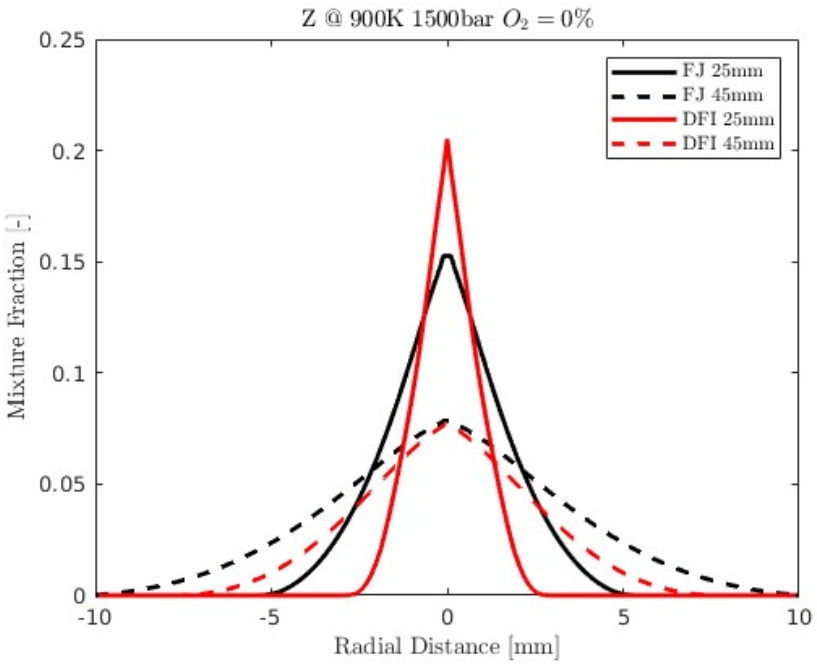

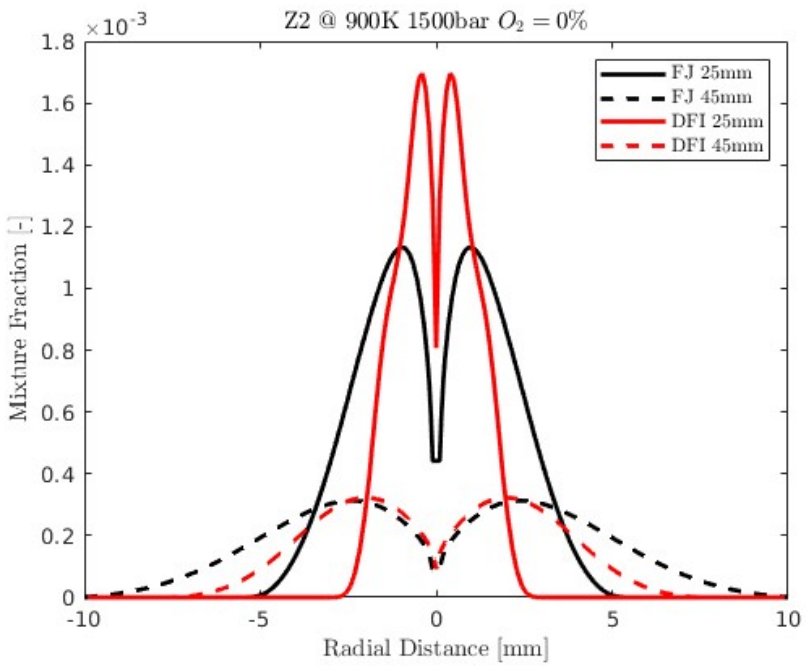

Figure 5.3: Numerical results from CFD simulations: comparison between FJ and DFI trends

By looking at both the mixture fraction and the mixture fraction variance fields, it is possible to comprehend the benefits introduced with the DFI technology: at the same distance along the injection axis, the duct enables keeping higher fuel concentration compared to the conventional case, and this is due to a difference related to the flow momentum evolution: in fact, the counter-pressure offered by the duct is significantly lower than the one observable for the free-spray case, and so the fuel diffusion is more limited. This last aspect leads to higher values for the mixture fraction variance, due to the fact the diffusion rate is lower than the free-spray condition. Only at 45mm from the injector nozzle, the fuel concentrations along the main axis are the same, but the mixture fraction field associated with the DFI technology is narrower than the free-spray one. The following figure offers a comparison between FJ and DFI in terms of turbulent kinetic energy:

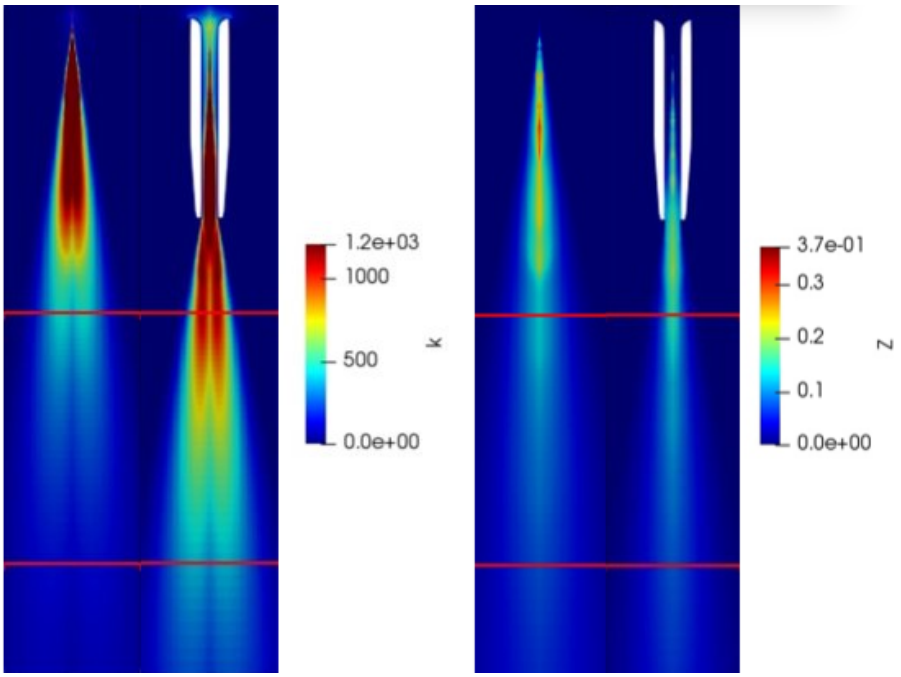

Figure 5.4: Turbulent kinetic energy and mixture fraction field comparison between FJ and DFI under non-reacting conditions and 900K ambient temperature at 25mm and 45mm from injection nozzle

By looking at the differences in terms of turbulent kinetic energy, further results can be introduced for describing the evolution of the velocity field inside the vessel: in this case, thanks to ParaView, a representation of the system evolution in the first instants of the injection process has been offered, with the relative comparison between FJ and DFI technologies. By looking at the following results, it is easy to appreciate how the velocity field along the injection axis is higher for the ducted approach rather than the conventional one: in this sense, the impact the surrounding air has on reducing momentum is more limited, and the fuel jet can maintain higher inertia during the penetration through the ambient air.

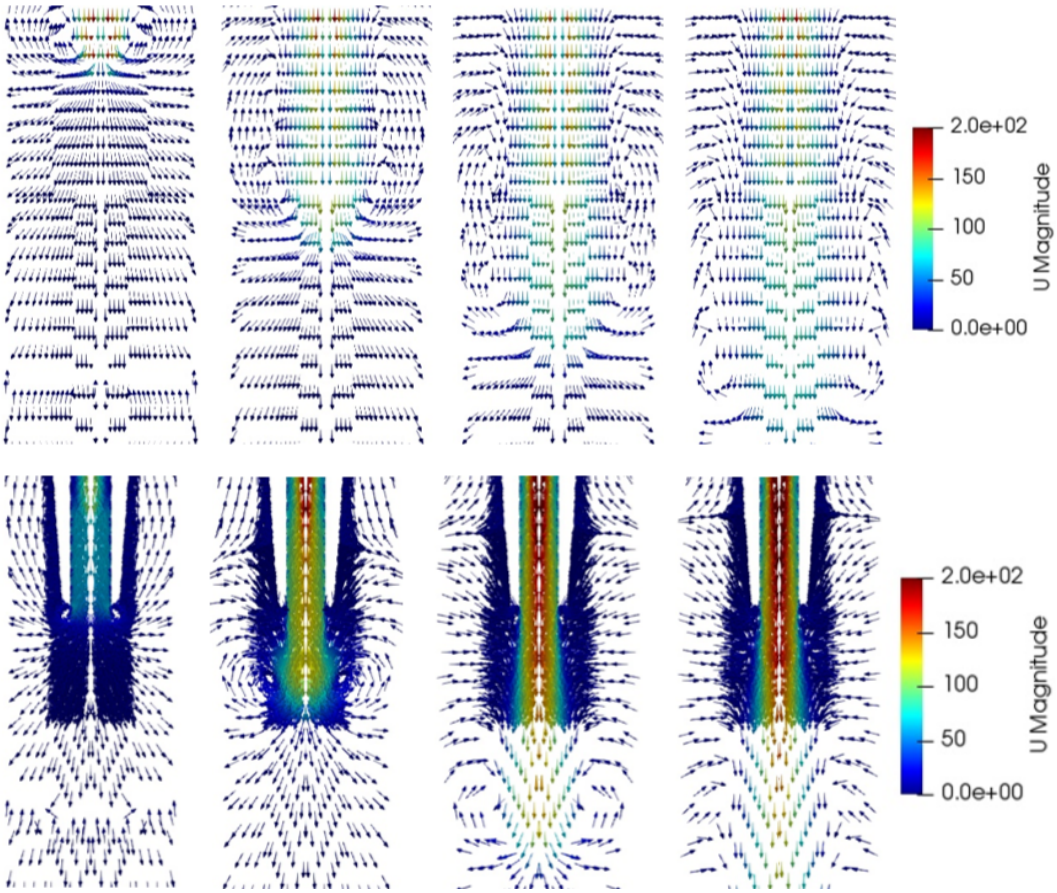

Figure 5.5: Velocity field variation associated with both FJ and DFI technologies from 0.1ms to 0.4ms

As described above, the introduction of the duct enables to keep high the fuel concentration along the injection axis, due to the lower counter-pressure acting against the fuel jet inside the duct: this trend is graphically confirmed by the higher extension of the region where the turbulent kinetic energy reaches the maximum value. This difference between the 2 technologies is confirmed by the comparison between the vapor and liquid penetration trends:

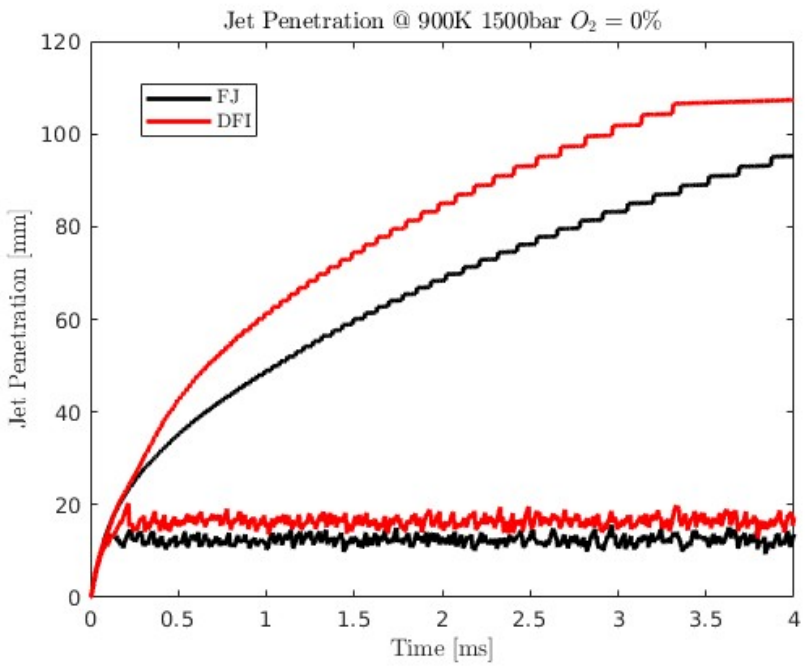

Figure 5.6: Jet penetration comparison between the FJ and the DFI technologies

The difference in terms of liquid length is very small, whereas the most evident discrepancy is associated with the vapor penetration trends: for the FJ the vapor penetration trend is almost linear, whereas the DFI trend is more curved. The difference is associated with the evolution of the fuel momentum along the propagation axis: the higher flow inertia achieved with the duct introduction is appreciated by the higher slope of the red curve compared to the black one. This means that, for the DFI solution, the fuel jet is able to better withstand the resistance introduced by the surrounding air, by reflecting lower fuel diffusion inside the vessel and also deeper penetration of the vapor phase.
Hereafter, a graphical comparison between the FJ and DFI technologies has been brought to the attention to resume all the differences previously highlighted: the spray evolution has been calculated thanks to the post-processing tool *ParaView*, which enabled to extract the spray evolution inside the vessel up to 0.4ms, so to be able to appreciate both the vapor and the liquid penetration in terms of mixture fraction field:

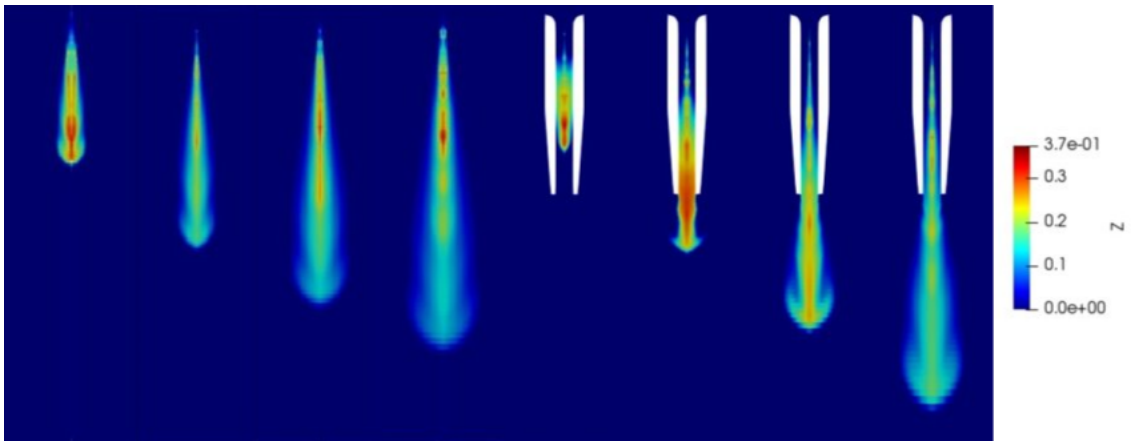

Figure 5.7: Spray evolution for the free-spray and DFI cases between 0.1ms and 0.4ms according to mixture fraction field

5.2. Reacting Analysis

The main target of the reacting analysis is to point out how a turbulent flame generates and stabilizes at a fixed ambient thermo-chemical state, emphasizing the conditions at which an ignitable air-fuel mixture is generated and the subsequent production of partially-oxidized elements that gives a measure of how efficient the combustion process is. This represents an evolution with respect to the non-reacting investigation since the combustion is studied in each of its aspects, rather than focusing only on the evolution of mixture fraction and velocity fields in space and time and, moreover, the presence of oxygen in the air represents a more realistic point of view for the analysis.
For analyzing the reacting case, the following table shows all the assumptions made on the different boundary conditions:

	value
Oxygen Concentration	15%, 21%
T_{amb} **[K]**	850, 900, 950
Combustion Model	PSR, ADF

Table 5.2: Analyzed operating conditions for the reacting case

In particular, for the CFD case validation, the attention is focused on a set of different quantities, used for describing the transient evolution of the reacting system from a

thermodynamic point of view:

- *Ignition Delay*: this parameter expresses the time interval in-between the injection time and the ignition time.
- *Lift-Off Length*: this parameter expresses the distance, from the injection point, at which the flame stabilizes under the set of thermal boundary conditions introduced in advance. In particular, its trend is described in the file *LOLOH14.dout*.
- *Heat Release Rate*: this quantity shows the rate at which the thermal energy is released during the combustion process.
- *Soot Mass*: this feature shows the effectiveness of the combustion process, and thus the percentage of injected fuel that gets correctly oxidized by the ambient air.

In the following sections, all these quantities have been compared then to the experimental results obtained by Sandia to validate the goodness of the numerical model adopted in this analysis.

5.2.1. Combustion models comparison

A first evaluation of the differences in terms of adopted chemical mechanisms has been developed by looking at the heat release rate trends: in fact, for fixed thermo-chemical boundary conditions, the difference between the two models is the accounting of both mass and energy diffusion for the process analysis. In particular, the following results are considered for an *LTC* case, the first group of images is referred to an ambient oxygen concentration equal to 15%, the other set of results is evaluated at 21%: the black curve is referred to as the *ADF* approach, and the red one to the *PSR*.

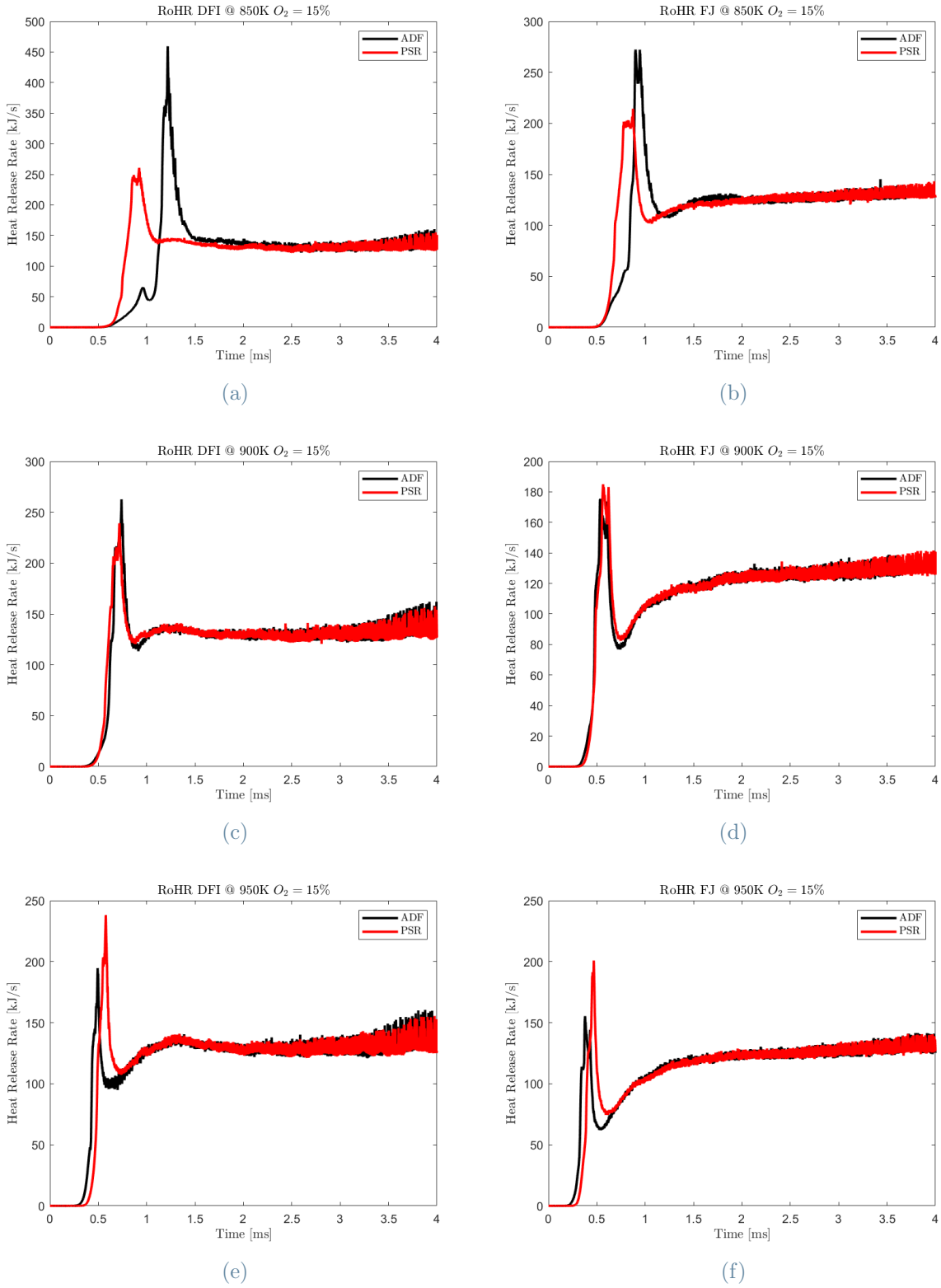

Figure 5.8: Effect of combustion mechanism on the heat release rate performance at 850K (a, b), 900K (c, d) and 950K (e, f) with $O_2 = 15\%$

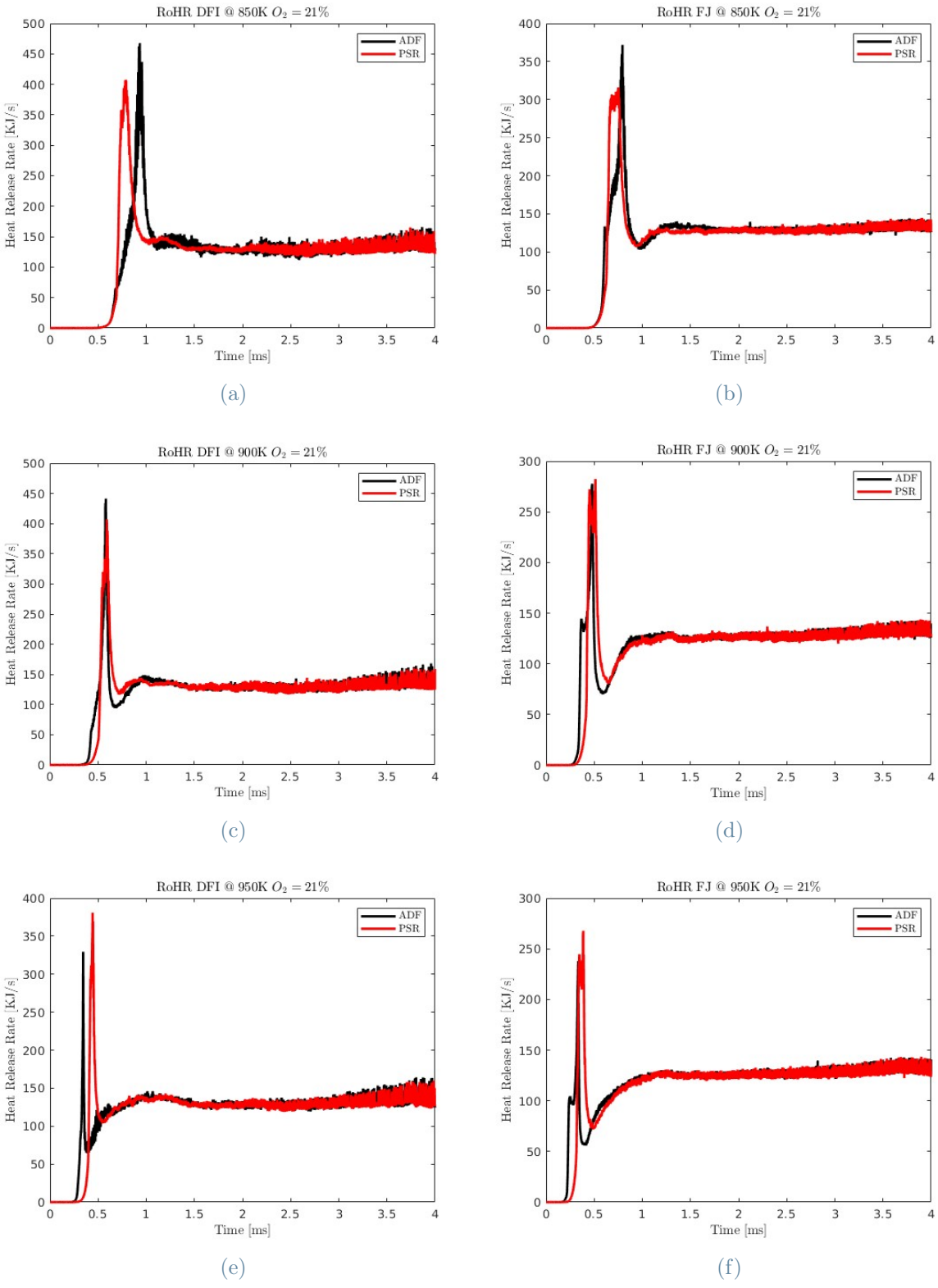

Figure 5.9: Effect of combustion mechanism on the heat release rate performance at 850K (a, b), 900K (c, d) and 950K (e, f) with $O_2 = 21\%$

As said before, the HRR gives a measure of the speed at which the heat is released as a consequence of the chemical reaction progress. It is possible to appreciate a relationship existing between the ignition delay and the maximum value of the heat release rate: generally speaking, an increase in the ignition delay corresponds to an increase in the maximum peak. This is due to the fact that the HRR trend also depends on the mixture's chemical composition: having enough time for observing the formation of a mixture with high homogeneity level, each point of the air-fuel system will ignite almost instantaneously, by releasing a large amount of energy.
Another aspect that has to be considered is related to the ambient oxygen concentration in the combustion vessel: in fact, by lowering the amount of oxygen, a higher amount of time is required for creating an air-fuel mixture able to auto-ignite at the same ambient conditions. Moreover, the maximum peak of the heat release rate is subjected to variations: in particular, by lowering the ambient oxygen, the mixture reactivity will be different at each point of the air-fuel system, obtaining a global reduction of the speed at which the thermal energy gets released by the oxidation reactions.
The comparison between the 2 adopted combustion models has also been done in order to find out which is the more accurate to reproduce the experimental results. Hereafter, results in terms of ignition delay and flame lift-off are proposed to better understand how a flame generates and stabilizes under variable thermal and chemical boundaries.

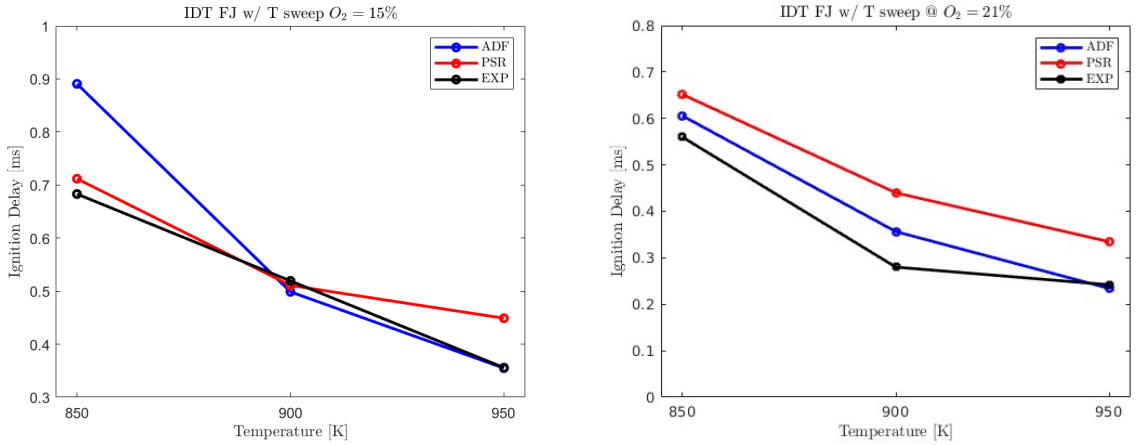

Figure 5.10: Ignition delay with FJ experimental results at $O_2 = 15\%$ and $O_2 = 21\%$

FJ	850K	900K	950K	Ambient O_2
ADF	0.89ms	0.50ms	0.35ms	
PSR	0.71ms	0.51ms	0.45ms	15%
Experimental	0.68ms	0.52ms	0.36ms	
ADF	0.61ms	0.36 ms	0.23ms	
PSR	0.65ms	0.44ms	0.33 ms	21%
Experimental	0.56ms	0.28ms	0.24ms	

Table 5.3: Ignition delay results and comparison among combustion mechanisms (ADF and PSR) and experimental data from Sandia for the FJ technology

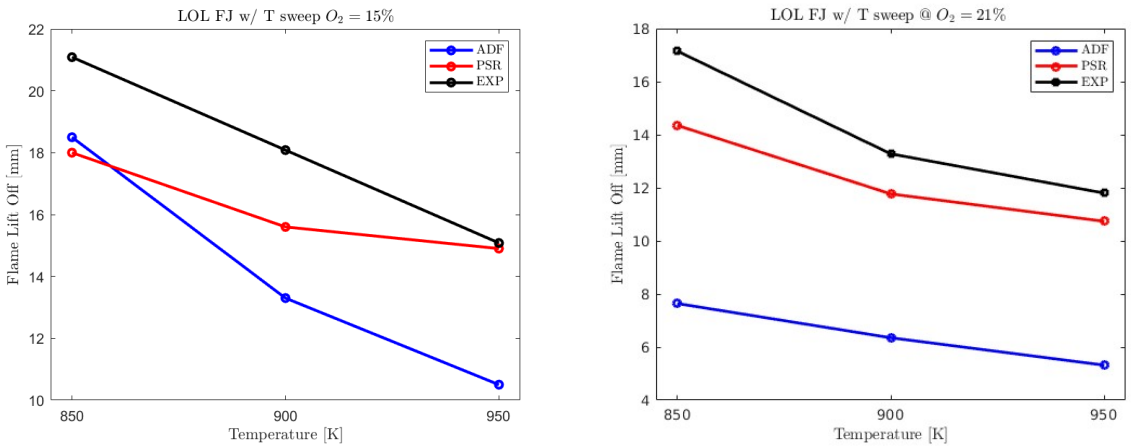

Figure 5.11: Flame Lift-Off with FJ experimental results at $O_2 = 15\%$ and $O_2 = 21\%$

FJ	850K	900K	950K	Ambient O_2
ADF	18.5mm	13.3mm	10.5mm	15%
PSR	18.0mm	15.6mm	14.9mm	
Experimental	21.1mm	18.1mm	15.1mm	
ADF	7.7mm	6.4mm	5.3mm	21%
PSR	14.4mm	11.8mm	10.7mm	
Experimental	17.2mm	13.3mm	11.8mm	

Table 5.4: Flame Lift-Off results and comparison among combustion mechanisms (ADF and PSR) and experimental data from Sandia for the FJ technology

By looking at the previous results associated with the FJ technology, it is possible to appreciate how good the PSR tabulation is to globally reproduce Sandia experimental results both at 15% and 21% O_2.
At 15%, ADF and PSR methods present an opposite trend for the ignition delay evaluation, due to the fact that the first one strongly overestimates the ignition phase at 850K and reproduces in a very good way the experimental trend at higher temperatures, whereas the PSR approach seems to be more accurate at lower temperatures. For what regards the lift-off length, the PSR approach is definitely the most accurate: increasing the temperature, the numerical and experimental trends continuously converge to the same value at 950K, whereas the ADF trend strongly diverges at increasing temperatures.
At 21%, the numerical ignition delay trends evaluated for both ADF and PSR tabulations overestimate the experimental trend, but the difference of values associated with the ADF approach is more limited than the other one. It is possible to appreciate how, at 950K, the ADF table reproduces in a very accurate way the data from Sandia. Talking about the flame lift-off, the PSR approach reproduces the experimental trend with a very high level of accuracy; instead, the ADF trend strongly underestimates the reference trend, and the difference between the 2 chemical mechanisms is very evident.

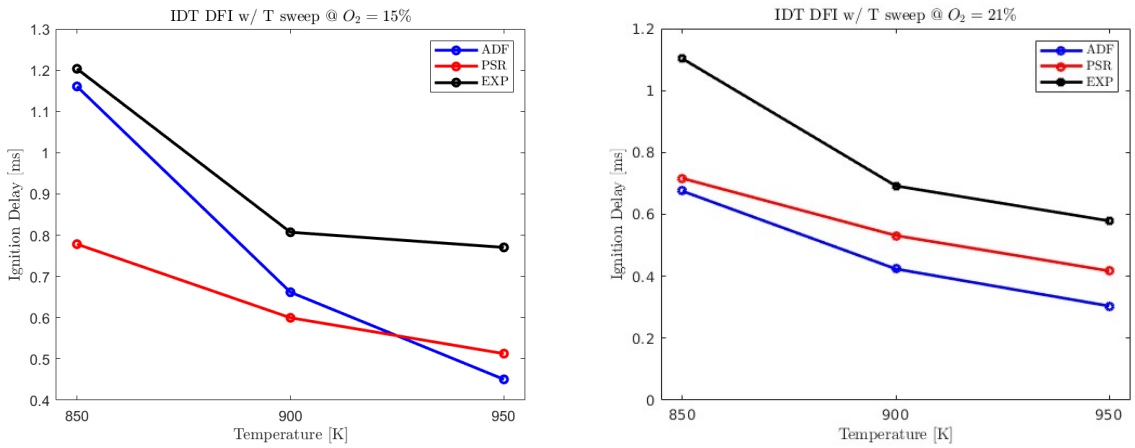

Figure 5.12: Ignition delay with DFI experimental results at $O_2 = 15\%$ and $O_2 = 21\%$

DFI	**850K**	**900K**	**950K**	**Ambient O_2**
ADF	1.16ms	0.66ms	0.45ms	
PSR	0.78ms	0.60ms	0.51ms	15%
Experimental	1.20ms	0.81ms	0.77ms	
ADF	0.72ms	0.53 ms	0.42ms	
PSR	0.68ms	0.43ms	0.31 ms	21%
Experimental	1.10ms	0.69ms	0.58ms	

Table 5.5: Ignition delay results and comparison among combustion mechanisms (ADF and PSR) and experimental data from Sandia for the DFI technology

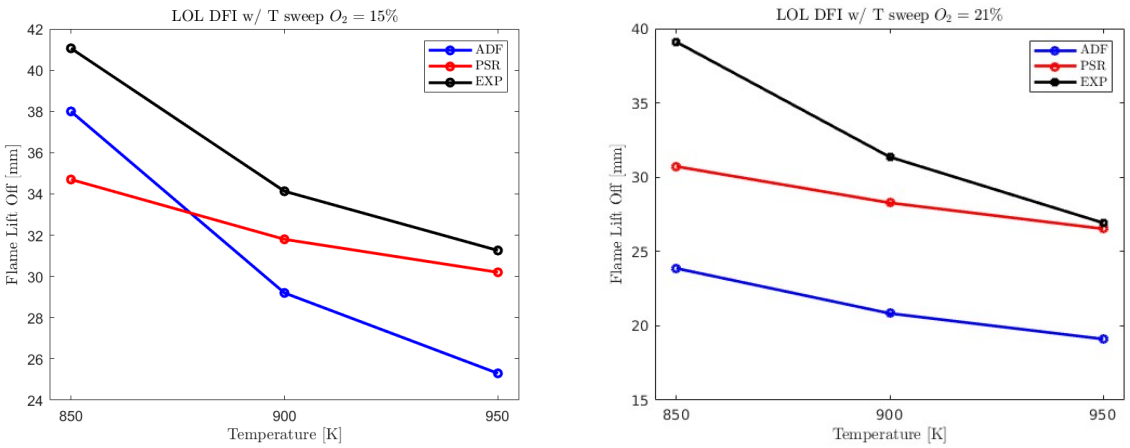

Figure 5.13: Flame Lift Off with DFI experimental results at $O_2 = 15\%$ and $O_2 = 21\%$

DFI	850K	900K	950K	Ambient O_2
ADF	38.0mm	29.2mm	25.3mm	
PSR	34.7mm	31.8mm	30.2mm	15%
Experimental	41.1mm	34.1mm	31.3mm	
ADF	23.9mm	20.8mm	19.1mm	
PSR	30.7mm	28.3mm	26.5mm	21%
Experimental	39.1mm	31.4mm	26.9mm	

Table 5.6: Flame Lift-Off results and comparison among combustion mechanisms (ADF and PSR) and experimental data from Sandia for the DFI technology

By looking at the previous results associated with the DFI technology, it is possible to appreciate how good the PSR tabulation is to globally reproduce Sandia experimental results both at 15% and 21% O_2.
At 15%, both ADF and PSR approaches underestimate the experimental trend of the ignition delay, although the PSR tabulation produces a trend that is almost parallel to the experimental one. On the other side, the ADF seems to reproduce quite well the Sandia data up to 900K: from that point on, the divergence between the profiles is significant. Looking at the lift-off length, the blue line associated with ADF diverges from reference data as the temperature increases; instead, the PSR tabulation produces a trend that rapidly converges to the black curve, observing an almost equal value at 950K.

At 21%, both ADF and PSR trends slightly underestimate the reference data associated with the mixture ignition delay, and it is also possible to appreciate the similarity existing between the trends obtained with the 2 tabulations. The discrepancy at 850K is very relevant, and by increasing the temperature, the PSR trend better reproduces the Sandia results. Looking at the flame lift-off, the PSR approach converges to the experimental trend by increasing the ambient temperature, whereas the ADF method strongly underestimated the Sandia results.

As previously introduced, the flame lift-off has been defined as the distance from the injector tip to the nearest location where 14% of the peak OH mass fraction is obtained. The hydroxyl OH is a very reactive radical that gets formed during the combustion process and, in particular, its mass concentration increases with the environment temperature. The following figures extracted from ParaView figure out the way OH concentration can be affected by environmental properties, both thermal and chemical and thus the variation of the hydroxyl affects the displacement of the flame lift-off. On the left the case at 15% O_2 is analyzed, whereas on the right side all the results associated to an oxygen concentration of 21% are reported:

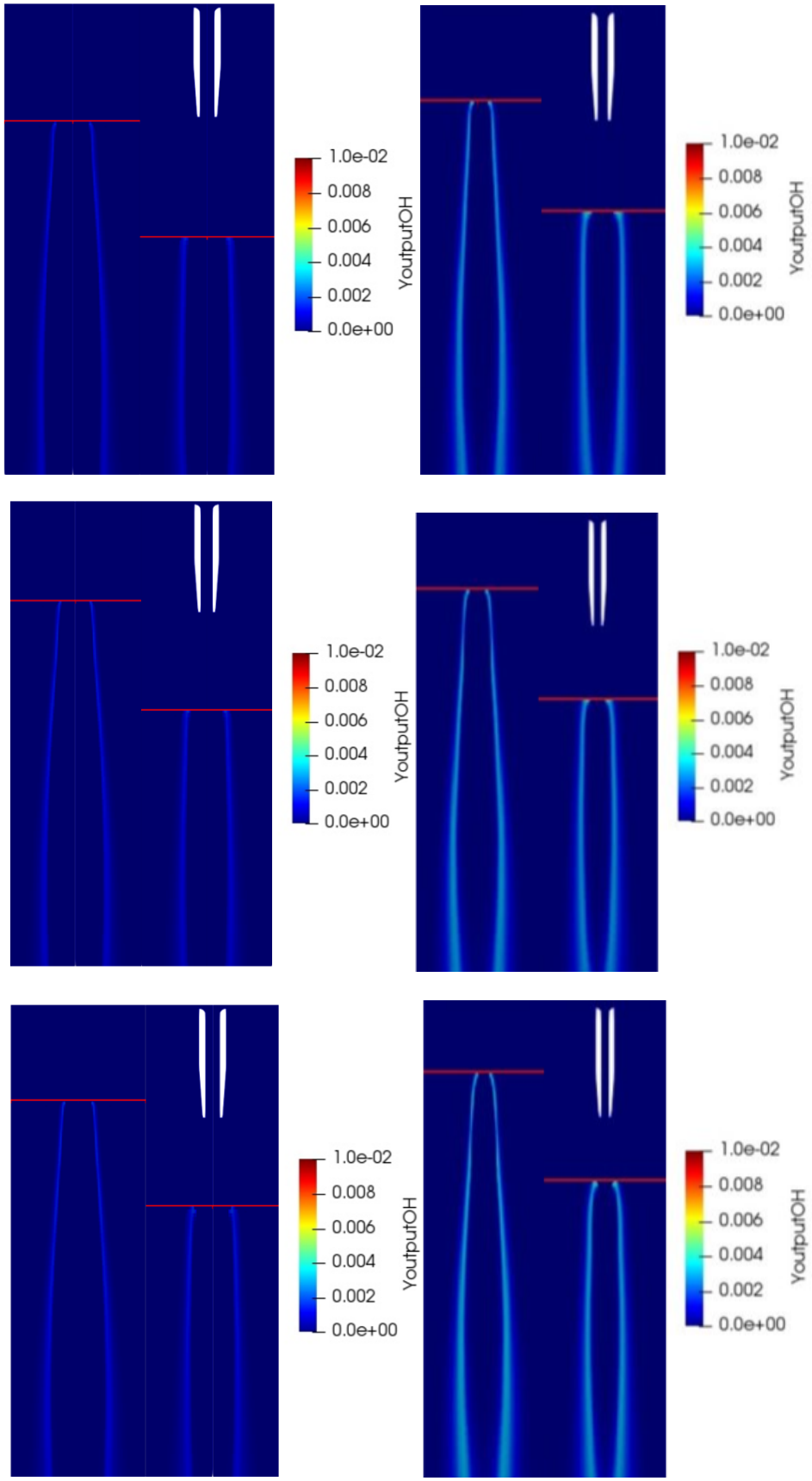

Figure 5.14: Variation of the OH production according to the environmental properties, related to ambient temperature (850K, 900K and 950K) and oxygen concentration (15% and 21%)

Ignition delay and flame lift-off are strictly related: if the mixture auto-ignition is anticipated due to high ambient conditions, the reaction rates are accelerated, and thus the OH formation; so, the flame stabilizes closer to the injection point. As it can be appreciated, the difference between the 2 mechanisms is more evident: the ADF method hugely underestimates the experimental trend, in particular at 850K where the difference is around 15mm, and the increase of temperature seems to reduce a little bit the discrepancy. The results are sharply better when the PSR tabulation is adopted: although an evident difference at 850K, the experimental global trend has been reproduced better, observing a data convergence with the increase of ambient temperature. Thus, the combustion mechanism that better approximates the Sandia experimental results is the PSR table: thus, the following graphical results extracted from ParaView are referred to that tabulation. Hereafter, results associated with flame temperature and equivalence ratio fields are introduced for 850K, 900K, and 950K respectively:

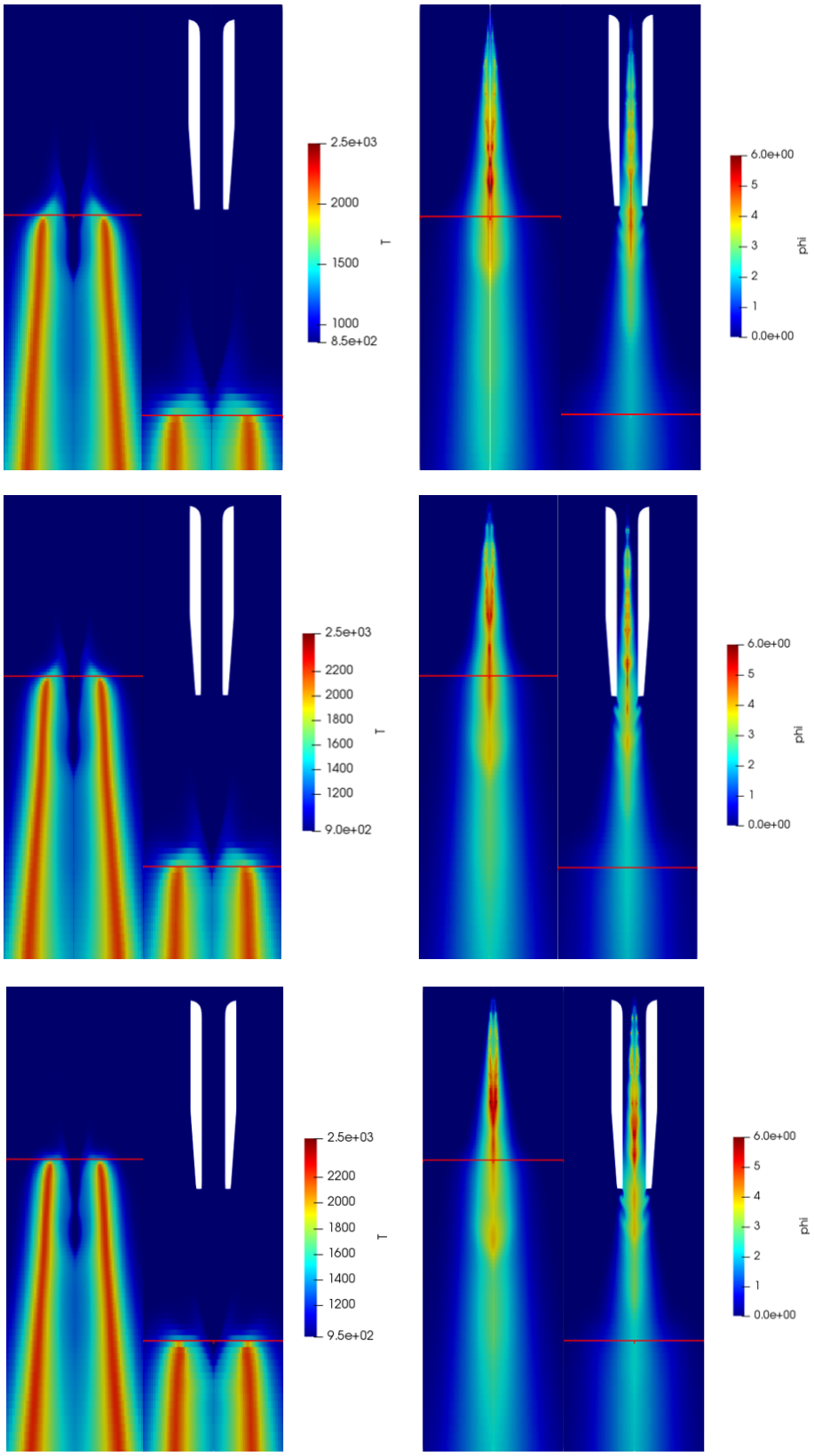

Figure 5.15: Graphical analysis for the flame temperature field (left) and for the ϕ field (right) at $O_2 = 15\%$: for each figure, a comparison between FJ and DFI can be appreciated

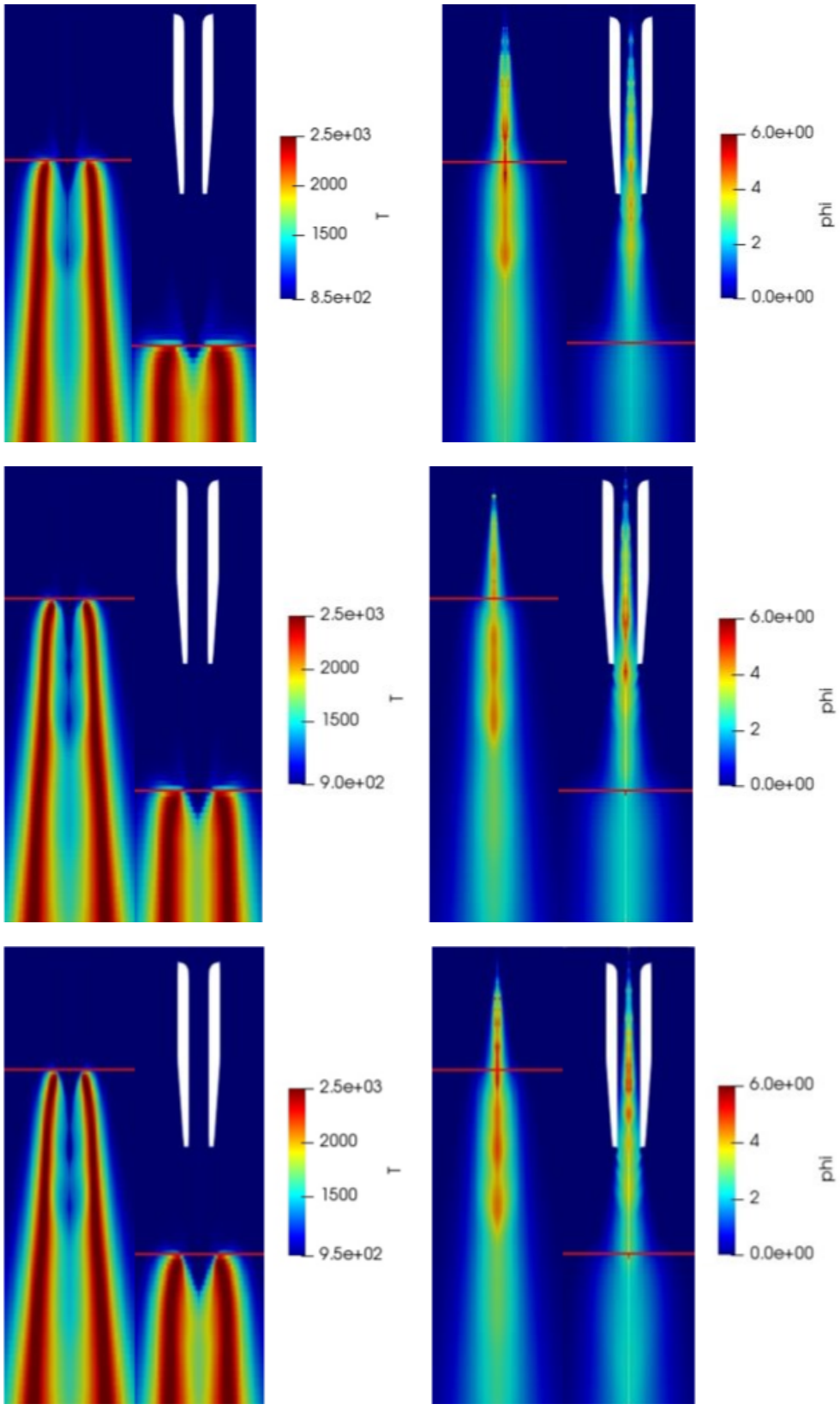

Figure 5.16: Graphical analysis for the flame temperature field (left) and for the ϕ field (right) at $O_2 = 21\%$: for each figure, a comparison between FJ and DFI can be appreciated

By looking at these images, the task of the DFI technology has been shown clearly: for each thermal condition of the combustion environment, the flame generated with the introduction of the duct significantly stabilizes farther from the injector nozzle than the conventional oxidation case: this is due to the fact that the fuel jet is able to maintain a higher momentum along the duct, so avoiding any critical interaction with the surrounding air that could lead to the formation of an inflammable mixture. The improvements achieved with the new technology can be further emphasized by looking at the equivalence ratio, ϕ, field: it is possible to appreciate that, at the same distance from the injector nozzle, the mixture fraction obtained with the ducted approach is significantly lower than the reference combustion case. The fact that the mixture is leaner, as said before, enables the faster release of thermal energy and moreover reduces the volume of produced soot.

5.2.2. Soot production analysis

As was said before, the introduction of the DFI technology has the target of creating a leaner mixture compared to the conventional combustion case, leading to a reduction of the produced soot volume. The production of partially-oxidized products determines the combustion efficiency, due to the fact that the soot tends to absorb part of the thermal energy released during the chemical process: thus, considering the same amount of potential energy introduced inside the system with the fuel, the lower the amount of soot the higher will be the net thermal power that can be exploited for other purposes, and thus the overall combustion efficiency.
Hereafter, the CFD results related to soot production will be reported, by focusing on the main differences between free-spray and DFI technology, and also the way soot varies according to the ambient thermo-chemical conditions. In particular, the evaluation of the soot production has been conducted only considering the PSR tabulation, since it has been demonstrated to produce the best similarities with experimental data from Sandia, especially for what concerns flame generation and stabilization inside the combustion environment.

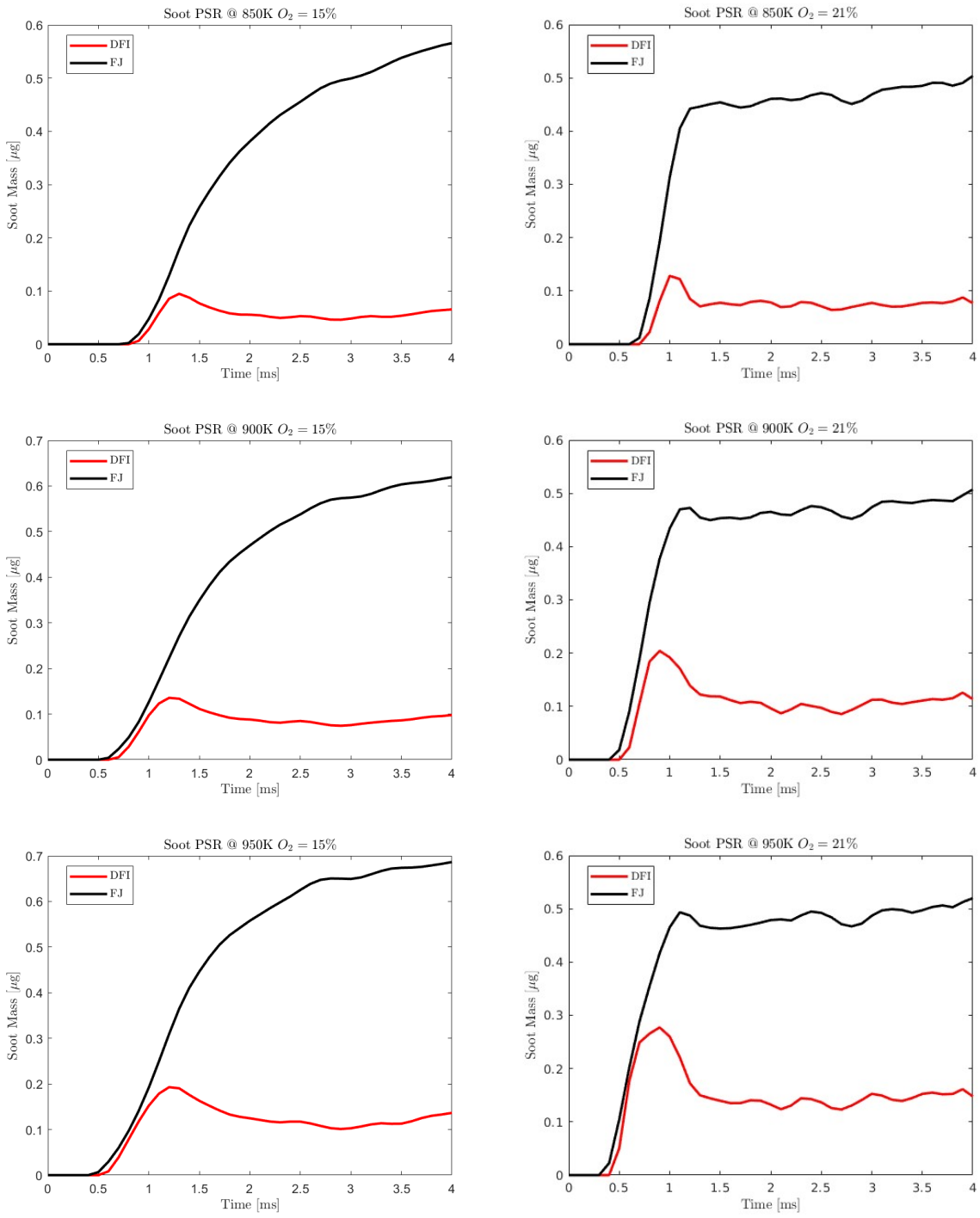

Figure 5.17: Soot production differences between FJ and DFI according to ambient oxygen concentration and ambient temperature

By looking at the previous results, it is possible to appreciate the impact the ambient thermo-chemical conditions have on the soot formation:

- *Temperature Effect*: considering constant oxygen concentration in the combustion environment, the increase of ambient temperature leads to anticipating the auto-ignition phase of the air-fuel mixture. The mixing phase is so limited by the low available amount of time, and the subsequent level of homogeneity for the mixture will be poor, leading to a bigger volume of partially-oxidized products.
- *Oxygen Effect*: considering constant ambient temperature inside the vessel, the trend of soot formation is quite different between the cases at 15% and 21%. Due to the fact O_2 acts as a catalyst for the chemical reaction, an increase in its concentration accelerates the auto-ignition phase of the mixture, and the poor level of homogeneity reached in the available time span brings to a sharper increase in soot production, up to the maximum value. From that point on, the soot formation seems to stabilize around a fixed value, that depends on the thermo-chemical evolution of the system toward the equilibrium: the higher the oxygen concentration, the faster will be the stabilization of soot production.

According to the results above reported, the oxygen effect determines some sensible variations of what regards the soot production curves profile for both FJ and DFI technologies. The largest discrepancy is associated with the FJ case: at 15% O_2, the soot production profile is constantly increasing over time and the trend stabilization verifies at 4ms, whereas at 21% O_2 the soot profile is steeper than the other one, and after 1ms the process stabilization occurs. At lower oxygen concentrations, the soot production stabilization is delayed due to the fact that there is not enough oxygen for compensating the introduced fuel mass: this is why the soot volume increases until the fuel injection goes on. Instead, at 21% O_2 there is enough oxygen concentration in the environment to compensate the introduction of the fuel mass: thus, the process will stabilize before the injection phase ends.
On the other side, the soot production observed by adopting the DFI technology does not seem to be so affected by the ambient O_2 concentration in the environment: in fact, the global trend in the 2 cases is quite similar and, moreover, the soot production stabilizes at the same value, once the thermal state of the vessel has been set. This can be connected to the higher jet penetration, and thus the possibility of better exploiting the available amount of oxygen in the environment.

Thanks to ParaView, it is possible to have a better understanding of the impact of the 2 technologies in terms of soot production: the following figures enable to appreciate, at 850K, 900K and 950K, the comparison between FJ and DFI for what concern the soot formation according to the ambient oxygen concentration:

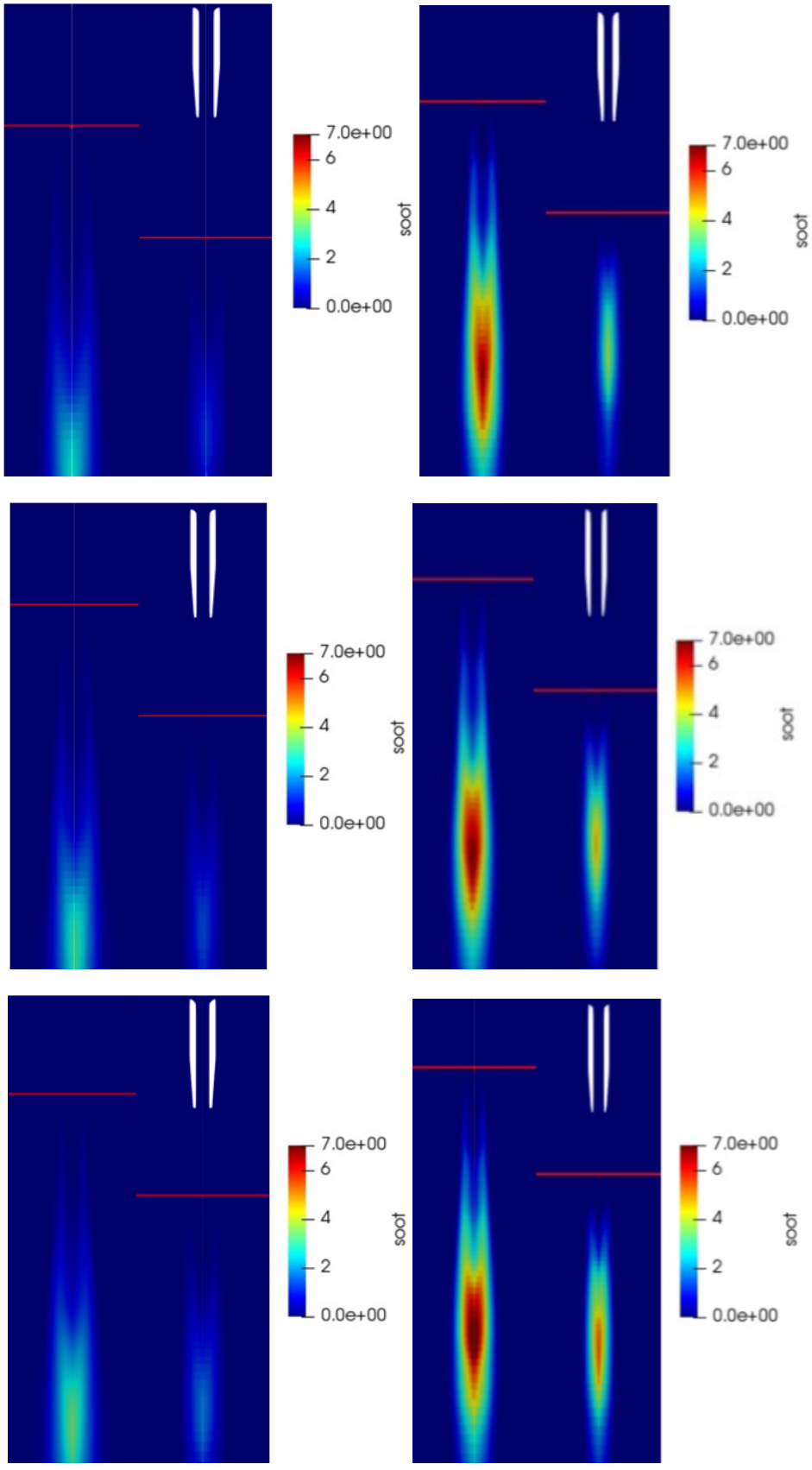

Figure 5.18: Graphical comparison for soot production from ParaView according to ambient temperature and oxygen concentration variations

6 | Conclusions and future developments

The activity presented in this thesis has the aim of pointing out the improvements, in terms of soot reduction and subsequent combustion efficiency, that the ducted fuel injection technology introduces with respect to the conventional process characterized by a free-spray jet.
The campaign started with the analysis of the experimental state-of-the-art Sandia National Laboratories achieved through the adoption of a constant-volume combustion vessel and an optical gear used for capturing the most important parameters related to turbulent flame generation and stabilization. This set of results, both associated with FJ and DFI technologies, has been used as a reference for the current activity: in fact, the study of both mechanisms has been possible by adopting a numerical approach thanks to the CFD computational software OpenFOAM, in order to reproduce the actual environment wherein turbulent combustion occurs. Once the computational domain and the injection system, with the respective boundary conditions, have been modeled so to be the same as the ones adopted by Sandia National Laboratories, the thesis activity has been divided into 2 different phases:

1. Validation of the adopted numerical model under no-reacting conditions: in this case, the numerical FJ case has been compared to the experimental spray A condition from Sandia National Laboratories, so to assess the goodness of the spray model. The numerical approach brought very accurate results similar to the reference ones, both associated with the mixture fraction field and the jet penetration inside the vessel: some discrepancies may be due to the data processing gear and the relative accuracy. Moreover, a brief comparison between FJ and DFI technologies, at non-reacting conditions, has been defined so to point out the main differences between them, according to the evolution of both mixture fraction field and jet penetration in space and time.

2. Once assessed the accuracy level of the numerical spray model, the analysis has been

extended to the reactive field. In this case, the experimental data associated with the flame generation and stabilization inside the vessel have been compared, for different thermo-chemical conditions, to the numerical ones obtained by considering two different combustion models: PSR and ADF. In most cases, both these two approaches underestimate the experimental results of Sandia National Laboratories, but globally the PSR approach is the one able to minimize the difference with the reference data: in fact, the accuracy level achieved with the ADF table is poor, in particular for the DFI analysis.

Due to the fact that PSR turned out to be the best chemical mechanism to reproduce the experimental results, this table has been considered for analyzing the differences in terms of soot production between FJ and DFI for a Low-Temperature Combustion: as it can be noticed from numerical results, the DFI introduces huge improvements related to the soot reduction for each analyzed the thermo-chemical condition of the vessel, so that the adopted numerical model can be observed as idoneous for future studies.

- The soot production observable with the DFI technology seems to be independent on the ambient oxygen concentration since for 15% and 21% O_2 the differences are very limited.
- Once the ambient oxygen concentration has been fixed, the effect ambient temperature has on the soot production is more evident for the DFI technology rather than the conventional free-spray case: by considering the same range of temperatures, an increase of 100K determines an increase in soot production for the DFI 10 times higher than the free-spray

DFI could be a key technology for future engines because it is an effective, conceptually simple, mechanical approach for lowering soot and perhaps other emissions, as well as potentially improving combustion efficiency. Still much remains to be investigated and learned about the DFI knowledge, so in the future scientific analysis can be further improved by quantifying the effects of ducts on entrainment and mixing rates, duct/spray misalignment, and eventually multiple injections. A wider sensitivity analysis on soot production varying duct diameter, length, stand-off distance, duct inlet/outlet geometries and overall cross-sectional profile (e.g. converging or diverging); duct material including heat transfer to or from the duct, and surface finish; fuel composition and properties effect can be investigated. In the end, accurate analysis of the duct in real engines, where the ambient thermodynamic conditions are time-varying, including impacts on efficiency, cold-start ability, and engine noise.

Bibliography

[1] J.B. Heywood. *Internal Combustion Engine Fundamentals*. McGraw-Hill, New York, 1988.

[2] G. Ferrari. *Motori A Combustione Interna*. Società Editrice Esculapio, 2016.

[3] Charles J Mueller, Christopher W Nilsen, Daniel J Ruth, Ryan K Gehmlich, Lyle M Pickett, and Scott A Skeen. Ducted fuel injection: A new approach for lowering soot emissions from direct-injection engines. *Applied energy*, 204:206–220, 2017.

[4] Christopher W Nilsen, Drummond E Biles, Brady M Wilmer, and Charles J Mueller. Investigating the effects of duct length and diameter and fuel-injector orifice diameter in a compression-ignition engine equipped with ducted fuel injection. *Applications in Energy and Combustion Science*, 7:100030, 2021.

[5] Charles J Mueller, Christopher W Nilsen, Drummond E Biles, and Boni F Yraguen. Effects of fuel oxygenation and ducted fuel injection on the performance of a mixing-controlled compression-ignition optical engine with a two-orifice fuel injector. *Applications in Energy and Combustion Science*, 6:100024, 2021.

[6] Brady M Wilmer, Christopher W Nilsen, Drummond E Biles, Charles J Mueller, and William F Northrop. Solid particulate mass and number from ducted fuel injection in an optically accessible diesel engine in skip-fired operation. *International Journal of Engine Research*, 23(7):1226–1236, 2022.

[7] Feng Li, Chia-fon Lee, Ziman Wang, Yiqiang Pei, and Guoxiang Lu. Impacts of duct inner diameter and standoff distance on macroscopic spray characteristics of ducted fuel injection under non-vaporizing conditions. *International Journal of Engine Research*, 22(5):1702–1713, 2021.

[8] Yuxin Zhang, Ziman Wang, Chia-fon Lee, Feng Li, and Han Wu. Analysis of mechanism of ducted fuel injection under non-vaporizing condition. *Fuel*, 305:121496, 2021.

[9] Feng Li, Chia-fon Lee, Ziman Wang, Fushui Liu, and Guoxiang Lu. Optical investi-

gation on impacts of ambient pressure on macroscopic spray characteristics of ducted fuel injection under non-vaporizing conditions. *Fuel*, 268:117192, 2020.

[10] Kenth I Svensson and Glen C Martin. Ducted fuel injection: Effects of stand-off distance and duct length on soot reduction. *SAE International Journal of Advances and Current Practices in Mobility*, 1(2019-01-0545):1074–1083, 2019.

[11] Russell Fitzgerald, Kenth Svensson, Glen Martin, Yongli Qi, and Chad Koci. Early investigation of ducted fuel injection for reducing soot in mixing-controlled diesel flames. *SAE International Journal of Engines*, 11(6):817–834, 2018.

[12] Shiro Tanno, Jun Kawakami, Koji Kitano, and Takeshi Hashizume. Investigation of a novel leaner fuel spray formation for reducing soot in diffusive diesel combustion-homogenizing equivalence ratio distribution in the lift-off region. Technical report, SAE Technical Paper, 2019.

[13] Christopher W Nilsen, Drummond E Biles, Boni F Yraguen, and Charles J Mueller. Ducted fuel injection vs. conventional diesel combustion. *SAE International Journal of Engines*, 14(1):47–58, 2021.

[14] Federico Millo, Andrea Piano, Benedetta Peiretti Paradisi, Cristiano Segatori, Lucio Postrioti, Luca Pieracci, Andrea Bianco, Francesco Concetto Pesce, and Alberto Vassallo. Ducted fuel injection: A numerical soot-targeted duct geometry optimization. *SAE International Journal of Engines*, 15(03-15-02-0014):297–317, 2021.

[15] F Millo, A Piano, B Peiretti Paradisi, L Postrioti, L Pieracci, A Bianco, FC Pesce, and A Vassallo. Ducted fuel injection: Experimental and numerical investigation on fuel spray characteristics, air/fuel mixing and soot mitigation potential. *Fuel*, 289:119835, 2021.

[16] RK Gehmlich, CJ Mueller, DJ Ruth, CW Nilsen, SA Skeen, and J Manin. Using ducted fuel injection to attenuate or prevent soot formation in mixing-controlled combustion strategies for engine applications. *Applied energy*, 226:1169–1186, 2018.

[17] Universitat Politecnica De Valencia. Cmt website, 2022.

[18] Daniel Pontoni. Modeling diesel combustion with tabulated kinetics and different flame structure assumptions. Master's thesis, Politecnico di Milano, 2016.

[19] CFD. Cfd-wiki, the free cfd reference, 2022.

[20] Jennifer C Beale and Rolf D Reitz. Modeling spray atomization with the kelvin-helmholtz/rayleigh-taylor hybrid model. *Atomization and sprays*, 9(6), 1999.

[21] Abderrahmane Aissa, Mohamed Abdelouahab, Abdelkader Noureddine, Mohammed Elganaoui, and Bernard Pateyron. Ranz and marshall correlations limits on heat flow between a sphere and its surrounding gas at high temperature. *Thermal science*, 19(5):1521–1528, 2015.

[22] OpenFOAM. Openfoam guide, 2022.

[23] Kin M Leung, Rune P Lindstedt, and William P Jones. A simplified reaction mechanism for soot formation in nonpremixed flames. *Combustion and flame*, 87(3-4):289–305, 1991.

[24] Tommaso Lucchini, Gianluca D'Errico, Tarcisio Cerri, Angelo Onorati, Gilles Hardy, et al. Experimental validation of combustion models for diesel engines based on tabulated kinetics in a wide range of operating conditions. *SAE technical paper*, 2017:1–15, 2017.

[25] JA Van Oijen and LPH De Goey. Modelling of premixed laminar flames using flamelet-generated manifolds. *Combustion science and technology*, 161(1):113–137, 2000.

[26] Tommaso Lucchini, Gianluca D'Errico, Angelo Onorati, Alessio Frassoldati, Alessandro Stagni, and Gilles Hardy. Modeling non-premixed combustion using tabulated kinetics and different flame structure assumptions. *SAE International Journal of Engines*, 10(2):593–607, 2017.

[27] Gianluca D'Errico, Tommaso Lucchini, Francesco Contino, Mehdi Jangi, and X-S Bai. Comparison of well-mixed and multiple representative interactive flamelet approaches for diesel spray combustion modelling. *Combustion Theory and Modelling*, 18(1):65–88, 2014.

[28] Alireza Ghasaemi. Numerical simulation of non-reactive evaporative diesel sprays using openfoam. Master's thesis, Politecnico di Milano, 2016.

[29] F Payri, R Novella, JM Pastor, and Eduardo Javier Pérez-Sánchez. Evaluation of the approximated diffusion flamelet concept using fuels with different chemical complexity. *Applied mathematical modelling*, 49:354–374, 2017.

[30] ECN. Engine combustion network, 2022.

List of Figures

List of Tables

List of Symbols

Variable	Description	SI unit
$\vec{\boldsymbol{a}}$	Flow acceleration	m/s^2
$\boldsymbol{B_0}$	KH model constants	–
$\boldsymbol{B_1}$	KH model constants	–
$\dot{\boldsymbol{c}}$	progress variable reaction rate	–
$\boldsymbol{c}$	Normalized progress variable	–
$\boldsymbol{c_p}$	Specific heat capacity	J/kgK
$\boldsymbol{C_1}$	k - ε model constant	–
$\boldsymbol{C_2}$	k - ε model constant	–
$\boldsymbol{C_3}$	RT model constant	–
$\boldsymbol{C_b}$	Levich's breakup length constant	–
$\boldsymbol{C_d}$	Injector nozzle global discharge coefficient	–
$\boldsymbol{C_D}$	Drag coefficient	–
$\boldsymbol{C_k}$	k - ε model constant	–
$\boldsymbol{C_\epsilon}$	k - ε model constant	–
$\boldsymbol{C_\mu}$	turbulent eddies constant	–
$\boldsymbol{d_n}$	Injector nozzle diameter	m
$\boldsymbol{D}$	Duct diameter	m
$\boldsymbol{D_m}$	Mass diffusion coefficient	m^2/s
$\boldsymbol{e}$	Specific total energy	J/kg
$\boldsymbol{E_a}$	Activation energy	J
$\boldsymbol{F_{aero}}$	Global aerodynamic force	N
$\boldsymbol{G}$	Stand-off distance	m
$\boldsymbol{h}$	Convective heat transfer coefficient	$W/m^2/K$
$\boldsymbol{h_{298,i}}$	Formation enthalpy of the i-th species	J/kg
$\boldsymbol{h_t}$	Specific total enthalpy	J/kg

Variable	Description	SI unit
$\boldsymbol{h_u}$	Specific enthalpy of the unburned mixture	J/kg
$\boldsymbol{H_v}$	Latent evaporation heat of fuel	J/mol
$\boldsymbol{HRR}$	Heat Release Rate	J/s
$\boldsymbol{k}$	Turbulent kinetic energy (TKE)	J
$\boldsymbol{k_f}$	Reaction rate constant	–
$\boldsymbol{K_n}$	Nozzle K-factor	–
$\boldsymbol{l}$	Turbulent length scale	m
$\boldsymbol{L}$	Duct length	m
$\boldsymbol{L_b}$	Break-up length	m
$\boldsymbol{Le}$	Lewis number	–
$\boldsymbol{LOL}$	Flame lift-off length	m
$\boldsymbol{m}$	Fluid mass	kg
$\boldsymbol{n}$	polytropic exponent	–
$\boldsymbol{n_i}$	Molar concentration of the i-th species	mol/m^3
$\boldsymbol{N}$	Soot density number	–
$\boldsymbol{NC}$	Cetane number	–
$\boldsymbol{Nu}$	Nusselt number	–
$\boldsymbol{Oh}$	Ohnesorge number	–
$\boldsymbol{p}$	Ambient pressure	Pa
$\boldsymbol{Pr}$	Prandtl number	–
$\boldsymbol{\vec{q}}$	Flow momentum	kgm/s
$\boldsymbol{q}$	Specific heat flux	J
$\boldsymbol{Q_d}$	Thermal power dispersed during combustion	J/s
$\boldsymbol{Q_r}$	Thermal power released during combustion	J/s
$\boldsymbol{r}$	Droplet radius	m
$\boldsymbol{R}$	Gas constant	J/kgK
$\boldsymbol{R1}$	Soot nucleation rate	$1/s$
$\boldsymbol{R2}$	Soot surface growth rate	$1/s$
$\boldsymbol{R3}$	Soot oxidation rate	$1/s$
$\boldsymbol{Re}$	Reynolds number	–
$\boldsymbol{ROI}$	Rate of injection	kg/s
$\boldsymbol{RR}$	Chemical reaction rate	$1/s$
$\boldsymbol{Sc}$	Schmidt number	–

Variable	Description	SI unit
Sc_t	Turbulent Schmidt number	$-$
T	Temperature	K
T_{amb}	Ambient Temperature	K
T_{ign}	Ignition Temperature	K
T_u	Unburned mixture temperature	K
Ta	Taylor number	$-$
$\bar{u}_p$	piston average speed	m/s
u	Turbulent characteristic velocity field	m/s
u_{rel}	relative motion speed	m/s
U	Internal energy	J
$\vec{V}$	Velocity field	m/s
$\bar{V}_i^{'}$	velocity field along the i-th spatial coordinate	m/s
V	gas volume	m^3
V_T	Thermophoretic speed	m/s
W	Mechanical Power exchanged with piston	J/s
We	Weber number	$-$
We_{cr}	Critical Weber number	$-$
x_b	fraction of burned fuel	$-$
x_i	i-th spatial coordinate	$-$
Y_i	Mass fraction of i-th element	$-$
$\tilde{Z}^{''2}$	Mixture fraction variance	$-$
Z	Mixture fraction	$-$
α	Thermal diffusivity	m^2/s
α_a	Actual air-to-fuel ratio	$-$
α_s	Stoichiometric air-to-fuel ratio	$-$
α_t	Turbulent thermal diffusivity	m^2/s
γ	specific heat ratio	$-$
δ_t	Dynamic boundary thickness	m
δ_v	Thermal boundary thickness	m
ΔG	Gibbs Free Energy	J
ε	TKE dissipation rate	Js/m
κ	Conductive heat transfer coefficient	$W/m^2/K$

Variable	Description	SI unit
$\boldsymbol{\Lambda_{KH}}$	Critical KH wavelength	m
$\boldsymbol{\Lambda_{RT}}$	Critical RT wavelength	m
$\boldsymbol{\mu_i}$	Chemical potential of the i-th species	J/mol
$\boldsymbol{\mu_t}$	Turbulent eddies viscosity	Pas
$\boldsymbol{\nu_i^{'}}$	Stoichiometric coefficient of the i-th species	$-$
$\boldsymbol{\rho}$	Fluid density	kg/m^3
$\boldsymbol{\rho_u}$	Unburned mixture density	kg/m^3
$\boldsymbol{\sigma}$	Surface tension	Pa
$\boldsymbol{\bar{\tau}}$	Stress tensor	Pa
$\boldsymbol{\tau_a}$	chemical process time scale	s
$\boldsymbol{\tau_{bu}}$	characteristic breakup time	s
$\boldsymbol{\tau_t}$	physical process time scale	s
$\boldsymbol{\Phi}$	Equivalence ratio	$-$
$\boldsymbol{\Phi_0}$	Initial state of thermo-chemical system	$-$
$\boldsymbol{\chi}$	Scalar dissipation rate	$1/s$
$\boldsymbol{\chi_{st}}$	Stoichiometric scalar dissipation rate	$1/s$
$\boldsymbol{\dot{\omega}_i}$	Reaction rate of the i-th species	$1/s$
$\boldsymbol{\omega}$	wave oscillating frequency	$1/s$
$\boldsymbol{\Omega}$	Control volume	m^3
$\boldsymbol{\Omega_{KH}}$	Critical KH frequency	$1/s$
$\boldsymbol{\Omega_{RT}}$	Critical RT frequency	$1/s$
$\boldsymbol{\Theta}$	Crank Angle	deg